Reviews of Geophysics

REVIEW ARTICLE
10.1029/2024RG000867

Meteorological Tsunamis: From Local Hazard to Global Relevance

Ivica Vilibić[1,2], Petra Zemunik Selak[3], and Jadranka Šepić[4]

[1]Division for Marine and Environmental Research, Ruđer Bošković Institute, Zagreb, Croatia, [2]Institute for Adriatic Crops and Karst Reclamation, Split, Croatia, [3]Institute of Oceanography and Fisheries, Split, Croatia, [4]Faculty of Science, University of Split, Split, Croatia

Key Points:

- Minute-scale sea level oscillations, including meteotsunamis, significantly contribute to extreme sea levels worldwide
- Generated though atmosphere-ocean resonances, meteotsunamis can have from local to global impact and be destructive at certain locations
- Reliable estimates of meteotsunami hazard in present and future climates, along with effective forecasting and warning, remain a challenge

Correspondence to:
I. Vilibić,
Ivica.vilibic@irb.hr

Citation:
Vilibić, I., Zemunik Selak, P., & Šepić, J. (2025). Meteorological tsunamis: From local hazard to global relevance. *Reviews of Geophysics*, *63*, e2024RG000867. https://doi.org/10.1029/2024RG000867

Received 15 APR 2025
Accepted 17 SEP 2025
Corrected 13 OCT 2025

This article was corrected on 13 OCT 2025. See the end of the full text for details.

Abstract Research on meteorological tsunamis or meteotsunamis—long ocean waves in the tsunami frequency band generated by propagating atmospheric disturbances which resonantly enhance ocean waves—has grown significantly in recent decades. This expansion is due to progress in (a) ocean and atmospheric measurements, including advanced instrumentation with higher precision and smaller sampling time steps, as well as installation of meteotsunami tracking measurement networks, (b) ocean and atmospheric data products, including those related to the upper atmosphere and ionosphere, and (c) supercomputing capabilities and sophisticated atmosphere-ocean models that successfully simulate both atmospheric planetary processes and mesoscale systems capable of generating meteotsunamis, as well as sea level response to these. Meteotsunamis can induce multi-meter sea level oscillations in harbors and low-lying areas, leading to severe flooding, infrastructure damage, injuries, and sometimes fatalities. Traditionally, meteotsunami research focused on individual event analyses using available sea level and lower-layer atmospheric observations. Recently, efforts have shifted toward global hazard mapping, the development of forecast and early-warning systems, and toward quantifying projected meteotsunamis intensity and frequency, using climate models. The January 2022 eruption of the Hunga Tonga-Hunga Ha'apai volcano, which generated acoustic-gravity waves that circled the globe, has spurred research of planetary meteotsunami waves and their potential to pose coastal hazards worldwide. Additionally, meteotsunamis radiate acoustic-gravity waves vertically, creating ionospheric oscillations detectable through electron content variations. This review will cover the mentioned developments and conclude with a discussion of research gaps and potential directions for further studies.

Plain Language Summary Sea level extremes are an emerging topic in the era of climate change, as most coastal damage and impacts occur during such events. One of the underrated phenomena contributing to these extremes are meteorological tsunamis or meteotsunamis—long ocean waves in the tsunami frequency band resonantly generated by traveling air pressure/wind disturbances—which are known to substantially impact certain coastlines and locations, causing deaths, injuries, and damage to coastal infrastructure, ships and yachts, buildings, and households, as well as affecting navigational safety. Until about a decade ago, research on meteotsunamis was mostly localized, focusing on specific meteotsunami hotspots. However, in recent years, research has become more global. This was made possible by the development of high-precision oceanic and atmospheric instruments that collect data at minute or higher resolutions, as well as ultra-high-resolution atmosphere-ocean models capable of reproducing meteotsunamis, supported by high-performance computing facilities. This review summarizes all aspects of meteotsunamis, from available data, products, and tools that can be used for research, to an in-depth exploration of the science behind the phenomenon, and its impact on coastal regions. It also discusses the development of forecasting and early-warning systems. Finally, the review provides recommendations for future research directions on this hazardous phenomenon.

Author Contributions:
Conceptualization: Ivica Vilibić, Petra Zemunik Selak
Funding acquisition: Ivica Vilibić, Jadranka Šepić
Methodology: Ivica Vilibić
Supervision: Ivica Vilibić
Visualization: Petra Zemunik Selak, Jadranka Šepić
Writing – original draft: Ivica Vilibić, Petra Zemunik Selak, Jadranka Šepić
Writing – review & editing: Ivica Vilibić, Petra Zemunik Selak, Jadranka Šepić

1. Introduction

Although not unified under a single name or with a comprehensive understanding of the physical processes underlying the phenomenon, meteorological tsunamis, or meteotsunamis, have been known since ancient times. For instance, when the Arabs landed in the 9th century in what is now Mazara del Vallo, located on the south-western coast of Sicily (Italy), they encountered extraordinary propagating bores in the estuary of the local river. These waves endangered their fleet. This phenomenon, recurrent with varying intensity, led to the river being named Mazaro, meaning "possessed" (Šepić, Vilibić, et al., 2018).

Another legend from the small village of Vrboska (Hvar, Croatia) describes how a meteotsunami unified two communities located on opposite shores of a long inlet that were in religious conflict (Šepić & Orlić, 2025b). On the Good Friday of 1614, during a procession held because of bloody tears observed on a crucifix, a violent meteotsunami, locally called "šćiga," struck. It prevented the procession from crossing the bridge over the inlet, forcing participants to traverse all inlet communities. The villagers interpreted this as a divine sign to end their confrontations and unify.

Many similar ancient accounts likely describe violent, destructive ocean waves of non-seismic origin (see more in Section 5.1). These waves are not triggered by earthquakes, aerial or submarine landslides, asteroid impacts, or volcanic caldera collapses but rather by atmospheric processes, and were recognized to correlate with rapid changes in air pressure or wind in the early 20th century (Caloi, 1938; Fonteserè, 1934; Honda et al., 1908; Nomitsu, 1935). Locally, meteotsunamis can reach heights of several meters—much higher than local tides or storm surges at some locations—causing significant impacts on coastal infrastructure and populations, particularly in microtidal regions like the Mediterranean Sea, the Great Lakes, the Japan Sea, and the Baltic Sea (Monserrat et al., 2006; Rabinovich, 2020; Vilibić et al., 2021).

The phenomenon has earned distinct local names worldwide, including "rissaga" or "ressaca" in the Balearic Islands and southeastern Spain (Monserrat, Ramis, & Thorpe, 1991; Ramis & Jansà, 1983; Tintoré et al., 1988), "šćiga" or "štiga" in the Adriatic (Hodžić, 1979/1980; Orlić, 1980, 2015), "abiki" in southwestern Japan (Akamatsu, 1982; Hibiya & Kajiura, 1982; Honda et al., 1908), "marrubbio" or "marrobbio" in Sicily (Candela et al., 1999; Colucci & Michelato, 1976), "milghuba" in Malta (Airy, 1878; Drago, 2009), and "Seebär" in the Baltic Sea (Defant, 1961; Metzner et al., 2000; Piotrowski et al., 2017; Renqvist, 1926). Other locations, such as the Great Lakes, the Persian Gulf, and the northern Algerian coast, have also experienced deadly meteotsunamis (Heidarzadeh et al., 2020; Okal, 2021a; Vilibić et al., 2016).

Advancements in technology—particularly in cost-effective, accurate sea level monitoring—have greatly improved the development and management of sensors capable of detecting minute-scale oscillations. Additionally, rapid and reliable real-time transmission of measured data (NOAA, 2025; Pérez Gómez et al., 2022; VLIZ/IOC, 2025) has facilitated better quantification of meteotsunami events, including assessment of hazards by moderate and weaker minute-scale sea level occurrences, referred to as nonseismic sea level oscillations at tsunami timescales (NSLOTTs; Vilibić & Šepić, 2017; Williams, Schultz, et al., 2021; Zemunik, Denamiel, Šepić, & Vilibić, 2022). Though these oscillations often appear as a part of the background signal, they can significantly increase coastal sea level hazards (Ruić et al., 2023).

An additional challenge is defining meteotsunamis amidst the background of all high-frequency sea level oscillations with atmospheric sources, that is, NSLOTTs. For other types of tsunamis, even centimeter-high waves are classified as tsunamis if their source is verified. Applying the same definition to meteotsunamis would imply their constant presence, as infragravity or other minute-frequency waves of various heights are continuously generated and radiated through the oceans (Bertin et al., 2018; Rawat et al., 2014). At the moment, there is no unified criterion for the definition of a meteotsunami within the scientific community. Early meteotsunami studies were based on the meteotsunami impact on the coast (e.g., flooding, damage, drowning, strong currents). Newer studies aim to set a quantitative threshold for meteotsunami definition: Orlić (2015) and Šepić and Orlić (2025a) defined meteotsunamis as long ocean waves exceeding 1 m in height—the height was selected with a presumption that it will normally lead to flooding of the Adriatic Sea coastaline. Other studies which are based on instrumental data adopted various thresholds, e.g., of sea level or energy exceeding 3 to 6 standard deviations (e.g., Dusek et al., 2019; M. S. Kim et al., 2019), or a fixed threshold for specific stations (e.g., Bechle et al., 2016; Pattiaratchi & Wijeratne, 2014; Rabinovich & Monserrat, 1996, 1998; Šepić et al., 2012). Most recent studies combine these criteria with additional necessary conditions, such as meeting the above criteria at least at two nearby tide gauges (Dusek et al., 2019; M. S. Kim et al., 2021) or ability to associate the meteotsunami occurrence with a convective system (e.g., Williams, Schultz, et al., 2021) or to a specific signal detectable in atmospheric time series (e.g., in air pressure, wind or convective potential energy; Dusek et al., 2019; Pellikka et al., 2020). Furthermore, some meteotsunami studies restrict the sea level analysis to periods shorter than: (a) 2 hr (e.g., Zemunik, Denamiel, Šepić, & Vilibić, 2022; Zemunik, Denamiel, Williams, & Vilibić, 2022); (b) 3 hr (Rabinovich & Monserrat, 1996); (c) 6 hr (Šepić, Vilibić, Lafon, et al., 2015); and (d) even 10 hr (Ferrarin et al., 2023). With this in mind, we propose to use the term meteotsunami to refer either to devastating and damaging NSLOTT events or—in the case of no damage—to the most extreme of NSLOTT events. Most extreme NSLOTT events can be defined

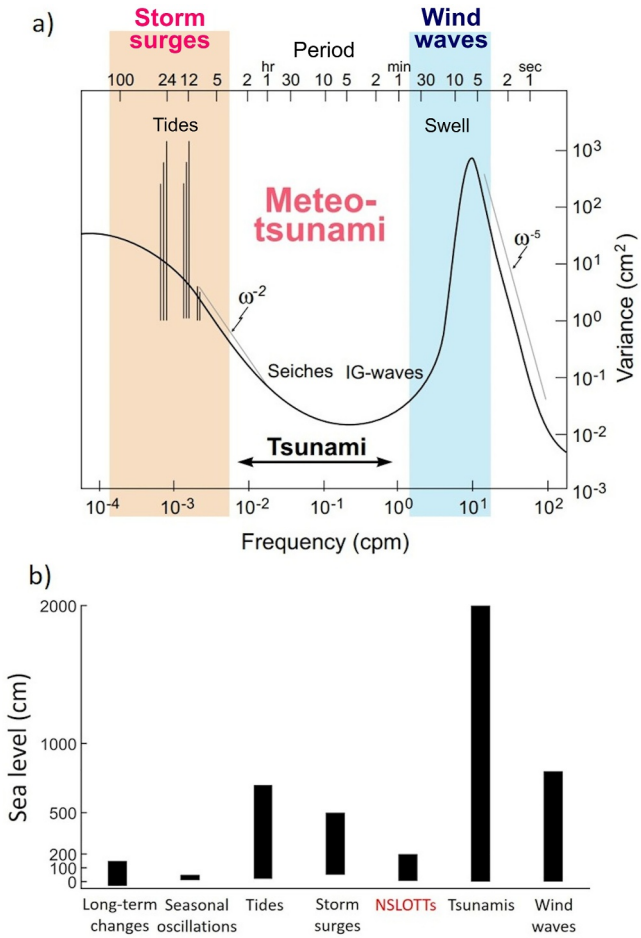

Figure 1. (a) Spectrum of surface gravity waves in the ocean (after Rabinovich, 2020); (b) Comparison of the most common ranges (i.e., not counting specific extreme events/locations) of different components of coastal sea levels oscillations: long-term changes (change of mean sea level over a century), seasonal oscillations, tides, storm surges, nonseismic sea level oscillations at tsunami timescales (including meteotsunamis), other types of tsunamis and wind waves (significant wave height).

as those events during which wave heights surpass a certain high percentile——to be defined by the community——but higher than 99.99 percentile. for example, Ruić et al. (2023) show that high-frequency sea level oscillations measured at 18 Adriatic Sea tide gauge stations, surpass 99.993 percentile 2.5–4.5 times per year per stations. Thus, we conclude that meteotsunamis represent the most extreme of NSLOTTs, lying in the tail of distribution of heights of NSLOTTs.

Meteotsunamis, jointly with tsunamis, seiches and infragravity waves, occupy a frequency range devoid of regular oceanic sea level energy (Figure 1a). This is a range for which a renowned oceanographer W. H. Munk observed: "*The most conspicuous thing about long waves in the open ocean is their absence*" (Munk, 1962; Rabinovich, 2020). However, like other tsunami types (Monecke et al., 2008; Satake & Atwater, 2007), meteotsunamis can be highly destructive, even though catastrophic meteotsunamis occur only once every several decades or centuries at any particular location (Jansà & Ramis, 2021). While the wave amplitude and inundation levels, even of the strongest meteotsunamis, are, in general, significantly lower than those of the moderate to strong seismic tsunamis, meteotsunamis still pose significant threats to numerous coastal communities.

Despite the progress in meteotsunami research, integrating minute-scale sea level hazards into global sea level studies remains incomplete, primarily due to low coverage and quality of available minute sea level measurements. Further, current numerical models struggle to replicate atmospheric and oceanic processes at kilometer and sub-kilometer scales (Lam et al., 2023). By contrast, reproduction of sea level phenomena like storm surges (Bernier et al., 2024; Muis et al., 2020; Pringle et al., 2021) and hurricanes (Bloemendaal et al., 2020; Needham et al., 2015) are well-established. NSLOTTs (including meteotsunamis), however, can contribute to sea level extremes by more than 40% in some basins, such as the Mediterranean and the Caribbean (Vilibić & Šepić, 2017). Excluding NSLOTTs from coastal hazard assessments can result with underestimation of future sea level threats, as their impact is, at endangered regions, comparable to projected sea level increases due to climate change., thus underscoring the need to include NSLOTTs in coastal risk assessments.

This review will discuss two additional topics, not previously covered in meteotsunami review papers: (a) planetary-scale meteotsunami waves caused by violent volcanic explosions, such as the Hunga Tonga-Hunga Ha'apai eruption in January 2022 (Matoza et al., 2022); (b) effects of meteotsunamis on the ionosphere, which is realized through the propagation of acoustic-gravity atmospheric waves generated by meteotsunamis.

The structure of this review is as follows. Section 2 introduces the similarities and differences between meteotsunamis and other types of tsunamis. Section 3 presents the observing systems and preferred standards for measuring meteotsunamis and tsunamigenic atmospheric processes. Section 4 explores the physics underlying the transfer of energy from the atmosphere to the sea, focusing on resonance mechanisms such as Proudman and Greenspan resonances. It also discusses how coastal topography and harbor resonance amplify these waves near the coastline. Section 5 includes a global survey of meteotsunamis, their contributions to sea level extremes during extreme coastal hazard events, and a review of regional and local meteotsunami catalogs and climatologies based on observations and instrumental data. Section 6 reviews the atmospheric processes responsible for generation of tsunamigenic atmospheric disturbances. Section 7 examines the connection between meteotsunamis, NSLOTTs and broader synoptic patterns in some basins. It presents research linking specific synoptic patterns to meteotsunamis, which may aid forecasting efforts. Section 8 discusses present day meteotsunami forecasting and early warning systems capabilities. It also assesses their associated coastal risks, and explores potential impacts of future climate change on meteotsunami hazards. Section 9 introduces meteotsunamis caused by globally

propagating air pressure disturbances triggered by explosive volcanic eruptions. Section 10 discusses the effects of meteotsunami waves on the ionosphere, including the generation and amplified propagation of acoustic-gravity waves detectable by modern global navigation satellite systems. The review concludes with a tentative (but not exhaustive) list of research gaps in meteotsunami science in Section 11. These gaps may provide valuable guidance for future research aimed at quantifying various aspects and consequences of this rare yet powerful phenomenon.

2. Tsunamis Versus Meteotsunamis

The distinctions between meteotsunamis and other tsunami types (e.g., seismic, landslide, volcanic, asteroid impact) are well-documented (Monserrat et al., 2006). The primary difference lies in the generating force of the ocean waves. Seismic tsunamis are caused by impulsive events, that is, by the sudden uplifting or downlifting of a large oceanic mass during earthquakes (lasting seconds to minutes). These events release free long ocean gravity waves in directions which are influenced by fault characteristics and bathymetry (Allan et al., 2012; Cheung et al., 2013). The similar holds for tsunamis generated by asteroid impact and sudden (short lasting) submarine volcanic eruptions. On the other hand, tsunamis generated by submarine and subaerial landslides, might also have a component of continuous forcing of sea level due to a large volume sliding down the slope (Benjamin, 2015; Fine et al., 2003). Meteotsunamis are generated by continuous forcing, that is, by propagating atmospheric disturbances, with forcing that lasts from tens of minutes to hours. Meteotsunami amplification depends on the intensity, size, and shape of the atmospheric disturbance, as well as the ocean bathymetry. When the speeds of the atmospheric disturbance and long ocean waves align, Proudman resonance amplifies the long ocean waves (discussed further in Section 4.1). If conditions are suboptimal, that is, if speeds do not match, meteotsunami waves form as wave packages comprising both forced and free waves, with free waves radiating due to velocity differences (Grue et al., 2022; Tonegawa & Fukao, 2022; Wijeratne & Pattiaratchi, 2024).

Upon reaching coastlines or encountering topographical obstacles, meteotsunamis and other tsunami types behave identically. They refract around islands, reflect off shores, concentrate energy at steep shelf breaks, focus energy over submarine canyons and ridges, and amplify due to coastal shoaling and harbor resonance (Kowalik et al., 2008; Okal, 2021b; Orlić et al., 2010; Pasquet & Vilibić, 2013; Rabinovich et al., 2021; Z. Y. Ren et al., 2023; Šepić, Rabinovich, & Sytov, 2018; Vennell, 2010; Xiong et al., 2017). A summary illustrating the similarities and differences between meteotsunamis and other types of tsunamis is provided in Table 1.

Another difference between meteotsunamis and other types of tsunamis is in the fact that the former represent only the extreme tail—the strongest events—of all NSLOTTs observed at a given location (as discussed in Section 1). In contrast, seismic, landslide, or volcanic tsunamis have no height-surpassing threshold in their definitions—even a centimeter-scale sea level oscillation caused by the respective tsunamigenic force is defined as a tsunami. This definition, however, cannot be applied to meteotsunamis, because background sea level oscillations at tsunami timescales occur quasi-continuously due to persistent atmospheric processes that generate weak long ocean waves. Notably, significant lowering of the threshold for defining meteotsunamis would increase the number of recorded events at a single station to hundreds per year, rendering research impractical. Nevertheless, even sub-threshold NSLOTTs generally share the same generation mechanisms as documented for meteotsunamis (see more in Section 4.3).

The classification of meteotsunamis as a type of tsunami has been a subject of a long-standing debate. Consequently, meteotsunamis have not yet been officially recognized as a tsunami hazard and are not included in global hazard or risk assessments or early warning system implementation plans (e.g., Amato, 2014; Wächter et al., 2012). Despite this, the term "meteotsunami" was introduced nearly a century ago by Nomitsu (1935) and later gained prominence through Defant's (1961) classical textbook and subsequent studies (e.g., Bryant, 2001; Rabinovich & Monserrat, 1996, 1998). From a coastal observer's perspective, all types of tsunamis, including meteotsunami can be regarded as "waves in a harbor," which corresponds to the direct translation of the original Japanese term for tsunami.

The lack of recognition of meteotsunamis within the tsunami research community may arise from the traditional focus of this community on seismic, geological, risk management, and social science disciplines, rather than on atmospheric sciences. As a result, meteotsunamis have often been overlooked or misclassified in historical tsunami catalogs, frequently labeled as "unknown" events or mistakenly attributed to meteorological phenomena such as storm surges (e.g., Lander et al., 1993; Maramai et al., 2014; Soloviev et al., 2000; Tinti et al., 2004). Early

Table 1
Similarities and Differences Between Tsunamis and Meteotsunamis

	Tsunamis	Meteotsunamis
Similarities	Long ocean waves	
	Time scales: from a few minutes to a few hours	
	Spatial scales: from a few hundred of meters to hundreds of kilometers	
	Similar spectral characteristics	
	Destructive effects on the coast, including occurrence of strong currents	
	Resonance effects (for landslide tsunamis only)	
	Coastal amplification	
Differences	Source at or near the sea bottom through seafloor or mass displacement (aside for tsunamis generated by asteroid impact and aerial landslides)	Source at the sea surface through air pressure or wind forcing
	Impulse-type generation (aside for landslide tsunamis) and gravitational restoration as forcing	Continuous generation through resonances acting on the sea surface
	Energy spreading by free waves	Energy spreading by forced and free waves
	Wave height to several tens of meters	Wave heights to several meters
	Destructiveness: potential high loss of human lives, destruction of whole coastal cities and shorelines	Destructiveness: potential loss of a few human lives or injuries, limited destruction and flooding of coastal regions
	Spatial coverage: from local to global	Spatial coverage: from local to regional (except for planetary meteotsunami waves)
	Predictivity: not possible for the source region, quite hard for near-field regions while fairly accurate for far-field regions	Predictivity: less accurate everywhere, due to continuous ocean forcing by the atmosphere which is rapidly changing in four-dimensional time-space

warning tsunami systems predominantly target seismic tsunamis, which are indeed the most devastating (Bernard & Titov, 2015). Nevertheless, the percentage of meteotsunamis recorded in catalogs has increased. e.g., Gusiakov (2021) reports 4.1% meteotsunamis for all tsunami events in the 4000-year long period till the end of the 20th century, while this number increases to 5.8% for events occurring in the 21st century only. Instructively, the increase is a result of better detection of meteotsunamis in the instrumental era (e.g., Gusiakov, 2019, 2021). This figure could be even higher, as existing tsunami catalogs are not optimized to archive meteotsunamis, and the definition of a meteotsunami is still not unified (Gusiakov, 2021).

Recent efforts to integrate meteotsunamis into the tsunami research community have gained momentum, driven by the involvement of atmospheric scientists and global meteorological and oceanographic organizations, such as International Association of Meteorology and Atmospheric Sciences (IAMAS) and Intergovernmental Oceanographic Commission (IOC). These organizations have started working on developing standard procedures for meteotsunami detection and early warning (Angove et al., 2021; Necmioglu et al., 2023; UNESCO/IOC, 2025).

Importantly, meteotsunamis also cannot be classified as storm surges (although they were occasionally mistaken for these, particularly in older storm surge catalogs, e.g., Needham & Keim, 2012). Storm surges represent non-oscillatory forced responses of sea level to atmospheric or other (like hydrological) forcings (Pugh & Woodworth, 2014; Resio & Westerink, 2008; von Storch & Woth, 2008). By contrast, meteotsunamis exhibit wave-like behavior (encompassing both forced and free waves) and share key physical characteristics with tsunamis, such as reflection, refraction, shoaling, and run-up (Monserrat et al., 2006). The generation mechanisms of storm surges and meteotsunamis also differ fundamentally: storm surges are produced by large-scale atmospheric pressure anomalies and wind stress acting on the ocean surface, driving quasi-static ocean adjustments through the inverse barometric effect and frictional forces at the sea surface. Meteotsunamis, in contrast, are dynamically generated through resonant energy transfer from atmospheric disturbances to the ocean, where static responses are multiplied. Temporal and spatial scales of storm surges and meteotsunamis are likewise distinct. Storm surges typically span periods from several hours to a few days and involve quasi-monotonic rises or falls in sea level over hundreds to thousands of kilometers (Pugh & Woodworth, 2014). Meteotsunamis, on the other hand, are characterized by oscillatory sea-level and current patterns, have shorter periods—from a few minutes to a few hours—and wavelengths ranging from a few kilometers to several tens of kilometers.

3. Observing Meteotsunamis

3.1. Sea Level Records Versus Meteotsunami Prerequisites

Reliable records of meteotsunamis are essential for several purposes: (a) understanding the atmospheric and oceanic interactions that drive meteotsunamis, thereby enhancing comprehension of coastal dynamics, (b) assessing hazards and managing risks to mitigate impacts and build resilience, and (c) developing early warning systems to prevent potential human and material losses. Traditional tide gauges primarily recorded continuous sea level variations using daily or weekly charts (UNESCO/IOC, 1985), after which the charts were digitized and hourly data obtained. Some older sea level measurements were based on recording high and low waters only. The sea level data were often further processed with a particular aim. For instance, the Permanent Service for Mean Sea Level (PSMSL, https://psmsl.org, Woodworth & Player, 2003) collects monthly time series in order to track and quantify changes in mean sea level (e.g., Church & White, 2006). Other active data sets, such as those from the University of Hawaii Sea Level Center (UHSCL, https://uhslc.soest.hawaii.edu) and the Global Extreme Sea Level Analysis (GESLA, https://www.gesla.org, Haigh et al., 2023), were created to collect hourly or higher resolution (if available) sea level records, to allow for research on extreme sea levels, such as storm surges (e.g., Marcos et al., 2015). Before the 2004 Sumatra-Andaman tsunami (Fujii & Satake, 2007), measurements of sea levels with minute-scale or higher resolution were unavailable globally—although some tide gauge networks were recording with such resolution (e.g., the Croatian tide gauge network, Vilibić, Domijan, & Čupić, 2005; Vilibić, Orlić, et al., 2005). Similarly, meteotsunami studies have long required high-resolution measurements of atmospheric variables (e.g., air pressure and wind), which were historically standardized at hourly or 10-min intervals by national meteorological agencies—which are resolutions insufficient for quantifying meteotsunami sources. Therefore, the historical meteotsunamis were studied through digitizing both sea level and air pressure/wind records at a minute resolution (e.g., Hibiya & Kajiura, 1982; Orlić, 1980; Šepić, Vilibić, & Belušić, 2009; Šepić et al., 2012), by deploying process-oriented field experiments (e.g., LAST-97 experiment on the Balearic Islands, Monserrat et al., 1998), or by collecting eyewitnesses' reports (e.g., Vučetić et al., 2009).

High-quality sea level records for studying meteotsunamis and other high-frequency ocean and atmospheric phenomena have only emerged in recent decades, supported by advances in instrumentation, computational resources, data transmission, and storage technologies. Modern systems, such as pressure and radar sensors (for sea level measurements), now offer high temporal resolutions, operate reliably under various environmental conditions, and are more cost-effective and easier to maintain. However, accurate meteotsunami measurements depend on several factors. First, given the short periods of meteotsunamis (from a couple to tens of minutes), sea levels should be recorded with at least a minute time step to avoid undersampling and to capture waves in their full height (Vilibić & Šepić, 2017; Vilibić et al., 2016). Second, the data should ideally be of high quality to minimize errors, reduce quality-control efforts, and ensure precision (UNESCO/IOC, 2020; Zemunik et al., 2021a). Finally, spatially dense local networks of stations, like the Balearic VENOM network, are needed to provide adequate spatial coverage and facilitate tracking of meteotsunami propagation and amplification (e.g., Frank-Comas et al., 2021; Ramos-Alcántara et al., 2025). Using multiple instrument types for cross-validation also enhances data robustness and helps identify potential errors.

3.2. Databases and Repositories Available for Meteotsunami Research

Global and regional sea level monitoring networks support meteotsunami detection and research. The IOC Sea Level Station Monitoring Facility (SLSMF, https://www.ioc-sealevelmonitoring.org, VLIZ/IOC, 2025) integrates minute-resolution data from numerous tide gauge networks worldwide. The data are raw and not quality-controlled (as evident from Figure 2), however they are extremely useful for operational purposes, that is, for real time tsunami forecasts and warnings, as these data allow for a fast assessment of propagating tsunamis. Research-quality data products like Minute Sea Level Analysis (MISELA, Zemunik et al., 2021b) can be derived from these raw data sets following extensive quality screening (Zemunik et al., 2021a). The National Oceanic and Atmospheric Administration (NOAA) operates an extensive network of tide and water-level stations across the United States and its territories, providing minute-resolution data (NOAA, 2025). Additionally, the NOAA's Deep-ocean Assessment and Reporting of Tsunamis (DART) system, though primarily designed for tsunami detection, can also provide data relevant to meteotsunamis (Titov & Moore, 2021). The Joint Research Center (JRC; JRC, 2025) has played a key role in European tsunami warning system by integrating regional and global tide gauge data, maintaining historical event databases, and developing modeling tools for hazard maps and risk assessments.

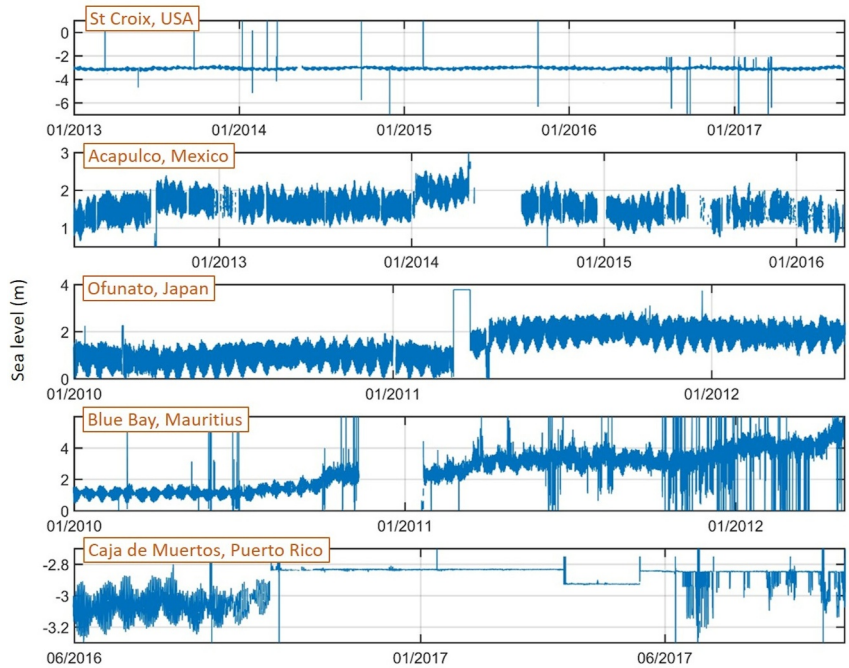

Figure 2. Examples of raw minute sea level series as received by the Intergovernmental Oceanographic Commission Sea Level Station Monitoring Facility, with different problems in recording (data spikes, reference level shifts, instrument drifts, data gaps, other instrument malfunctions).

JRC's Inexpensive Device for Sea Level Measurements (IDSL) network, with sub-minute sampling resolution, has significant potential for studying meteotsunami processes. Along the east Japanese coast, high-resolution S-net bottom array, consisting of 150 seafloor observatories equipped with ocean bottom pressure sensors and seismometers (Mulia & Satake, 2020), is also able to successfully capture meteotsunami waves (Kubota et al., 2021). Another sea bottom cable observatory, the Canadian NEPTUNE network, has the same potential for capturing meteotsunamis (Barnes et al., 2011; Rabinovich et al., 2023). Additionally, numerous national agencies now measure sea level with a minute resolution, and might have quality checked sea level data within their repositories (see, e.g., Pérez Gómez et al., 2022, for description of the Mediterranean and the Black Seas sea level networks).

3.3. Ancillary Observations for Meteotsunami Research

Atmospheric observations are also vital for a comprehensive understanding of meteotsunamis (Anderson et al., 2015; Vilibić et al., 2004). Minute-scale air pressure data from microbarographs are crucial for detecting rapid pressure changes and characterizing the timing, magnitude, spatial variability, and speed of meteotsunamigenic disturbances. While three microbarographs may suffice for basic detection (Monserrat & Thorpe, 1992; Šepić & Vilibić, 2011; Zemunik, Bonanno, et al., 2021), dense regional networks of tens of stations is a must to provide detailed spatial and temporal coverage, aiding accurate reproduction of meteotsunami events (Rabinovich et al., 2021; Villalonga et al., 2024). Similar considerations apply to wind speed and direction measurements, particularly in shallow basins where wind effects may equal or surpass those of air pressure (e.g., Chesapeake Bay, Šepić & Rabinovich, 2014; the Great Lakes, Bechle & Wu, 2014). In addition to traditional in situ measurements of air pressure and wind, modern weather radars, alone or in conjunction with in situ measurements and numerical models, can track atmospheric systems like squall lines and thunderstorms linked to meteotsunamis (Anderson et al., 2015; Kazeminezhad et al., 2021; Sibley et al., 2021; Titov & Moore, 2021; Wertman et al., 2014). Satellite observations, such as cloud-top temperature and speed analysis, can also be used to quantify speeds of meteotsunamigenic systems and their potential to generate meteotsunamis (Belušić & Strelec Mahović, 2009; Vilibić et al., 2010). High-frequency radar measurements of surface ocean currents and waves can further elucidate meteotsunami propagation and amplification in coastal areas (Domps et al., 2022; Dzvonkovskaya et al., 2019; Lipa et al., 2014). Finally, novel monitoring techniques, such as underfloor

muography, which measures density-dependent high-energy muons interacting with fluids, also offer unique possibilities for meteotsunami quantification (Tanaka et al., 2022).

4. Generation of Meteotsunamis

Meteotsunamis are generated through multiple resonant processes upon which their strength depends. These processes include: (a) existence of an intense, high-frequency atmospheric disturbance (an air pressure or wind disturbance) which travels over the ocean and has a period of change ranging from minutes to a few hours, (b) resonant energy transfer between the atmosphere and ocean, which can amplify the initial inverse barometer effect and wind forcing ocean response by an order of magnitude, (c) amplification of meteotsunami waves as they approach shallower continental shelf regions due to shoaling, and (d) further amplification within harbors or bays due to harbor resonance. Similar generation processes generally explain weak NSLOTTs as well, although with each or most of processes having weaker intensity. This section will provide details on the most important aspects of meteotsunami generation.

4.1. Atmosphere-Ocean Resonances

In the study of meteotsunamis, understanding the transfer of energy from atmospheric forcing to the ocean is essential to explain how seemingly moderate atmospheric disturbances can produce large, destructive ocean waves. Resonance mechanisms—specific conditions under which the characteristics of the atmospheric disturbances aligns with those of ocean waves or basin oscillations—are central to this amplification. Through the process of resonant energy transfer, amplitudes of long ocean waves increase significantly, making resonance a key driver in the formation of meteotsunamis.

Atmospheric pressure oscillations that generate meteotsunamis, even in extreme cases, initially trigger only minor changes in sea level, typically a few cm. However, substantial sea level oscillations develop through different types of resonance along the path of the traveling atmospheric disturbance.

4.1.1. The Proudman Resonance

The concept of Proudman resonance, a process that was introduced by British oceanographer Joseph Proudman in his seminal study in 1929 (Proudman, 1929) (and termed Proudman resonance by Orlić, 1980), provides a theoretical foundation for understanding the amplification of barotropic waves in response to moving atmospheric pressure disturbances. Under typical conditions, atmospheric disturbances passing over the ocean induce small sea level changes, primarily governed by the inverse barometric effect. However, Proudman's theory explains that a resonant energy transfer occurs when the speed of the atmospheric disturbance aligns with the speed of long waves in the ocean—a condition quantified by Froude number. The Froude number is given by:

$$Fr = \frac{U}{c}, \tag{1}$$

where U represents the speed of the moving atmospheric pressure disturbance and $c = \sqrt{gh}$ is the speed of long ocean waves (g is the gravity, h is the depth of the ocean).

The height of the generated waves can be approximated using the following expression (Proudman, 1929):

$$\tilde{\zeta} = \frac{\Delta\overline{\zeta} c^2}{c^2 - U^2} = \frac{\Delta\overline{\zeta}}{1 - Fr^2}, \tag{2}$$

where $\Delta\overline{\zeta} = \frac{-\Delta P_a}{\rho g}$ represents the sea level change due to the inverse barometric effect (corresponding to ~1 cm of sea level change per 1 hPa of air pressure change), ΔP_a is the change in atmospheric pressure, and ρ is the density of seawater. Thus, the height of resulting ocean waves is highly dependent on the Froude number. In theory, if Froude number $Fr \approx 1$ (i.e., $U \approx c$), following Equation 2, the waves could become infinitely amplified over flat boundless ocean. Naturally, this does not occur due to nonlinear effects which become important for large wave heights, bottom friction and limited widths of shelf breaks over which Proudman resonance occurs. When $Fr << 1$ (i.e., $U << c$), the atmospheric disturbance moves slower than long waves, and the wave height

approximates the effect of the inverse barometric effect, as seen in deeper water conditions. In contrast, when $Fr >> 1$ (i.e., $U >> c$), the atmospheric disturbance moves faster than long waves, which reduces the time available for energy transfer to the ocean. As a result, no significant waves are generated because the pressure disturbance travels too quickly to generate an intense oceanic response (Monserrat et al., 2006; Pattiaratchi & Wijeratne, 2015; Proudman, 1929), while weak ocean waves are freely radiated from the moving air pressure disturbance.

Numerous studies have demonstrated the occurrence of Proudman resonance in observations and through analytical approximations and numerical modeling. This resonance was suggested as a dominant mechanism in many meteotsunami events worldwide, including regions such as the Adriatic Sea (Orlić, 1980; Šepić, Vilibić, & Belušić, 2009), the Western Mediterranean (Garcies et al., 1996; Ličer et al., 2017), the Great Lakes (Bechle et al., 2015), east Asia (Hibiya & Kajiura, 1982; Kwon et al., 2021), northern Europe (Pellikka et al., 2014; Tappin et al., 2013), and many others. In order to investigate optimal conditions under which Proudman resonance occurs, many studies have utilized modeling experiments to understand the impact of bathymetry, characteristics of atmospheric forcing, interactions with tides, etc. (Bubalo et al., 2018; Y. X. Chen & Niu, 2018; Kakinuma & Kosugi, 2024; Niu & Chen, 2020; Vilibić, 2008; Williams, Horsburgh, et al., 2021).

To quantify the spatial extent of the region where resonant conditions remain near critical, as defined by the Froude number, the fractional Proudman length (Pl) has been introduced (Cheng et al., 2022; Ličer et al., 2017; Pellikka et al., 2022; Šepić, Međugorac, et al., 2016). Pl is defined as:

$$\mathrm{Pl} = \frac{L_{\mathrm{Fr\_crit}}}{L_{\mathrm{tot}}}, \tag{3}$$

where L_{Fr_crit} is the distance over which Froude number (Fr) falls close to 1 (e.g., within range of $0.95 < Fr < 1.05$ or $0.9 < Fr < 1.1$, depending on the study, meaning the disturbance speed closely matches the wave speed dictated by the bathymetry) and L_{tot} is the total distance traveled by the disturbance (Šepić, Međugorac, et al., 2016). Thus, Proudman length represents the percentage of the atmospheric disturbance trajectory over which Proudman resonance conditions are met, indicating the part of the trajectory that promotes strong wave growth. Interestingly, the correlation between Proudman length and strength of a meteotsunami might not be high, for two reasons: (a) there are many other processes in complex bathymetries that shape the meteotsunami height, like reflection, refraction and tunneling of the ocean wave energy over ridges and canyons (Seelam et al., 2016; Šepić, Rabinovich, & Sytov, 2018; Thiebaut & Vennell, 2011; Titov et al., 2005; Vennell, 2010; Yoon, 2002), and (b) the intensity of the meteotsunami waves rapidly weakens when moving from fully resonant conditions ($Fr = 1$), so that large waves resonantly generated in one part of the ocean may dissipate as free waves in other parts where resonance conditions are not fully met (Šepić, Vilibić, & Fine, 2015; Vilibić, 2008). This might be relevant particularly in macro-tidal regions, where the tidal elevation may substantially lower the resonance conditions (up to 25%) during the long-lasting meteotsunami generations and fully resonant conditions cannot be achieved during a single meteotsunami event. However, in such locations, super-resonant conditions may occur during the falling tide and counter-currents, resulting in even larger meteotsunami amplification (up to 6 %) than for the full Proudman resonance conditions ($Fr < 1$, Williams, Horsburgh, et al., 2021).

The transition of forced waves to free waves usually occurs when the speed of atmospheric disturbance and the speed of long ocean waves differs ($U \neq c$). This speed mismatch may occur due to fluctuations of speed and intensity of the atmospheric disturbance over time, and due to changes in bathymetry that result with changes of speed of long ocean waves, thus disrupting resonance conditions. The transition of waves on the step was described by C. J. R. Garrett (1970), while Vennell (2007) explored the transition over the ridge. Specifically, if $c < U$, the forced wave arrives to the coast before the free wave and vice versa (Grue et al., 2022; Orlić et al., 2010). Here, it is also worth mentioning that meteotsunamis waves hitting a sharp shelf break—like the tsunami waves (Heron & Dzvonkovskaya, 2015)—reflect much of their energy back in the form of free waves that can hit shorelines hours after the generation of the offshore generated forced ocean waves through the Proudman resonance (Pasquet & Vilibić, 2013; Šepić, Rabinovich, & Sytov, 2018; Wertman et al., 2014).

4.1.2. The Greenspan Resonance

While Proudman resonance is the most well-known mechanism involved in the amplification of meteotsunami waves, other resonance phenomena, such as Greenspan resonance, also play an important role in certain coastal environments. Greenspan resonance (Greenspan, 1956) describes a specific type of wave amplification phenomenon occurring in the coastal zone. This resonance occurs when the speed of a moving atmospheric pressure disturbance along the coast aligns with the propagation speed of edge waves (Niu, 2020, 2021; Seo & Liu, 2014). Edge waves are a type of gravity waves that are generated through reflection and refraction of energy within the continental shelf and that propagate parallel to the shore, with their amplitude decaying offshore (Munk et al., 1956; Ursell, 1952). The dispersion relation for edge waves is given as:

$$\sigma^2 = gk \sin[(2n+1)\beta], \tag{4}$$

where σ is the wave frequency, k is the alongshore wavenumber, n is the edge wave mode and β is the beach slope angle.

The phase speed of the edge waves can then be expressed as:

$$c = \frac{g}{\sigma}\tan[(2n+1)\beta]. \tag{5}$$

Matching of the speed of one of the edge wave modes with the speed of atmospheric disturbance along the coast facilitates a resonant energy transfer, causing amplifications of the edge wave amplitude.

Several studies demonstrated that the Greenspan resonance was responsible for the meteotsunami waves development, although the community is still in favor of quoting the Proudman resonance, even if the resonance is occurring over complex and sloping topographies over which the Proudman resonance almost cannot exist. This refers, for example, to the Yellow Sea (J. Kim et al., 2022) where the speed of the meteotsunami wave mismatch the estimates by the Proudman theory. In the middle Adriatic, a complex bathymetry off islands have slopes that may serve as a resonator for traveling disturbances, in particular if traveling quasi-parallel with the slope (Šepić, Međugorac, et al., 2016). Some studies acknowledged the interplay of both Proudman and Greenspan resonance, for example, in the Great Lakes, where different parts of lake are prone to different types of resonance (Bechle & Wu, 2014; Bechle et al., 2015), southern Australia (Wijeratne & Pattiaratchi, 2024) of Gulf of Bothnia in the Baltic Sea (Pellikka et al., 2022). Propagation of hurricanes can also result with meteotsunami waves, in particular if speed of hurricane parallel to the coastline matches speed of the edge waves on a shelf (J. Kim & Omira, 2024; Yankovsky, 2008, 2009). The interplay between the Proudman and the Greenspan resonance and their contribution to meteotsunamis is an open research question, in particular in determination of the distance from the coastline where the different resonances start to dominate.

4.2. Coastal and Harbor Resonances

Atmosphere-ocean resonances can amplify waves advancing from the open ocean or alongshore regions. However, even under ideal resonance conditions, the generated waves rarely reach amplitudes high enough to cause hazardous oscillations. The exceptions occur at straight coastlines with very wide shelves (e.g., longer than 100 km) over which resonant processes may result with destructive meteotsunami waves (e.g., the 1992 Daytona Beach meteotsunami, Churchill et al., 1995, the 2017 Dayyer meteotsunami, Heidarzadeh et al., 2020, etc.). The destructive potential of incoming meteotsunami waves can increase substantially if the waves interact with coastal features, such as bays, harbors, or other semi-enclosed basins, where additional amplification mechanisms, like harbor resonance, can occur.

The phenomenon of wave amplification in bays and harbors can be explained through several stages that consider changes in wave height due to specific factors such as decreasing water depth, narrowing bay geometry, and internal reflections and harbor resonance within the bay. Orlić et al. (2010) demonstrated that such amplification occurs in three steps. The increase of wave height due to effects of shoaling and narrowing of the harbor can be expressed by the Green's Law (Lamb, 1932):

$$\overline{\zeta_h'} = F_2\overline{\zeta_m},\ F_2 = \left(\frac{b_m}{b_h}\right)^{1/2}\left(\frac{h_m}{h_h}\right)^{1/4}, \tag{6}$$

where b is the width and h is the depth of the basin, and subscripts m and h denote the mouth and head of the basin, respectively. This equation shows that wave heights increase as the basin narrows ($b_m > b_h$) and becomes shallower ($h_m > h_h$).

Further, waves are reflected at the head of the basin, leading to the amplification approximated by Lamb (1932):

$$\overline{\zeta_h''} = F_3\overline{\zeta_h'}, \tag{7}$$

where $F_3 = 2$ is the factor of wave height increase due to its reflection.

Finally, the waves that are reflected at the head return to the bay mouth, where they can be superimposed to the incoming long ocean waves. If the period of the incoming waves aligns with the period of the eigen modes of a bay, harbor resonance takes place. The last stage of wave amplification is given by Orlić et al. (2010):

$$\overline{\zeta_h'''} = F_4\overline{\zeta_h''},\ F_4 = \frac{1 - \exp\left[\frac{-2(1-R)}{T_0}t_e\right]}{1-R}, \tag{8}$$

where T_0 is the period of the fundamental eigen mode, t_e is the time since the bay began oscillating and R is the reflection coefficient at the bay mouth. Here, $R = 0$ represents full energy dissipation, while $R = 1$ means no energy loss.

The amplification of long waves entering a harbor from the open sea due to harbor resonance can also be approximated by:

$$H^2(f) = \frac{1}{\left[1 - \left(f/f_0\right)^2\right]^2 + Q^{-2}\left(f/f_0\right)^2}, \tag{9}$$

where f represents the frequency of the incoming long wave, f_0 is the natural (resonant) frequency of the harbor, and Q is the quality factor, which quantifies the energy damping within the system (Monserrat et al., 2006) (similar to R in Equation 8). When the two frequencies match ($f = f_0$), the amplification achieves value $H^2(f) = Q^2$. At frequencies much lower than the resonant frequency ($f \to 0$), the amplification factor approaches unity, indicating minimal amplification. Conversely, at frequencies much higher than resonant frequency ($f \to \infty$), the amplification factor tends to zero, showing negligible influence of the waves on the harbor oscillations.

Narrow, elongated inlets such as fjords or harbors with constricted entrance are prone to resonant oscillations due to high Q-factor. This phenomenon is described by Miles and Munk (1961) and known as the "harbor paradox." The paradox explains how narrowing a harbor entrance, which is intended to protect it from external disturbances like wind waves and swell, can instead intensify internal oscillations due to resonance. Nevertheless, despite a high Q-factor which is essential for harbor oscillations, exceptionally strong oscillations can only occur when the two frequencies (f and f_0) align, that is when "internal resonance" between the incoming ocean waves and the harbor eigen modes occurs (Rabinovich, 1993). The characteristics of the excited harbor oscillations depends on the shape of the basin. Wilson (1972) provided a comprehensive summary of eigen modes for basins with different geometric shapes, which often serve as approximations for the typically irregular configurations of natural features such as lakes, bays, inlets, and harbors (Figure 3).

Indeed, there are many harbors, bays and inlets which possess a high amplification factor and—when an open ocean wave advances toward them—amplification at their ends may increase the initial height of the disturbance for several times. For example, modeling study of the 15 June 2006 meteotsunami in Ciutadella (Spain) indicate a quadrupling of wave height due to shoaling in front of the inlet and further tripling of wave height due to processes inside the harbor, in total increasing the ocean waves generated by the Proudman resonance for an order of

Basin type		Profile equation	Periods of free oscillation				
Description	Dimensions		Fundamental T_0	Mode ratios T_S/T_I $[n = (s+1)/2]$			
				$n=0$	1	2	3
Rectangular	Rectangular	$h(x) = h_1$	$2.000\,[2L/(gh_1)^{1/2}]$	1.000	0.333	0.200	0.143
Rectangular	Triangular	$h(x) = h_1 x/L$	$2.618\,[2L/(gh_1)^{1/2}]$	1.000	0.435	0.278	0.203
Rectangular	Semiparabolic	$h(x) = h_1(1 - x^2/L^2)$	$2.220\,[2L/(gh_1)^{1/2}]$	1.000	0.409	0.259	0.189
Triangular	Rectangular	$b(x) = b_1 x/L$ $h(x) = h_1$	$1.308\,[2L/(gh_1)^{1/2}]$	1.000	0.435	0.278	0.230
Triangular	Triangular	$b(x) = b_1 x/L$ $h(x) = h_1 x/L$	$1.653\,[2L/(gh_1)^{1/2}]$	1.000	0.541	0.374	0.283
Semielliptic	Semiparaboloidal	$b_1/L = 2$ $= 4/3$ $= 1$ $= 2/3$	$2.220\,[2L/(gh_1)^{1/2}]$	1.000	0.707 0.554 0.447 0.317	0.578 0.493 0.468 0.455	0.378 0.323 0.264 0.185
Semicircular	Semiparaboloidal	$h(x) = h_1(1 - r^2/L^2)$	$2.220\,[2L/(gh_1)^{1/2}]$	1.000	0.707	0.578	0.500

Figure 3. Modes of free oscillations in semi-closed basins of simple geometric shape (after Rabinovich, 2009, modified from Wilson, 1972).

magnitude (Vilibić et al., 2008). Similar ratios for the shoaling and harbor resonance have been estimated for the Nagasaki meteotsunami of 31 March 1979 (Hibiya & Kajiura, 1982; Monserrat et al., 2006). Although the highest wave amplitudes are reached for offshore meteotsunami waves advancing quasi-perpendicularly to a bay or harbor, edge waves advancing along the coastline may also excite strong eigen oscillations in bays when there is a matching of frequencies between the advancing edge wave and the harbor eigen periods (Sun & Niu, 2021). At end, it is worth mentioning that the same principle as for harbor resonance are valid on larger scales, for example, for tidal resonance, in which period of tides are close to the period of eigen oscillations of a basin. The examples are, among others, the Bay of Fundy (C. Garrett, 1972), the Ungava Bay (Arbic et al., 2007), the Adriatic Sea (Medvedev et al., 2020), the Gulf of Gabes (Sammari et al., 2006), in which either diurnal or semidiurnal components are amplified for an order of magnitude, like meteotsunamis in harbors with high amplification factors.

4.3. Impact of Changing Atmospheric Disturbances and Bathymetry on Meteotsunamis

Once generated in the open ocean through the Proudman resonance, meteotsunami waves do not necessarily reach high or destructive amplitudes upon arriving at the coastline. This might occur due to the following reasons: (a) changing resonant conditions over long shelves, which are highly sensitive to small variations in ocean depth. In

such cases, resonant conditions may not be sustained over an offshore segment, causing the waves to dissipate as free waves; (b) changes in intensity and speed of the atmospheric disturbance. A lack of continuous forcing can significantly weaken meteotsunami waves generated at more distant locations (e.g., hundreds of kilometers away); (c) sharp bathymetric features near the coastline, which can reflect, refract, or dissipate incoming waves, or alternatively, channel their energy toward specific coastal segments.

To evaluate spatial forcing over the shelf surrounding the Balearic Islands, Ličer et al. (2017) conducted sensitivity studies and concluded that the Proudman resonance over the shelf between Menorca and Mallorca (approximately 40 km long), located offshore of the meteotsunami hotspot Ciutadella, acts as a key build-up basin for destructive meteotsunamis there. In contrast, the longer (ca. 80 km) but more distant Mallorcan shelf regions do not substantially contribute to the intensity of meteotsunamis at Ciutadella. Šepić, Vilibić, and Fine (2015) performed sensitivity studies for the northern Adriatic meteotsunamis by varying the speed and propagation direction of the atmospheric disturbance. They found that the largest contributions to meteotsunami height come from amplifications within the last 30 km of the shelf near a hotspot. Conversely, "early" generation of intense meteotsunami waves farther offshore (e.g., along the western Adriatic shelf, 60–70 km from the hotspot) results in wave heights more than twice as small compared to those produced under local resonant conditions.

Furthermore, a linear change in the amplitude of a traveling air-pressure disturbance (from zero to a constant value) produces a quadratic change in meteotsunami wave amplitude over a flat sea, yielding wave heights up to two times smaller at a coastline than those generated by disturbances of the constant intensity over the same area (Williams, Horsburgh, et al., 2021). Therefore, weaker meteotsunamis may occur in association with rapidly intensifying meteotsunamigenic systems, such as mesoscale convective cells, which evolve over just a few tens of kilometers while advancing toward the coast, compared to the fully developed convective systems that travel over the same ocean path.

Finally, as with tsunamis (Iglesias et al., 2014), the energy of meteotsunami waves can be redistributed and funneled by underwater channels or ridges toward particular coastal segments. This was demonstrated through numerical modeling for the 2014 Odessa meteotsunami. Šepić, Rabinovich, and Sytov (2018) showed that the meteotsunami wave could have been generated approximately 200 km offshore, first reflected from the shelf break toward the coast and then channeled toward specific sections of the coast by an underwater ridge.

In conclusion, all of these effects jointly modulate the intensity of meteotsunamis along coastlines. However, their compound impacts in the real ocean are still not fully understood (see Section 11.3.3).

5. Mapping of Meteotsunamis and High-Frequency Sea Levels

5.1. Meteotsunamis: Local Phenomenon Occurring Worldwide

At their strongest, meteotsunamis are extreme and dangerous waves that cause destruction (Monserrat et al., 2006; Pattiaratchi & Wijeratne, 2015; Rabinovich, 2020; Vilibić et al., 2016), either by themselves or by contributing to an ongoing storm surge and to storm surge-related infragravity waves, swells and wind waves (e.g., Medvedev et al., 2022). The strongest meteotsunamis lead to high run-ups and inundation, as well as to destructive currents (e.g., Jansá et al., 2007; Linares et al., 2019; Sallenger et al., 1995; Vilibić et al., 2004; Vučetić et al., 2009; Yoo et al., 2010).

The first records describing probable meteotsunamis come from a legend related to the Muslim conquest of Sicily in the 9th century (Šepić, Vilibić, et al., 2018), an event in Ciutadella from the 15th century (Balearic Islands) related to sinking of two ships and a drowning of a man due to strong currents (Jansà & Ramis, 2021—citing the Juries of the Island of Menorca, 1465), and a religious festivity legend from the early 17th century in connection with the flooding of Vrboska village (island of Hvar, Adriatic Sea) (Šepić & Orlić, 2025b). These earliest records are followed by the 18th and 19th century newspaper reports of sudden and dangerous long ocean waves which were later (mostly in the 21st century) identified as likely meteotsunamis. Haslett and Bryant (2009), Thompson et al. (2020), and Lewis et al. (2023) list probable and confirmed 18th–21st century UK meteotsunamis, beginning with the event of November 1, 1755, followed by a further 9 events in the 18th century and 26 in the 19th century. Further east, Brüggermann (1779) reports on the Baltic Sea event on the Rega in 1757, which according to a description was also a possible meteotsunami. Given the abundance of meteotsunamis recorded along the coasts of Japan, Korea and China, it is safe to assume that historical reports of sudden long ocean waves exist for these locations as well—but we are not currently aware of these reports. The extreme meteotsunamis of the 20th and

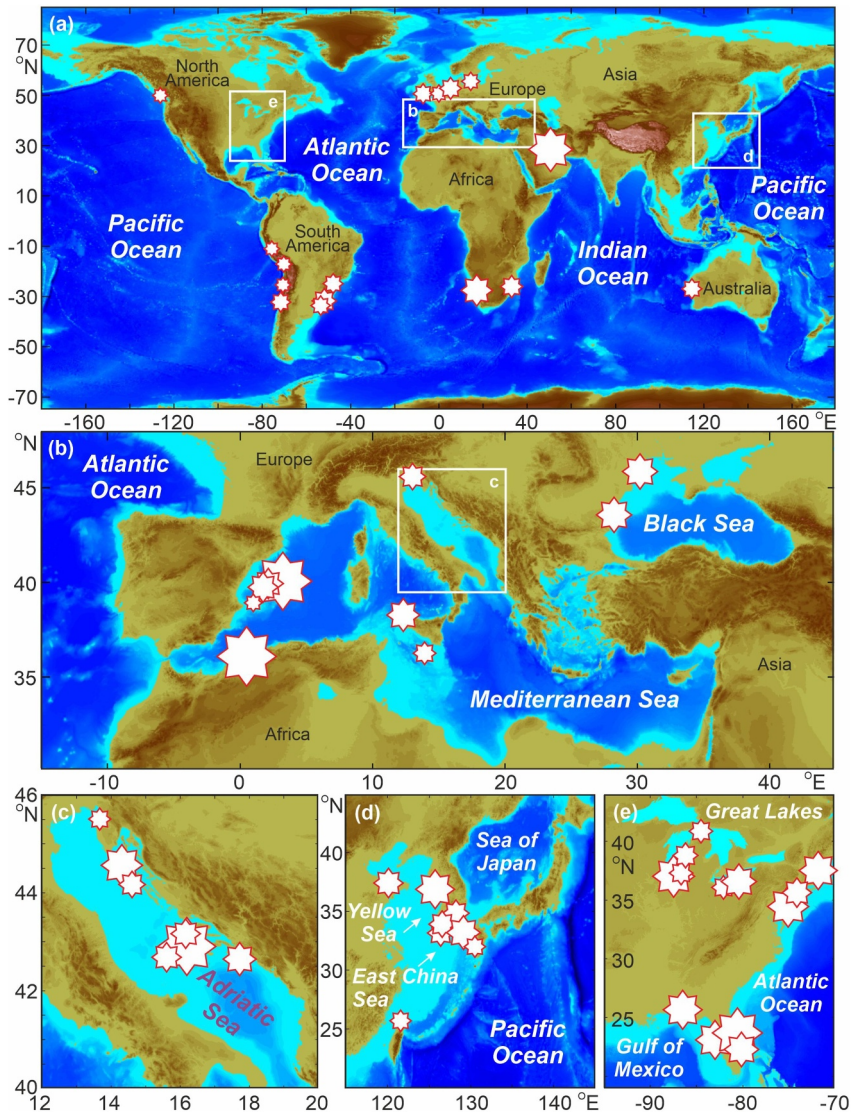

Figure 4. The world map with proven occurrences of meteotsunamis (modified from Rabinovich, 2020). Size of the star is proportional to the intensity of the event.

21st centuries have been increasingly well documented thanks to significant advances in measurement techniques and networks, as well as much better dissemination of information.

Although meteotsunamis occur on all coasts of the world (Figure 4), their strength is highly spatially-dependant with some regions clearly standing out. These regions are: the Great Lakes (e.g., Bechle et al., 2016; Donn & Ewing, 1956; W. M. Ewing et al., 1954), the east coast of the USA and Canada (Bailey et al., 2014; Churchill et al., 1995; Mercer et al., 2002; Sallenger et al., 1995; Wertman et al., 2014; Whitmore & Knight, 2014; Šepić & Rabinovich, 2014), the Gulf of Mexico (Alfonso-Sosa, 2016; Olabarrieta et al., 2017; Paxton, 2016; Paxton & Sobien, 1998), the Brazilian coast (Rabinovich, 2020), the Argentinian coast (Dragani et al., 2002), the United Kingdom (Haslett & Bryant, 2009; Lewis et al., 2023; Thompson et al., 2020), the Mediterranean Sea with the Balearic Islands (Jansà, 1986; Jansà & Ramis, 2021; Jansà et al., 2007) and the Adriatic Sea (Orlić, 2015; Šepić & Orlić, 2025a; Vilibić & Šepić, 2009) as well as two close but distinct hotspots, the Yellow Sea and the East China Sea (Cho et al., 2013; B.-J. Choi et al., 2014; Hibiya & Kajiura, 1982; M.-S. Kim et al., 2017, 2021; Tanaka, 2010; X. Wang et al., 1987; Yoo et al., 2010). The estimated and measured heights (where available) of the strongest and most destructive meteotsunamis in each of the region are listed in Table 2. Depending on the atmospheric forcing and the bathymetry off a meteotsunami hotspot, meteotsunamis can manifest as a single wave (mostly occurring

Reviews of Geophysics

10.1029/2024RG000867

Table 2
List of Selected Major Meteotsunami Hot-Spots With the Most Destructive Meteotsunami Events, Including the Occurrence Date and Maximum Wave Height (Witnessed—In Black, or Measured—In Red) and Their Impact

Region	Location	Date of the event	Observed max. wave height (m)	References	Impact
Mediterranean Sea	Vela Luka	21 June 1978	6–8	Orlić (1980), Vučetić and Barčot (2008), Vučetić et al. (2009), Orlić et al. (2010)	One hundred eighty-eight inundated households, damaged furniture, electrical appliances, installations, and food supplies; destroyed shops, markets, cars parked along the seaside, and boats which were moored in the harbor; 7 million US$ damage (at that time)
	Ciutadella	15 June 2006	4–5	Jansà et al. (2007), Vilibić et al. (2008)	More than 40 boats sunk or damaged; economic loss of a few tens of millions of euros (at that time)
	Mostaganem	3 August 2007	7–10	Okal (2021a)	Severe damage along the coast; 12 people killed; The atmospheric source of the event is indicated by seismic observations
Black Sea	Odessa	27 June 2014	2	Šepić, Rabinovich, and Sytov (2018)	Twelve people injured, of which two adults and four children taken to a hospital
East China Sea	Nagasaki	31 March 1979	4	Hibiya and Kajiura (1982)	Significant damage; three people killed
Yellow Sea	Boryeong	4 May 2008	1.3	Yoo et al. (2010)	Thirty-six people washed into the sea; 9 killed and 15 suffered serious injuries
Pacific Ocean	Southern Japan	4 September 2009	2.6	Heidarzadeh and Rabinovich (2021)	Damage of coastal infrastructure; Strong coastal currents; deaths due to Typhoon Jebi impact
The Great Lakes	Chicago	26 June 1954	3	W. M. Ewing et al. (1954), Bechle and Wu (2014)	Damages and flooding of coastal structures; eight people killed
	Southern shores of Michigan	4 July 2003	0.3	Bechle and Wu (2014)	Damage on coastal structures; strong rip currents; seven people killed
US East Coast	Daytona Beach	3 July 1992	3	Sallanger et al. (1995), Churchill et al. (1995)	Seventy-five minor injuries; damage to several tens of vehicles
	MA and NJ coasts	13 June 2013	2	Wertman et al. (2014), Bailey et al. (2014)	Several divers dragged by the waves; several people knocked into the water
West Australia	Fremantle	17 August 2014	0.5	Pattiaratchi and Wijeratne (2015)	Strong currents ripped car carrier and cargo ships from the wharf, colliding and badly damaging railway bridge on a major route that was then closed for 2 weeks
Southeast Africa	Dwarskersbos	27 August 1969	2.9	Okal et al. (2014)	Damage to some waterfront houses; several light boats and poultries were lost
Persian Gulf	Dayyer	19 March 2017	2.4	Salaree et al. (2018), Heidarzaleh et al. (2020), Kazeminezhad et al. (2021)	Damage to ca. 300 fishing and recreational boats and 85 coastal households; five people killed and 22 injured
Brazil	Pântano do Sul	19 November 2009	3	Candella and de Araujo (2021)	Considerable damage of cars, fishing boats, restaurants, and various beach infrastructure; one fisherman slightly injured

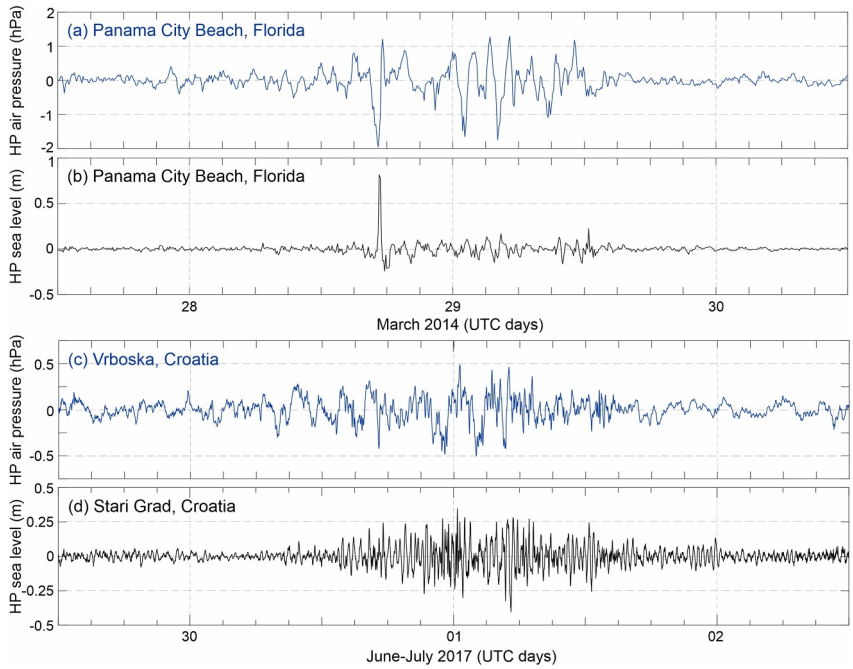

Figure 5. High-pass air pressure and sea level series measured during meteotsunamis that manifested as follows: (a, b) a single wave meteotsunami—Panama City (Florida) event of 28 March 2014; (c, d) a train of meteotsunami waves—Stari Grad (Croatia) event of 30 June 2017. The Stari Grad and Vrboska stations are within 8 km of each other. The Panama City series were measured with a 6-min time step, and the Croatia series with a 1-min time step. All series were high-pass filtered with a 3-hr Kaiser-Bessel window.

at an open coast), a train of waves (mostly occurring in a harbor or a bay) and can be superimposed on other processes driving extreme sea levels, like storm surges. Examples of such events are provided in Figures 5 and 6.

In other regions, meteotsunamis can make an important contribution to the overall sea level variability (e.g., Vilibić & Šepić, 2017, for global records; de Jong & Battjes, 2004; de Jong et al., 2003, 2021, for Rotterdam, Netherlands; Pattiaratchi & Wijeratne, 2014, 2015 for Australia), but appear to reach smaller, mostly non-damaging wave heights (although related currents can still be exceptionally strong and cause damage, e.g., Pattiaratchi & Wijeratne, 2015). The Baltic Sea, for one, attracts our attention, as historical reports indicate occurrence of destructive meteotsunamis, whereas no recent destructive events have been reported (Pellikka et al., 2014, 2022). For example, Brüggeman (1779) (cited here through Piotrowski et al., 2017), when writing about the 1757 Rega River flooding reports "… *in calm and bright weather, the Baltic coast near Trzebiatów on Rega River suddenly was rolling so much that a ship, moored in the harbor, was snatched away by high waves and shifted far onto the land. After that (rolling) was repeated three times, the sea became calm again. Local people call this phenomenon the Seebär*…".

In addition, there are also areas for which we are only aware of the very strong and destructive events, for example, the Dayyer event (Iran) in 2017, in which 5 people were killed and 22 more injured (Heidarzadeh et al., 2020; Kazeminezhad et al., 2021; Salaree et al., 2018), the Mostaganam event (Algeria) of 2007, where long ocean waves, suspected to be a meteotsunami, killed 12 people (Okal, 2021a), and the Dwarskersbos event (South Africa) of 1969, when the coastal run-up reached 2.9 m (Okal et al., 2014). More details on some of these events are provided in Sections 8.1.1 and 8.1.2. It is possible that these were unique events, but it is also possible that other events have occurred in these regions but are unknown to us due to lack of measurements and a lower availability of information from these countries.

In general, stronger meteotsunamis (higher waves/stronger currents) occur:

1. in the mid-latitudes,
2. along coastal stretches in front of which there is a shelf of considerable width/length, and
3. in bays and harbors with high amplification factors (Rabinovich, 2009).

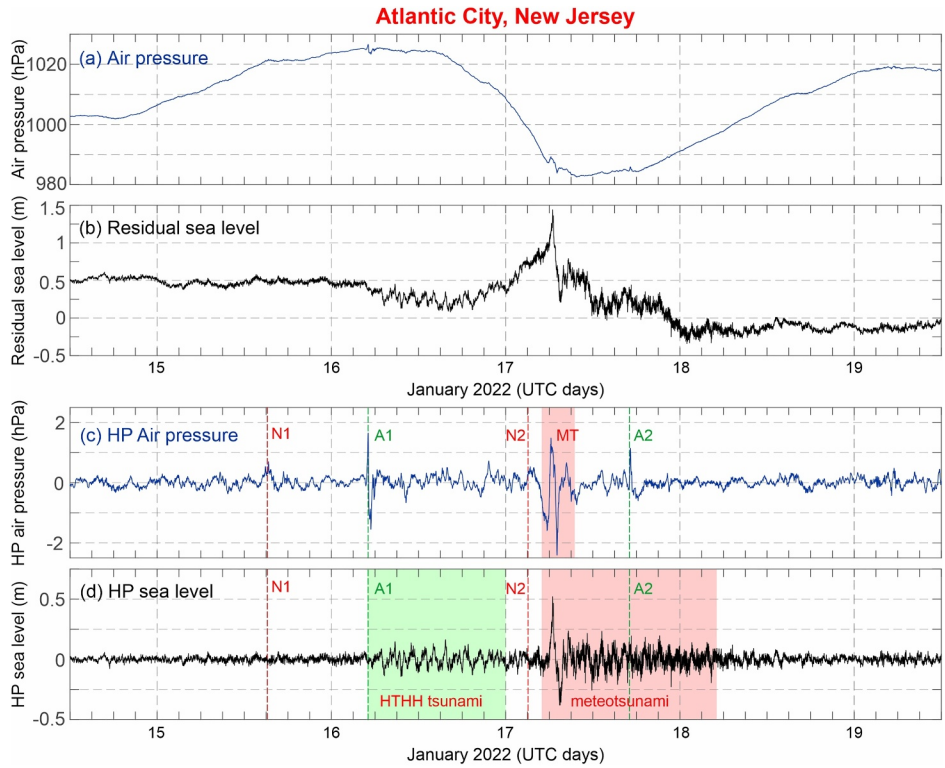

Figure 6. Atlantic City time series representing a triple jeopardy event consisting of a storm surge, a meteotsunami, and the Hunga Tonga-Hunga Ha'apai (HTHH) planetary tsunami waves (see more in Section 9): (a) original air pressure; (b) residual sea level; (c) high-pass (HP) air pressure; (d) high-pass sea level. Times corresponding to the HTHH waves arriving from the "pole" (N1, N2) and "antipole" (A1, A2) are indicated in (c), and (d). A meteotsunamigenic disturbance (MT) is marked in (c). HTHH tsunami and local meteotsunami are marked in (d). All series were measured with a 1-min time step. The series shown in (c) and (d) were high-pass filtered with a 3-hr Kaiser-Bessel window. A wider analysis of the event can be found in Rabinovich et al. (2025).

And weaker meteotsunamis occur:

1. in the low latitudes,
2. along coastal stretches in front of which there is no or only a very narrow shelf, and
3. in bays and harbors with low amplification factors, and along the open coast.

The higher frequency of strong meteotsunamis in the mid-latitudes is related to the higher frequency of tsunamigenic atmospheric disturbances in these latitudes compared to the lower latitudes. The greater frequency relates to both good weather meteotsunamis associated with atmospheric gravity waves (AGWs) and remote convective processes, and to bad weather meteotsunamis associated with thunderstorms, squall lines, cold fronts, extratropical and tropical cyclones, with the latter two not occurring at the lowest latitudes due to absent or weak Coriolis force (Stull, 2017). In their global studies of NSLOTTs, Vilibić and Šepić (2017) and Zemunik, Denamiel, Williams, and Vilibić (2022) show that variance of high-frequency sea level oscillations is correlated with the mean speed of wind at 500 hPa level, with the strongest mid and upper tropospheric winds blowing over the mid-latitudes. Nevertheless, one should bear in mind that low-income countries with less developed measurement networks are located in the low latitudes—and part of the absence of events could be due to a sparser measurement network (Vilibić & Šepić, 2017; Zemunik, Denamiel, Šepić, & Vilibić, 2022) and less availability of information.

The presence of wide shelves facilitates the generation of strong meteotsunamis through resonant processes (e.g., Proudman resonance; more details on generation of meteotsunamis are given in Section 4). The advantage of a wide shelf, when it comes to meteotsunami generation, can be easily deduced from the comparison between the east and west coasts of North America. Although meteotsunamis have been observed on both coasts (e.g., on the east coast: Bailey et al., 2014; Churchill et al., 1995; Mercer et al., 2002; Sallenger et al., 1995; Šepić &

Rabinovich, 2014; Wertman et al., 2014; Whitmore & Knight, 2014; and on the west coast: Rabinovich et al., 2021, 2023; Thomson et al., 2007), significantly stronger events have been observed on the east coast in front of which there is a wide shelf than on the west coast in front of which there is a much narrower shelf. In other regions where meteotsunamis are a common phenomenon, the most vulnerable coastal sections are also next to shelves of considerable width (Figure 4).

Atmospheric disturbances (see examples in Figures 5 and 6) generate long ocean waves as they propagate over the shelves (see Section 4). If the speed of an atmospheric disturbance coincides with the speed of long ocean waves, a forced long ocean wave with continuously increasing height is generated. This ocean wave propagates together with an atmospheric disturbance, which is in turn mainly advected by the mid and upper troposphere winds (Šepić, Vilibić, Rabinovich, & Monserrat, 2015). It could therefore be assumed that meteotsunamis will be most frequent and strongest on the coasts toward which the winds of the middle and upper troposphere are blowing. In mid-latitudes, the jet stream is mostly westerly (although with variations from southwesterly to northwesterly, end even southerly to northerly), suggesting that strong meteotsunamis should propagate from these directions toward the "opposite" coasts. This assumption is confirmed for numerous regions. For example, in the Mediterranean Sea, most destructive meteotsunamis are observed on the southward to westward looking coasts when strong mid-tropospheric southwesterly winds are blowing (Pupić Vurilj et al., 2023; Vilibić et al., 2021). In the Sea of Japan and the East China Sea, the strongest events are also recorded on the coasts of Japan (Hibiya & Kajiura, 1982; Tanaka, 2010) and Korea (M.-S. Kim et al., 2017, 2021) toward which jet streams (strong mid- and upper tropospheric winds) are directed. However, there are exceptions to the rule. Destructive meteotsunamis have been observed along the east coast of the USA (Rabinovich, 2020), although upper tropospheric winds direct atmospheric disturbances offshore. It was shown however that the US East Coast meteotsunamis usually propagate together with atmospheric disturbance offshore—but then, upon reaching the shelf break, ocean waves reflect westward from the shelf edge toward the east coast of the USA (Bailey et al., 2014; Pasquet & Vilibić, 2013), while the atmospheric disturbances continue propagating eastward.

Finally, the earliest studied meteotsunamis were exceptionally strong manifestations of seiches, occurring at the so-called "meteotsunami hotspots", that is, harbors and bays with high amplification factor (W. M. Ewing et al., 1954; Hibiya & Kajiura, 1982; Jansà, 1986; Orlić, 1980; Rabinovich, 2009). The advantage of such micro-locations for generation of strong meteotsunamis can best be inferred from climatological studies on meteotsunamis conducted by analyzing decadal 6-min (for US), 15 min (for UK) or 1-min sea level time series. Such studies are provided by Bechle et al. (2016) for the US Great Lakes coast, Dusek et al. (2019) for the US East Coast, Williams, Schultz, et al. (2021) for Northwest Europe, Pellikka et al. (2020, 2022) for the Baltic Sea, Lewis et al. (2023) for the United Kingdom and Ruić et al. (2023) for the Adriatic Sea. These studies all show a very strong dependence of the median and maximum meteotsunami heights on the exact location of the tide gauge station, with Ruić et al. (2023) concluding that the strongest high-frequency sea level oscillations occur at tide gauges located in narrow bays or channels, while the weakest occur along the open coast or at the entrance to wide bays. Incoming long ocean waves can trigger seiches of bays and channels, with a possible strong amplification occurring when frequency of incoming long ocean waves matches frequency of seiches (Raichlen, 1966; see also Section 4.2 of this paper for more details).

Nonetheless, exceptional events have also been reported at the open coasts. Rabinovich (2020), in his review of meteorological tsunamis which have occurred since the 1992 Daytona event, lists 49 strongest events, of which a little more than one third (i.e., 18 events) have occurred along an open coast/beach (e.g., Alfonso-Sosa, 2016; Anderson et al., 2015; Churchill et al., 1995; Olabarrieta et al., 2017; Paxton, 2016; Paxton & Sobien, 1998; Šepić, Rabinovich, & Sytov, 2018; Whitmore & Knight, 2014). In contrast to harbor/bay meteotsunamis, which usually have the shape of a seiche, open coast meteotsunamis usually have the shape of a large solitary wave (see examples of both types in Figure 5), which often hits the coast unexpectedly (Rabinovich, 2020). Generation of such a solitary wave (soliton) has been explained by the specific interplay of meteotsunami forcing (i.e., resonant processes over the shelf) and nearshore bathymetry (Sheremet et al., 2016).

5.2. Individual Versus Combined Contribution of Meteotsunamis to Extreme Sea Levels

Rabinovich (2020) classifies the strongest known meteotsunamis since 1992 as "good weather" or "bad weather" events based on a qualitative assessment of the general weather situation. Here, good weather means fair surface weather with no or weak winds, no rain and thunderstorms, and bad weather means the presence of tropical or

extratropical cyclones or storms, squall lines, severe thunderstorms and strong surface winds. Therefore, for good weather meteotsunamis the wind contribution to the resonant transfer of energy toward the ocean is absent or quite marginal to the contribution of the respective air pressure disturbance, while both wind and air pressure forcing may be relevant during bad weather meteotsunamis (see more in Section 5.3). The ratio of contributions is also dependent on the ocean depth, as wind become generally more important in very shallow basins (Šepić, Vilibić, & Fine, 2015; Šepić & Rabinovich, 2014; Shi et al., 2019). This classification can be roughly translated into a classification based on the background sea level, where good weather usually corresponds to an average background sea level and bad weather usually (but not exclusively) indicates an elevated background sea level due to an ongoing storm surge. Of the 49 meteotsunami events listed in Rabinovich (2020), about a quarter (12 events), are identified as bad weather events.

The oldest accounts of strong meteotsunamis refer to good weather events, which were mostly characterized by a sudden onset of sea level oscillations along with an apparent absence of significant atmospheric forcing (herein, significant atmospheric forcing would imply a large "cyclonic" pressure drops or strong winds, thunderstorms, etc.). Such was the 27 June 1954 Lake Michigan event that claimed lives of 5 people (W. M. Ewing et al., 1954), the 21 June 1984 Ciutadella rissaga with a height of ∼3 m (Jansà, 1986), the Great Vela Luka flood of 21 June 1978 with seiches of at 6–8 m height (Orlić et al., 2010; Vučetić et al., 2009), and the Nagasaki abiki of 31 March 1979 (Hibiya & Kajiura, 1982) with ∼4 m high waves that caused drowning of 3 people. Subsequent research revealed that good weather events mostly occur in the warmer season and are usually associated with: (a) AGWs maintained through wave-duct (e.g., Monserrat & Thorpe, 1992; Šepić, Vilibić, & Belušić, 2009), wave CISK (convective instability of the second kind; e.g., Belušić et al., 2007) or both (e.g., Tanaka, 2010), (b) pressure jumps associated with thunderstorms (e.g., Jansá et al., 2007) which do not necessarily pass directly over the affected areas so that the weather appears "fair" to an observer.

The bad weather events have been less studied, at least until recently, because the effects of meteotsunamis in these situations are often superimposed to other processes, that is, storm surges, infragravity waves, swells and wind waves (see an example in Figure 6). For this reason, only the very strong and/or destructive bad weather meteotsunamis were investigated. These include meteotsunamis that occur due to pronounced atmospheric pressure changes and strong winds in: (a) extratropical cyclones (e.g., Carvajal et al., 2017; Linares et al., 2016; Mercer et al., 2002); (b) tropical cyclones (e.g., Anarde et al., 2021; Ding et al., 2011; Dolgikh et al., 2023; Ke & Yankovsky, 2011; Lin & Wu, 2021; Ma et al., 2015; Mecking et al., 2009; Shi et al., 2020); (c) mesoscale convective systems (Kazeminezhad et al., 2021; Sibley et al., 2021); (d) squall lines (e.g., Bechle et al., 2016; M.-S. Kim & Woo, 2021); (e) derechos (e.g., Bailey et al., 2014; Šepić & Rabinovich, 2014; Wertman et al., 2014); and (f) cold fronts (e.g., de Jong & Battjes, 2004; de Jong et al., 2003; Perez et al., 2022).

Research of the joint effects of storm surges, infragravity waves, seiches and meteotsunamis on total sea level extremes has only recently been initiated. For example, Rabinovich et al. (2023), in their study on the effects of extratropical cyclone Songda on the coasts of British Columbia and Washington, show that extreme sea levels were reached through a combined effect of a storm surge, meteotsunamis and infragravity waves. The importance of high-frequency sea level oscillations (such as meteotsunamis) for the total sea level height reached during storm surges has been emphasized by other authors as well, for example, Suursaar et al. (2006) for Storm Gudrun in the Baltic Sea, Pérez Gómez et al. (2021) for storm Gloria in the western Mediterranean, Heidarzadeh and Rabinovich (2021) for Typhoons Lionrock and Jebi on the coasts of Japan, Medvedev et al. (2022) for Typhoon Maysak in Korea and the Sea of and Ferrarin et al. (2023) for a flooding of Venice on 12 November 2019. etc. An interesting event occurred between 16 and 18 January along the mid-US East Coast (Figure 6), during which three processes—planetary meteotsunami waves coming from the Hunga Tunga-Hunga Ha'apai eruption, meteotsunamis caused by propagating air pressure disturbances and storms surges—occurred almost simultaneously (Rabinovich et al., 2025). In addition to analysis of individual events, Ruić et al. (2023) conducted the first statistical analysis of the contribution of high-frequency sea level oscillations to total residual sea level maxima of the Adriatic Sea, reaching conclusions that high-frequency sea level oscillations (such as meteotsunamis) can dominate positive sea level extremes, or, even when not dominating them, significantly contribute to total sea level height. Additionally, Shi et al. (2020) have done a similar research by assessing contribution of meteotsunamis to total sea levels during the North Atlantic tropical hurricanes.

5.3. Air Pressure Versus Wind Disturbances Generating Meteotsunamis

In general, generation of meteotsunamis by traveling air pressure disturbances has been considered as the dominant in comparison to generation by the wind disturbances (Monserrat et al., 2006; Pattiaratchi & Wijeratne, 2015). This particularly holds for relatively deeper parts of coastal regions, as the wind-induced sea level changes (e.g., for storm surges) are inversely proportional to the ocean depth (e.g., for the frictionless one-dimensional problem):

$$\frac{\partial \zeta}{\partial x} = \frac{\tau_x}{\rho\, g\, H}, \tag{10}$$

where ζ is sea level displacement along x, τ_x is the wind stress, ρ and H are ocean density and depth, while g is the gravity. Convincingly, the shallower is the ocean or a water body, the larger is the sea level response to the wind forcing. This equation holds for slow ocean processes like storm surges, but also—similarly to the air pressure forcing (Equation 2)—is valid for dynamically amplified sea level response to traveling wind disturbances.

Indeed, analyses of observations and numerical simulations have shown that wind can be important in very shallow coastal regions and even in inland water bodies. For example, Shi et al. (2019) numerically reproduced winter meteotsunamis (here equivalent to bad weather meteotsunamis) along the wide shelf of the northern Gulf of Mexico, demonstrating the dominance of wind forcing at depths shallower than 15 m. Similarly, Šepić, Vilibić, and Fine (2015) reached the same conclusion in sensitivity modeling studies of meteotsunamis in the northern Adriatic Sea, where winds can make a substantial contribution only in very shallow coastal regions. In deeper coastal areas (e.g., 30–80 m), wind may still play a significant but not dominant role compared to air pressure forcing (Vilibić, Domijan, & Čupić, 2005; Vilibić, Orlić, et al., 2005). In such cases, wind contributes primarily at longer periods (e.g., generating seiches with periods greater than 1 hr, while having only a minor effect on sea-level oscillations with periods from a few minutes to a few tens of minutes), and only under very strong winds (>20 m/s), typically accompanying bad weather meteotsunamis.

In North America, derechos—severe convective storms that can travel eastward for more than a thousand kilometers and produce gale-force winds (>20 m/s) together with intense air pressure oscillations (exceeding several hectopascals)—can generate meteotsunamis through both air pressure and wind forcing (Guastini & Bosart, 2016; Šepić & Rabinovich, 2014). The generation mechanism is dominated by wind forcing in very shallow regions, such as Chesapeake Bay with an average depth of 6.4 m, while in deeper regions, such as Lake Erie or along the US East Coast, air pressure forcing dominates or acts exclusively. Finally, strong seiches in very shallow coastal water bodies (e.g., lagoons or marine lakes shallower than 5 m) are almost exclusively generated by winds (Niedda & Greppi, 2007; Vilibić et al., 2025), consistent with the absence of good weather meteotsunamis in such basins.

5.4. Global Studies

Researchers have conducted systematic global investigations of meteotsunamis and other atmospherically induced high-frequency sea level oscillations, both from an observational perspective and based on the global instrumental data sets. The seminal paper by Monserrat et al. (2006) that strongly advertised the term meteotsunami to the tsunami and geosciences community also listed the number of meteotsunami events, in particular referring to the most damaging ones that occurred over global coastlines. Pattiaratchi and Wijeratne (2015) listed 35 meteotsunami hotspots and the documented wave heights of meteotsunami, pointing out that meteotsunamis are an underrated phenomenon in studies of extreme sea levels and providing some examples for the Australian coastline. Vilibić et al. (2016) provided spatial plots of worldwide meteotsunamis, with more detailed view on the Mediterranean Sea, aiming to list some of major research gaps in the global research of meteotsunamis. Gusiakov (2019) examined all tsunamis occurring between 1900 and 2019 and estimated the type and various parameters of the largest tsunami occurring each year, showing that meteotsunamis were the strongest tsunamis observed globally during 9 years (7.5% of all examined years). The average maximum wave run-up for these events was 4 m, much less than for seismic (9.2 m), landslide (65.4 m) and volcanic (30.4 m) tsunamis. Finally, Rabinovich (2020) described in detail 49 meteotsunami events, indicating the type (more in Section 5.2) and intensity of events, and documenting also the impact and the damage that resulted from these meteotsunami events.

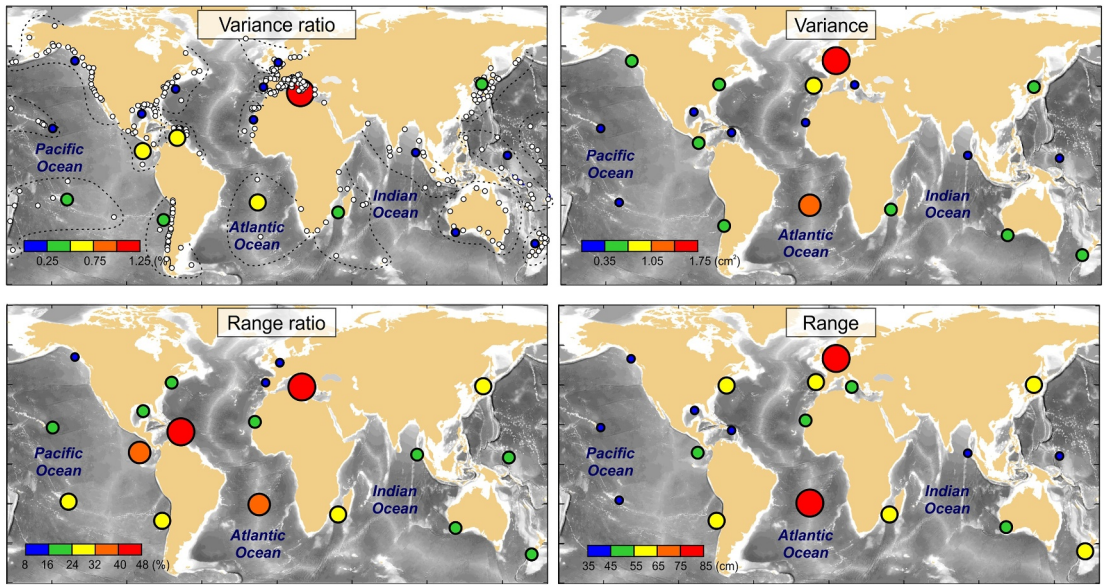

Figure 7. Ratio between nonseismic sea level oscillations at tsunami timescales (NSLOTTs) and total sea level variances (upper left) and their maximum ranges (lower left), as well as NSLOTT absolute variance (upper right) and maximum ranges (lower right), all averaged over coherent areas (after Vilibić & Šepić, 2017).

With the development of global sea level products at a minute timescale (more in Section 3.2), global studies based on worldwide sea level observations were initiated. The first such study, conducted by Vilibić and Šepić (2017), introduced the term "NSLOTT," which has since been adopted by other researchers (Williams, Schultz, et al., 2021; Zemunik, Denamiel, Šepić, & Vilibić, 2022; Zemunik, Denamiel, Williams, & Vilibić, 2022) and is referring to all high frequency (period from 2 min to a few hours) sea level oscillations observed at tide gauges induced by processes in the atmosphere. Their findings revealed that while the contribution of NSLOTT variance to the overall sea level variance is in general relatively small, the maximum NSLOTT range can contribute more than 40% of the overall maximum sea level range in low-tidal areas (Figure 7). Moreover, a distinct zonal pattern of NSLOTTs was identified, with variance doubling from the tropics and subtropics to the mid-latitudes at particular location. This pattern suggests a link between mid-tropospheric jet, tsunamigenic AGWs and long ocean waves, as will be explained in more detail in Section 7.1.

Zemunik, Denamiel, Šepić, and Vilibić (2022) advanced this research by constructing a global climatology of NSLOTTs over a predefined sub-region, estimating their average variance to very low values, from 0.24 cm^2 in the Baltic Sea to 6.57 cm^2 along the Pacific coast. However, the amplification of oscillations during the strongest NSLOTT events compared to background oscillations were estimated up to 100, in particular over some regions, where the amplification is attributed to both local bathymetries and intensity and frequency of atmospheric processes in a region. Additionally, they found that NSLOTTs are typically not isolated phenomena. During extreme events, about a quarter of the strongest occurrences are synchronized across stations within a radius of several hundred kilometers from a central "beacon" station.

5.5. Regional and Local Meteotsunami Climatologies and Catalogs

In regions or meteotsunami hotspots with a long history of meteotsunami observations or sufficient minute-resolution sea level data to establish climatologies, local (station-wise) and regional (e.g., country- or basin-wide) meteotsunami catalogs and climatologies have been developed. Two prominent Mediterranean meteotsunami hotspots exemplify this: the Adriatic Sea (Croatian coast) and Ciutadella (Menorca, Spain). Orlić (2015) documented meteotsunami events starting with Vela Luka meteotsunami of 1931, with the earliest occurrences based mostly on written accounts from local enthusiasts (Tabain & Tabain, 1994). The catalog was later transferred online and expanded with additional 15 events (totaling 36 events at the moment), all with heights above 1 m, and all described in detail (Šepić & Orlić, 2025a). The online version of the Adriatic Sea meteotsunami catalog also details the synoptic patterns associated with meteotsunami events.

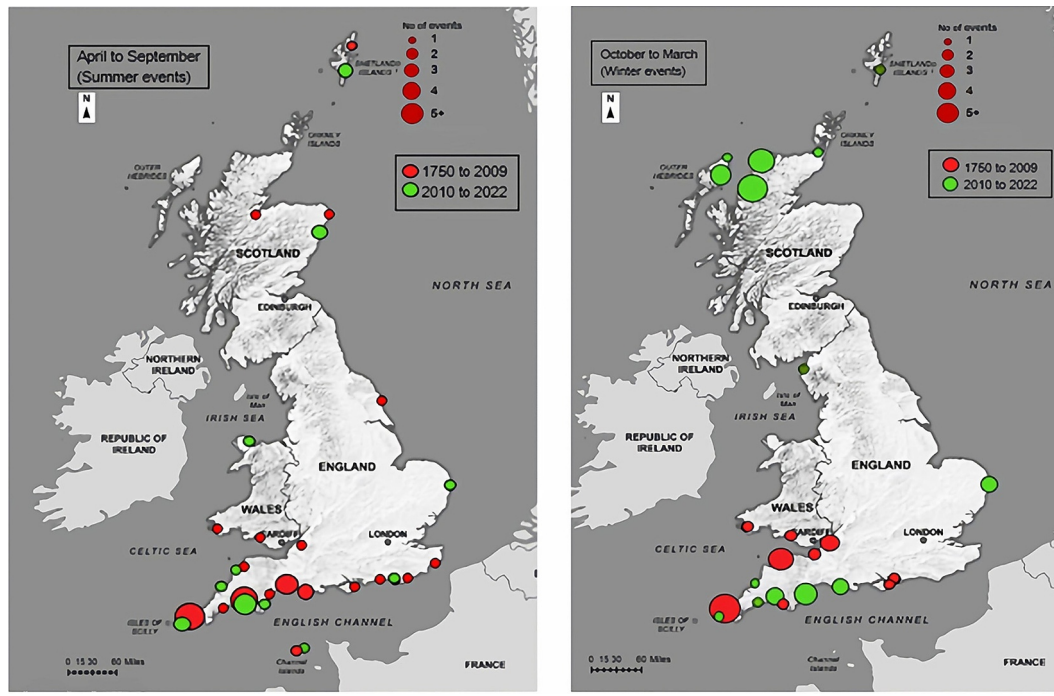

Figure 8. Seasonal and locational distribution of maximum wave heights from 1750 to 2022. Numbers of events at specific locations are represented by dot size as shown in the key (after Lewis et al., 2023).

For Ciutadella, no dedicated meteotsunami catalog has been published, but data from the region has been extensively used in various studies, particularly those focused on forecasting. The Spanish Meteorological Service (AEMET) classifies observed events as moderate (amplitude of 20–70 cm), high (amplitude of 70–100 cm), very high (amplitude of 100–200 cm) or extreme (amplitude > 200 cm), based on observed or eye-witnessed wave amplitude in Ciutadella Harbor (Jansà & Ramis, 2021). Studies by Romero et al. (2019) and Vich and Romero (2021) used data on 126 recorded rissaga events to assess a meteotsunami forecasting system, while Šepić, Vilibić, and Monserrat (2009) used 32 rissaga events, with data on events extracted either from previous research studies or from available sea level measurements, to quantify the simultaneity between the Balearic and the Adriatic meteotsunamis.

In the UK, records of historical meteotsunami events date back to the 18th century. Initial studies focused on "summer-type" meteotsunamis (Haslett et al., 2009; more on classification in Section 7.2). The studies were later expanded to include events as far back as the 18th century (Thompson et al., 2020) and recent occurrences from the instrumental era (Lewis et al., 2023), as well as "winter-type" events. UK meteotsunamis are most frequent along the southwestern and southern coasts, near locations where Joseph Proudman developed his resonance transfer theory (Proudman, 1929). The UK authors use several criteria for definition of a meteotsunami event: (a) wave height >20 cm with 2–120 min period oscillations registered at two or more tide gauge stations, (b) atmospheric criteria requiring either convective mesoscale weather system or wind/air pressure jump higher than a given threshold, and (c) geological criteria, which discriminates atmospheric from non-atmospheric tsunamis. Notably, winter-type meteotsunamis are stronger along northern UK coastlines, whereas summer-type events are less common in these regions (Figure 8; Lewis et al., 2023). Historical records indicate more summer events, whereas the instrumental era reveals a predominance of winter events. This discrepancy suggests winter meteotsunamis were less noticeable historically due to their overlap with storm surges and waves, whereas summer meteotsunamis during calm weather posed a higher risk to communities.

The longest meteotsunami climatology has been documented for the Finnish coast, where Pellikka et al. (2020) examined sea level charts back to 1922 and recent 15-min and 1-min instrumental records measured during the summer period (May-October). They used different criteria for detecting meteotsunamis at charts and within instrumental records, assessing the period of oscillations (below 2 hr) and putting variable threshold between

stations, due to their different bathymetry characteristics. In total, 121 meteotsunami events were extracted and analyzed, conjoined with a rapid change in air pressure occurring shortly before or simultaneously with the sea level oscillations in 70% of all events. Also, the authors found that meteotsunamis are strongly connected with lightning over the region, pointing to the existence of strong convective systems during most of summer events.

Examination of sea level charts was also a basis for constructing the pointwise meteotsunami climatology for the northern Adriatic. Šepić et al. (2012) used a single station (Rovinj) placed at the open coast. For that reason (open coast), the threshold of wave height for a meteotsunami was set low, 0.25 m, yielding to 16 meteotsunami events over the 1955–2010 period (with the highest one reaching 0.60 m). Convective systems were present above the area during at least five strongest events (satellite images were not available for all events), and most of the events were conjoined with typical synoptic condition for the summer-type meteotsunamis (see more in Section 7.2).

Observational studies based on tide gauge measurements in Northwest Europe (Williams, Schultz, et al., 2021) show a higher occurrence of meteotsunamis in winter, with more than double the frequency compared to other seasons. However, a low threshold (meteotsunami event was defined as a NSLOTT surpassing 0.25 m that was conjoined with precipitation over a 6-hr interval) for defining meteotsunamis resulted in the inclusion of weak events, yielding to 349 detected events across 90 tide gauge stations during an 8-year period. Similarly, Dusek et al. (2019)—defining meteotsunamis as wave height surpassing 0.20 m for at least two tide gauges in a region—reported seasonal differences along the US East Coast, with maximum meteotsunamis occurring in summer along the southern, and in winter along the northern sections of the coast. Similarly, a low threshold for a meteotsunami yielded to approximately 25 meteotsunami events per year along the US East Coast. The Great Lakes climatology (Bechle et al., 2016) shows that most meteotsunamis occur between April and July, coinciding with the peak of derechos in the early warm season (Guastini & Bosart, 2016). Bechle et al. (2016) defined meteotsunamis as NSLOTTs with wave height above 0.3 m conjoined with air pressure rates of change or wind speed at neighboring meteorological station(s) surpassing 0.75 hPa/min or 10 m/s, respectively. Such a definition led to approximately 106 meteotsunami events per year.

Here, it should be emphasized that tide gauge sampling intervals are strongly influencing the detection of meteotsunami events, as, for example, the US East Coast and the Great Lakes climatologies were obtained from sea level data having resolution of 6 min, while UK climatology is based on 15-min sea level series.

In Southeast Asia, recent studies (Lin et al., 2024a) indicate that meteotsunamis, defined by a fixed wave height threshold of 30 cm over 1-min sea level measurements, occur nearly weekly. Winter meteotsunamis are linked to clustered storms, while late summer-autumn typhoon-induced meteotsunamis, though less frequent (ca. 20%), are significantly stronger. In estuarine systems like the Tamsui and Keelung Rivers near Taipei, meteotsunamis can propagate far inland, with higher-frequency signals (of ca. 20 min period) attenuated but lower-frequency components (of ca. 50 min period) persisting (Lin et al., 2024b). An older climatology (1957–1858, 1961–1981) for the Longkou Harbor (X. Wang et al., 1987), located in the northeast China, and facing the west, documented 137 meteotsunami events defined as events during which long waves had periods shorter than 155 min and heights above 40 cm (the authors called them "seiches"), exhibiting strong interannual variability but occurring mostly during summertime and peaking in July. Interestingly, on the opposite coastline of the Yellow Sea, that is, at approximately same latitude along the western coastline of South Korea, the 10-year climatology (2010–2019) indicates a shift in season with maximum meteotsunami occurrences in March-June period (M. S. Kim et al., 2021) and peak in April.

For the western Australian coast, Pattiaratchi and Wijeratne (2014) defined meteotsunamis as events during which wave heights of long ocean waves surpassed 0.4 m. Australian meteotsunamis were found to coincide with thunderstorms in summer and low-pressure systems in winter. Notably, Fremantle's record-breaking sea level (for entire 115 years of tide gauge operations) was attributed to the significant contribution of a meteotsunami (total sea level of 2.12 m; 0.61 m due to meteotsunami).

To conclude, various studies based on instrumental data and meteotsunami catalogs have proposed different definitions of meteotsunamis, as emphasized in Section 1. Several issues hinder the unification of such a definition, the most important being a subjective assessment of meteotsunamis and their definitions, as well as the discrepancy between events identified from eyewitness reports and those derived from instrumental records. Moreover, each of the latter categories carries its own inconsistencies. For example, historical meteotsunami catalogs based on eyewitness reports are influenced by coastal resilience—meteotsunami impacts in macrotidal

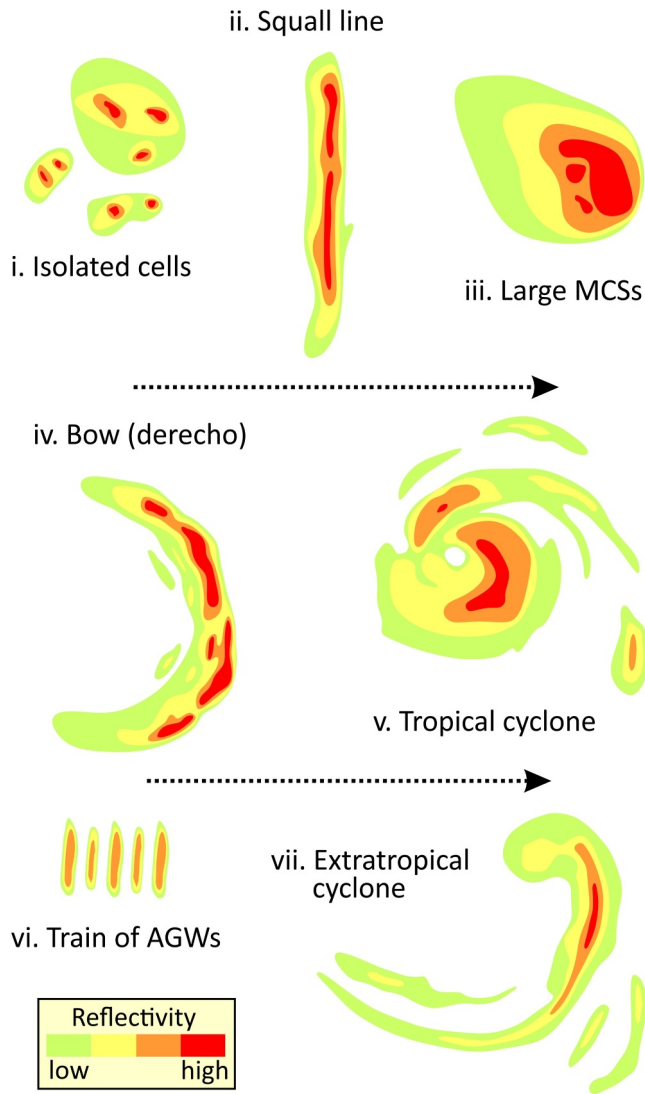

Figure 9. Different types of meteotsunamigenic atmospheric systems (mesoscale convective system; atmospheric gravity wave; types are partially described in Bechle et al., 2015). The arrows indicate moving rather than stationary systems.

regions such as the UK coast are generally much lower than in microtidal regions (see Section 8.1). In addition, such reports are often developed locally, as in Vela Luka (Orlić, 2015) or Ciutadella (Romero et al., 2019), implying that local bathymetric features and the subjective perspectives of researchers and communities play an important role in establishing thresholds for meteotsunami events (e.g., 1 m in Vela Luka, or 20 cm in Ciutadella). By contrast, developing an objective definition is more straightforward from instrumental records, where fixed or statistically defined thresholds can be applied (e.g., percentiles, such as the 99.993 percentile used by Ruić et al., 2023). For this reason, a single uniform definition of meteotsunamis cannot be established. Instead, we suggest defining meteotsunamis as the most extreme minute-scale oscillations in a given area, particularly those that are devastating or damaging.

6. Atmospheric Sources of Meteotsunamis

At the beginning of the 20th century Honda et al. (1908), Proudman (1929), Fonteserè (1934), Nomitsu (1935), Caloi (1938) and others have noticed a coincidence between rapid changes in atmospheric pressure and the occurrence of strong harbor or bay seiches. These coincidences, that is, simultaneous appearances of atmospheric and ocean fluctuations, were explained theoretically by Proudman (1929) and Greenspan (1956), as different types of atmosphere-ocean resonances. Their findings were later supported by numerous individual studies and numerical modeling experiments, of which some are described in other chapters of this paper. The importance of wind disturbances in the generation of long ocean waves has also been noted and studied (Platzman, 1958, 1965). In this chapter, we discuss the nature of tsunamigenic atmospheric pressure and wind disturbances, including the schematization of various types of tsunamigenic atmospheric systems (Figure 9).

6.1. Atmospheric Gravity Waves

AGWs (also known as internal gravity waves) are ubiquitous in the atmosphere: they are found at all its levels—from the planetary boundary layer to the ionosphere, have a wide range of wavelengths (10–1,000 km) and periods (10–200 min), and propagate both horizontally and vertically at speeds of ~1–~50 m/s (Nappo, 2002; Plougonven & Zhang, 2014). The restoring force for AGWs is buoyancy. When a parcel of air which is immersed in a stable atmosphere is lifted to a higher level, it cools adiabatically and becomes denser than the surrounding fluid and thus begins to sink to its initial position. However, due to inertia, it overshoots its original position. While it sinks, the parcel heats adiabatically, ending at a level where it has a lower density than its environment—positive buoyancy then causes the parcel to start rising again. These oscillations represent AGWs, the frequency of which is known as the Brunt–Väisälä frequency (N) and is given by:

$$N = \sqrt{\frac{g}{\theta}\frac{\partial \theta}{\partial z}} \tag{11}$$

where g is the gravity acceleration, θ is the potential temperature, and z is the vertical coordinate. If the AGWs propagate diagonally, or if the process involves moist adiabatic lifting/sinking, the equation for the frequency of the oscillations must be modified accordingly (Nappo, 2002).

For an initial displacement of a parcel to occur, and for an AGW to develop, a trigger is required. One of the most common triggers of AGWs is terrain. A horizontal atmospheric flow encountering an orographic obstacle (e.g., a ridge or a mountain) is likely to be displaced vertically, giving rise to one of two types of gravity waves generated

by terrain: *Lee waves* or *mountain waves*, with the former propagating only horizontally and the latter propagating both horizontally and vertically (Nappo, 2002). Dynamical instabilities in the middle and upper troposphere, which occur due to strong vertical wind shear and low static stability, are another potential trigger of AGWs (Gedzelman & Rilling, 1977; Keliher, 1975; Plougonven & Zhang, 2014). Other possible sources of AGWs include geostrophic adjustments (Gossard & Hooke, 1975), nonlinear wave-wave interaction (Fritts, 1982, 1984) and convective processes in thunderstorms of various types (e.g., Belušić et al., 2007; Tanaka, 2010).

In order for AGWs to generate meteotsunamis, they must:

1. extend from their generation level to the surface/ocean, where they manifest as pronounced atmospheric pressure and/or wind disturbances, and
2. propagate, without losing much of their energy, horizontally over the ocean long enough to generate a meteotsunami.

In the absence of a mechanism for energy conservation or renewal, AGWs lose most of their energy through vertical propagation before they propagate horizontally for even a single wavelength (Lindzen & Tung, 1976). A common mechanism for energy conservation is wave trapping (resulting in ducted AGWs), and a common mechanism for energy renewal is wave-CISK (Lindzen & Tung, 1976). We will now describe both mechanisms and list some of the meteotsunamis generated by such waves.

6.1.1. Ducted Atmospheric Gravity Waves

Ducted AGWs propagate horizontally through a stable atmospheric layer that serves as a duct (guide) and which is capped by a dynamically unstable layer (Lindzen & Tung, 1976; Nappo, 2002). A dynamically unstable layer is one in which there is either a strong vertical wind shear or static stability is very low (the Brunt–Väisälä frequency is close to zero), or a combination of both. The dynamical stability of the layer is usually assessed using the Richardson number Ri:

$$Ri = \frac{N^2}{\left(\frac{\partial u}{\partial z}\right)^2 + \left(\frac{\partial v}{\partial z}\right)^2} \tag{12}$$

where N is the Brunt–Väisälä frequency, u and v are the east-west and north-south components of the wind speed, respectively, and z is the vertical coordinate. In saturated, or almost saturated air, Equation 12 should be modified. If $Ri < 0.25$, a layer is dynamically unstable (e.g., Stull, 2017). When a vertically propagating wave is formed in a duct layer, it can either be partially transmitted through a dynamically unstable layer and partially reflected or completely reflected. The reflected component propagates to the surface, from where it is reflected upwards again. The upward and downward waves can then interfere constructively, resulting in AGWs that propagate horizontally through a duct layer for several wavelengths (Lindzen & Tung, 1976; Nappo, 2002). Whether the wave is partially or fully reflected at a capping layer and whether the interference of upward and downward wave will be positive or negative depends on the height of the reflecting layer and the vertical wavelength of the wave (Nappo, 2002), as well as on the wind speed within the reflecting layer. In situations where the wind speed in the dynamically unstable capping layer is equal to or very close to the phase speed of the AGWs in the duct layer, the ducted AGW can persist for a long time without the need for an additional energy source (Lindzen & Tung, 1976), thus having enough time to impact the ocean and generate meteotsunamis.

Jansà and Jansà (1980) (cited in Jansà & Ramis, 2021) suggested that the atmospheric pressure disturbances responsible for the formation of the rissagas in the Balearic Islands are surface manifestations of AGWs, and Monserrat and Thorpe (1992, 1996) deepened their findings by concluding that they are probably ducted AGWs. The conclusions of Monserrat and Thorpe (1992, 1996) are supported by the fact that the observed waves were relatively long-lived and non-dispersive (common characteristics of ducted AGWs), and that a typical vertical profile of the atmosphere (determined by a radio-sounding) at times of rissaga events was such that it favored the trapping of AGWs. The profile comprises a stable layer near the ground capped by a dynamically unstable layer in which wind speed is close to the determined phase speed of AGWs.

The concept of ducted AGWs as a source of meteotsunamis was later used to explain some other events, especially in the Mediterranean (e.g., the 2007 Ist meteotsunami, Šepić, Vilibić, & Belušić, 2009, several other events

in the Adriatic Sea, Vilibić and Šepić (2009), and a chain of the Mediterranean meteotsunamis in June 2014, Šepić, Vilibić, Rabinovich, & Monserrat, 2015). Ducted AGWs have also been proposed as a meteotsunami source for events in other locations, for example, the 2008 Boothbay event (Vilibić, Horvath, et al., 2014) and the East China Sea events (Tanaka, 2010), the latter jointly with wave-CISK.

It should be reiterated that processes within dynamically unstable layers can also lead to the generation of AGWs (Gedzelman & Rilling, 1977; Keliher, 1975; Plougonven & Zhang, 2014), that is, that a vertical atmospheric profile that enables the trapping of AGWs also supports their generation.

6.1.2. Atmospheric Gravity Waves Propagating With Wave-CISK

The term "conditional instability of the second type" (CISK) was first introduced by Charney and Eliasen (1964) to explain how cyclones can form in a conditionally unstable tropical atmosphere through the interaction of cumulus clouds and cyclonic motions: the clouds provide the latent heat for the cyclone, and the cyclonic motions provide the moisture for the clouds. Later, Lindzen (1974) developed a similar concept of cooperation between AGWs and convective motions (within cumulus clouds) and called it "wave-CISK": the process explains how convergence and upward motion in an AGW force moist convection and how the released heat provides energy for the wave. An overview of the various aspects of wave-CISK research is given by Houze (2004).

The wave-CISK mechanism was used by Belušić et al. (2007) to explain a tsunamigenic atmospheric pressure disturbance that produced extraordinary and destructive Adriatic meteotsunamis on 27 June 2003 (for a description of the event, see Vilibić et al., 2004). Belušić et al. (2007) have shown through data analysis (including radio-sounding, satellite imagery and air pressure measurements) and high-resolution numerical modeling (with a resolution of ∼4 km) that the AGW propagating along the long axis of the Adriatic Sea was "locked" to a thunderstorm cloud by a wave-CISK mechanism. This allowed both the cloud and the AGW to cross ∼500–600 km of the Adriatic long axis within 9 hr without losing much of their strength. Belušić and Strelec Mahović (2009) later showed that convective clouds were present over the area during three other strong meteotsunamis in the Adriatic and that the atmospheric pressure disturbance observed at the surface were likely related to these clouds, but they did not hypothesize on the nature of the relation.

Wave-CISK was also recognized as a likely mechanism for energy renewal by Horvath et al. (2018), who investigated the atmospheric forcing of the 25 June 2014 meteotsunami in the Adriatic Sea, and by Tanaka (2012), who investigated the 15 July 2009 meteotsunami in the Tsushima Strait (Japan). Tanaka (2010) investigated a destructive 25 February 2009 meteotsunami in the East China Sea and found that both the wave duct and wave-CISK were important in maintaining the AGW during this event.

6.2. Thunderstorm Clouds, Mesoscale Convective Systems, Squall Lines, Derechos

In addition to AGWs, numerous meteotsunamis were explained by convective processes in thunderclouds, mesoscale convective systems, derechos and squall lines. Bechle et al. (2015), for example, analyzed radar reflectivity imagery and assigned the Great Lakes meteotsunamis to one of eight categories: "convective cluster, convective complex, linear convection, bow convection (including derechos), extratropical cyclone, frontal (i.e., fronts associated with distant extratropical cyclones) and possible AGWs," with the majority of events (78%) associated with convective storms and only a very small fraction (<5%) associated with possible AGWs. Although convective storms can coexist with AGWs (and positively interfere with them through e.g., the wave-CISK mechanism), it is not necessary to invoke an AGW to explain a pressure jump within a thunderstorm cloud or a system.

The processes within a convective system (from the simplest single cell to mesoscale convective systems, squall lines and derechos to supercells) are such that they lead to low surface pressure under the convective updrafts and high surface pressure under the convective downdrafts—with the strong downdrafts also causing the wind gust fronts. During severe convection, surface pressure differences can become substantial, reaching several hPa within a few minutes. For example, the devastating Ciutadella meteotsunami of 15 June 2006 was associated with a convective pressure jump of 5 hPa within 10 min (Jansà et al., 2007; Vilibić et al., 2008). When convective storms propagate over an area that supplies them with moisture and heat (i.e., over a warm and moist air mass or over a warm ocean), they can persist long enough to impact the ocean and generate meteotsunamis through resonance processes.

A mesoscale convective system is a multicellular thunderstorm system that is usually organized in a narrow line of thunderstorms with heavy precipitation (Stull, 2017). Mesoscale convective systems are much more complex than individual thunderstorms, with a cumulonimbus cloud system extending over 100 km or more in at least one direction, and with a developed mesoscale circulation (Houze, 2004). These systems result in pronounced surface pressure gradients with a high-pressure perturbation positioned at the leading edge of a convective region (Houze, 2004). Such pressure perturbations can cause a meteotsunami, and mesoscale convective systems were indeed identified as meteotsunami sources, for example, of the 28–29 May 2017 meteotsunami along the English Channel and North Sea coast (Sibley et al., 2021) and the 19 March 2017 meteotsunami in the Persian Gulf (Kazeminezhad et al., 2021), among others.

Squall lines and derechos are special types of mesoscale convective systems. Within squall lines, many adjacent thunderstorms are combined into a long, narrow line that can be hundreds (to thousands) of kilometers long but is usually very narrow (15–400 km wide) and can last from several hours to several days (Stull, 2017). Derechos are basically squall lines which are bent into a shape called a bow echo. For a bow echo to be called a derecho, it must have winds that cause damage over a distance of at least 400 km, last for at least 3 hr and have wind speeds of over 26 m/s and gusts of over 33 m/s (Stull, 2017). Squall lines and derechos have been associated with many meteotsunamis, including the 1929 event in the UK (Douglas, 1929), other historic events in the UK (Haslett et al., 2009), events in the Great Lakes (Bechle et al., 2015, 2016), along the US East Coast (Bailey et al., 2014; Sallenger et al., 1995; Šepić & Rabinovich, 2014) and along the Yellow Sea (J. Kim & Woo, 2021).

Generation of meteotsunamis by convective cells along the cold front were studied by Bechle et al. (2015, 2016) for the Great Lakes, de Jong et al. (2003) for the southern North Sea (Port of Rotterdam), and by Perez et al. (2022) for the Rio de la Plata estuary.

6.3. Tropical Storms and Tropical Cyclones Rainbands

Tsunamigenic atmospheric pressure and wind disturbances can also occur within tropical cyclones, both due to the development of AGWs (Nolan & Zhang, 2017) and to convective processes in tropical cyclone eyewall and rainbands (bands of thunderstorms organized into spirals) (Shi et al., 2020).

Impact of tropical storms on onset of long ocean waves was documented by Mercer et al. (2002) for Tropical Storm Jose (1999) and Tropical Storm Helene (2000) over the Grand Banks, and later modeled by Mecking et al. (2009) for Tropical Storm Helene (2000). The occurrence of meteotsunamis during individual tropical cyclones (typhoons, hurricanes) has also been demonstrated. For example, Dusek et al. (2019) and Anarde et al. (2021) documented the impact of Hurricanes Irma and Harvey, respectively, on the Gulf of Mexico and Atlantic Coast of the USA. Heidarzadeh and Rabinovich (2021) studied extreme sea levels related to impact of Typhoons Lionrock and Jebi on the coasts of Japan, while Medvedev et al. (2022) examined the impact of Typhoon Maysak in Korea and the Sea of Japan. A more detailed, statistical study relating tropical cyclones to meteotsunamis was done by Shi et al. (2020). The authors have analyzed atmospheric and sea level data related to 97 tropical cyclones which propagated along the continental shelf of the Gulf of Mexico, Eastern United States, and Puerto Rico in the hurricane seasons of 1998–2018. In 49 (52%) of situations, meteotsunamis with elevation above 0.2 m were measured by at least one tide gauge, and in 8 situations meteotsunamis had heights above 0.4 m, with the maximum of 0.78 m measured at Freshwater Canal Locks (Louisiana) during Hurricane Harvey in 2017. The research demonstrated that tropical cyclones can trigger both single meteotsunami waves, and trains of meteotsunami waves, and that these waves can contribute significantly to total flooding height. A peculiar event was studied by Rabinovich et al. (2023): Typhoon Songda, after traveling along the coast of Japan, turned eastwards, transitioned into an extratropical cyclone, and jointly with two local northern Pacific extratropical cyclones formed surges and meteotsunamis along the Canada and US West Coasts. The listed research confirms that meteotsunamis and other long ocean waves should be considered when estimating danger from tropical and extratropical cyclones.

7. Synoptic Background of Meteotsunamis

7.1. Synoptic Patterns Observed During Meteotsunamis in Mid-Latitudes

Intense mesoscale atmospheric processes often emerge under specific large-scale synoptic conditions (de la Cámara & Lott, 2015; Plougonven & Zhang, 2014). For instance, strong temperature gradients in the atmosphere

can create frontal systems, which act as sources of AGWs. Similarly, convective systems which can also cause meteotsunamis develop in unstable atmospheric environments where warm, moist air interacts with cooler, drier air, resulting in intense upward and downward motions and related pressure jumps, and sometimes also AGWs (see Section 6.2).

The connection between synoptic-scale atmospheric conditions and meteotsunamis was first identified in the Balearic Islands. An early description of the atmospheric origin of the rissaga (the local term for a meteotsunami in the Balearic Islands) in Ciutadella was provided by Jansà and Jansà (1980) (cited through Jansà & Ramis, 2021), whereas the link to large-scale meteorological patterns was not established following the 1981 rissaga event. A detailed analysis of this event hypothesized, for the first time, the relationship between rissagas, pressure jumps, gravity waves, and specific synoptic patterns, including a recognition of well-defined vertical structure of temperature and wind fields (Jansà, 1986; Ramis & Jansà, 1983). Subsequent studies confirmed the typical synoptic conditions associated with rissagas (Garcies et al., 1996; Jansà et al., 2007; Monserrat, Ibberson, & Thorpe, 1991; Tintoré et al., 1988). Typical conditions include (a) inflow of warm and dry Saharan air at low levels (~850 hPa), (b) strong southwesterly winds exceeding 20 m/s at mid-tropospheric levels (400–700 hPa) with embedded dynamic instabilities, and (c) weak to moderate low-pressure systems near the surface.

Simultaneously, research on the origins of the "šćiga" (local term for meteotsunamis in the Croatian islands) events was conducted. Early study by Hodžić (1979/1980) suggested meteorological origin of the event, linking it to a specific synoptic situation. An attempt to connect Adriatic Sea NSLOTTs to specific synoptic patterns was undertaken by Šepić et al. (2008), who showed that strong sea level oscillations in Bakar were associated with southwesterly mid-tropospheric flow. Later case studies (e.g., Belušić & Strelec Mahović, 2009; Ruić et al., 2024; Šepić, Vilibić, & Belušić, 2009; Šepić et al., 2012) reinforced these findings, highlighting recurring synoptic conditions across the Adriatic, much alike to the ones found over the Balearic Islands.

Research of individual events extended across the Mediterranean, revealing shared synoptic features during numerous meteotsunamis. Šepić, Vilibić, et al. (2018) and Zemunik, Bonanno, et al. (2021) studied "marrobbio" events along Sicily's southwestern coast, using reanalysis and radio-sounding data to connect these phenomena to characteristic synoptic conditions. A 2014 event in Odessa, analyzed using satellite imagery, revealed convective clouds and typical synoptic patterns, both indicative of AGWs (Šepić, Rabinovich, & Sytov, 2018). This event was part of a series of destructive meteotsunamis spanning thousands of kilometers across the Mediterranean and Black Sea, where a synoptic pattern favorable to meteotsunami generation was tracked propagating eastward over several days (Šepić, Vilibić, Rabinovich, & Monserrat, 2015), coincident with meteotsunami occurrences over the area.

Systematic studies of the Mediterranean region were also done, including research on the co-occurrence of meteotsunamis in the Balearic and Adriatic seas under specific synoptic conditions. These studies confirmed the importance of upper-level instabilities in meteotsunami formation (Šepić, Vilibić, & Monserrat, 2009). Additionally, an analysis of averaged synoptic conditions during selected events from the 2010s across four Mediterranean areas revealed similar patterns in all Mediterranean regions (Šepić, Vilibić, Lafon, et al., 2015).

Research subsequently expanded globally. A seminal study by Vilibić and Šepić (2017) identified a significant (at $p < 0.01$) zonal correlation between NSLOTT range and mid-troposphere winds. Zemunik, Denamiel, Williams, and Vilibić (2022) further examined correlations between NSLOTTs and relevant synoptic variables, highlighting mid-troposphere wind speed and relative humidity as key factors for occurrence of NSLOTT events. Extreme events consistently featured strong and dynamically unstable mid-troposphere jet streams, low-troposphere thermal fronts, and nearby surface cyclones. Notably, differences between hemispheres emerged, with more pronounced thermal fronts and deeper cyclones associated to NSLOTT events in the Southern Hemisphere (Figure 10).

7.2. Summer-Type Versus Winter-Type Meteotsunamis

Distinct seasonal patterns emerge when comparing summer- and winter-type meteotsunamis, particularly in their driving mechanisms, associated atmospheric conditions, and geographic distributions. These differences arise from variations in the synoptic and mesoscale atmospheric processes that dominate during different times of the year, though these processes are not entirely exclusive to any particular season.

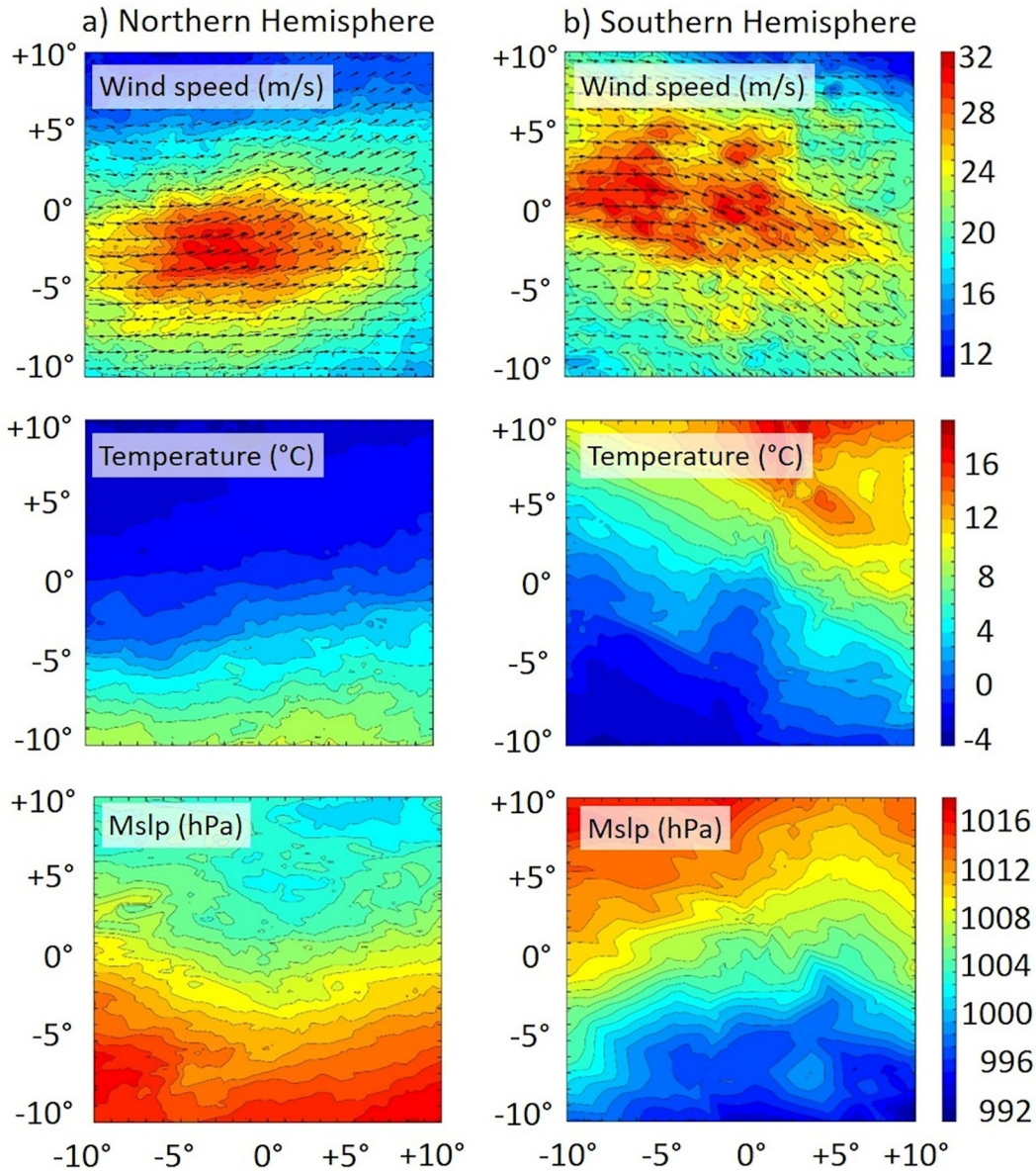

Figure 10. Wind speed and direction at 550-hPa level, temperature at 850-hPa level and mean sea level pressure averaged over all extreme nonseismic sea level oscillations at tsunami timescales (NSLOTT) events for the stations (centered in the middle of a domain) for which correlation between 550-hPa wind speed and NSLOTT range was higher than 0.4 on the (a) Northern, and (b) Southern Hemisphere (after Zemunik, Denamiel, Williams, & Vilibić, 2022).

Summer-type meteotsunamis are typically associated with rapid air pressure jumps triggered by intense mesoscale phenomena such as convective storms or frontal systems. These events often occur under specific synoptic-scale conditions, such as a mid-troposphere jet overtopping an inflow of dry low-troposphere air masses. This pattern is commonly observed over the Mediterranean region during the warm months, creating favorable conditions for meteotsunami formation. Consequently, meteotsunamis in the Mediterranean are most frequent in summer, reflecting the seasonal patterns conducive to their development (Monserrat et al., 2006; Vilibić et al., 2021).

Winter-type meteotsunamis, on the other hand, are commonly associated with cyclonic systems or strong cold fronts. Originating from extratropical cyclones and deep lows, winter meteotsunamis are typically linked to air pressure oscillations of lower intensity rather than the abrupt jumps recorded during summer events (Pellikka et al., 2022). Further, strong surface winds frequently accompany winter events. Still, the winter-type

meteotsunamis may be more destructive, as they are normally appearing jointly with a storm surge, thus potentially reaching quite extreme total sea levels (for example, Heidarzadeh & Rabinovich, 2021; Medvedev et al., 2022).

The wave ducting mechanism plays a dominant role in summer-type meteotsunamis by preserving the energy of air pressure disturbances (see Section 6.1), which facilitates resonant amplification. Additionally, surface winds during summer events are generally weak, minimizing disruption to the resonant processes. In the Mediterranean, associated atmospheric disturbances often approach from the southwest (Jansà & Ramis, 2021; Šepić, Vilibić, & Monserrat, 2009). In other regions, summer-type meteotsunamis may be associated with different synoptic patterns. For example, meteotsunamis associated with derecho events along the northeastern U.S. coast involve intense air pressure jumps accompanied by gale-force wind gusts. However, these events are also linked to strong mid-tropospheric jets (Fery & Faranda, 2024; Guastini & Bosart, 2016; Johns & Hirt, 1987).

The Adriatic Sea is another location where both summer and winter-type meteotsunamis occur (Šepić & Orlić, 2025a). Applying clustering methods to approximately 20 years of minute-resolution sea level data further highlights this distinction: winter-type meteotsunami patterns in the Adriatic Sea are characterized by pronounced mean sea level pressure gradients, favoring wind-induced storm surges, colder low-troposphere conditions, and the presence of a jet stream at the 500 hPa level, whereas summer-type patterns are associated to a weak mean sea level pressure fields, warmer low troposphere conditions, but also the presence of a jet stream at the 500 hPa level (Ruić et al., 2024).

Moving poleward, summer-type meteotsunamis become less frequent, while winter-type meteotsunamis become more prevalent. In Finland, Pellikka et al. (2022) presented a comprehensive 10-year analysis of meteotsunamis in the Baltic Sea, showing that winter-type events dominate, with some winter-type events occurring as late as May and June. Summer-type meteotsunamis in the Baltic resemble those in the Mediterranean, with the key difference being that the mid-tropospheric jet in the Baltic is southerly instead of south-westerly, as observed in the Mediterranean (Figure 11).

In general, winter-type meteotsunamis are stronger and more frequent in Northwest Europe than summer-type ones, as quantified by Williams, Schultz, et al. (2021). This study found that approximately half of these events are driven by quasi-linear systems embedded in cold fronts propagating eastward. In contrast, only about 20% of meteotsunamis in this region are driven by northeastward flows, following a synoptic setup similar to summer-type meteotsunamis.

8. Mitigating, Forecasting and Projecting Meteotsunami Hazards and Risks

8.1. Meteotsunami Risks

As highlighted in the introduction, meteotsunamis possess a significant level of destructiveness that can cause substantial damage and even loss of life, particularly in microtidal or non-tidal regions unaccustomed to large sea level oscillations (Rabinovich, 2020). It should be said that meteotsunamis occur with comparable strength in both microtidal and macrotidal regions (as it can be seen from listed events in Section 5 and presented theory in Section 4). These events have been recorded on every continent (see Section 5.1), impacting coastal households and facilities, infrastructure, road and rail transportation, navigation safety, ship moorings, aquaculture farms, and the safety of tourists and swimmers, among other. This section provides an overview of the most critical risks associated with meteotsunamis, including examples of notable events and human reactions linked to these phenomena.

8.1.1. Loss of Human Lives and Injuries

The height of meteotsunami waves can reach substantial levels in certain locations, posing significant risks by dragging people—such as local fishermen, tourists, coastal walkers, swimmers, and beachgoers—into the sea or lake. A list of the most destructive meteotsunamis is given in Section 5.1 in Table 2. Herein, we describe in slightly more detail the deadliest of these events. In the morning of 26 June 1954, the water level of Lake Michigan rose by about 2–3 m within minutes along the fishing piers in Chicago, submerging the lakefront and tragically killing eight people (Bechle & Wu, 2014; W. M. Ewing et al., 1954).

A more intense meteotsunami (with a crest-to-trough height of approximately 6–8 m and a period of 15–20 min) struck Vela Luka, Croatia, on the morning of 21 June 1978. Fortunately, no lives were lost during this event. This

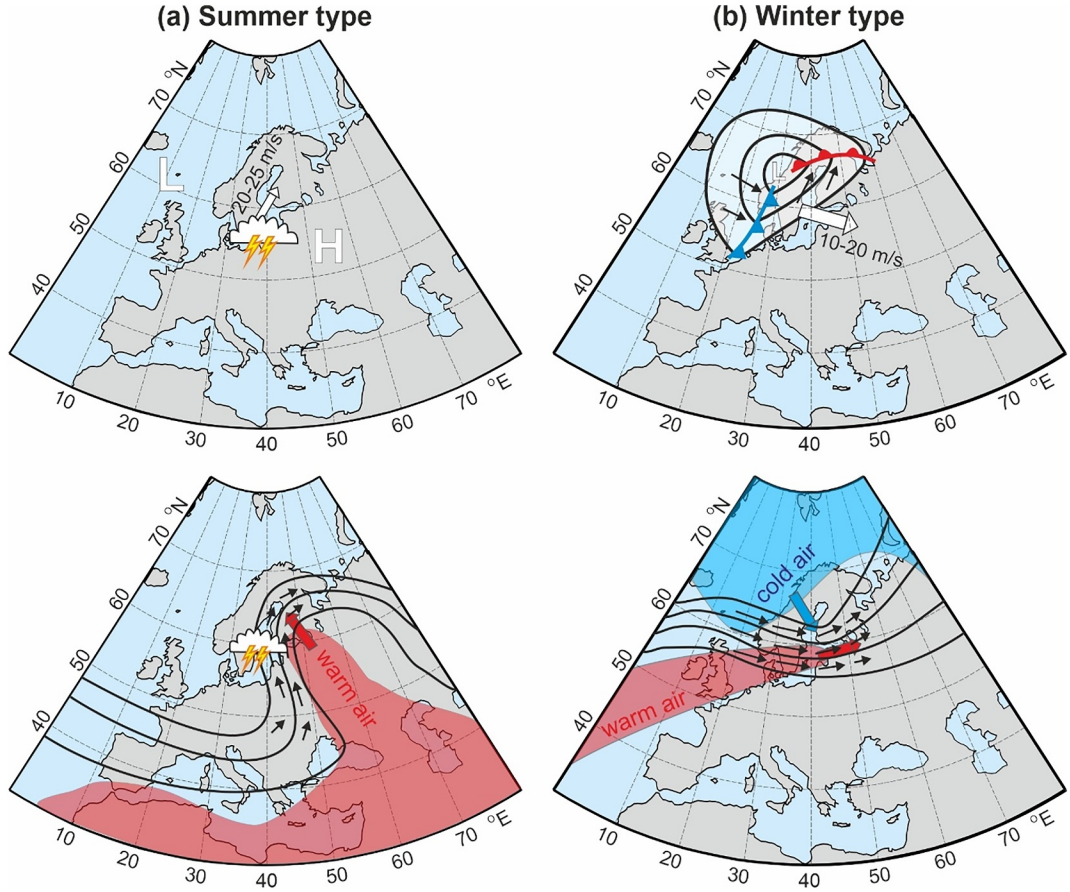

Figure 11. An illustration of: (top) dominant surface and (bottom) low and mid-tropospheric atmospheric conditions and weather systems observed during extreme meteotsunamis in the northern Baltic Sea during (a) mesoscale convective system (MCS)-driven summer-type events and (b) winter-type events associated with cold fronts. Red (blue) shaded areas in bottom plots indicate advection of warm (cold) air at the 850 hPa level; black lines (geopotential) and black arrows (wind) mark the position and direction of the 500 hPa jet stream. Filled arrows mark the general direction of movement of MCSs (white arrow), extratropical cyclones (white), and warm (red) and cold (blue) air advection, with average speed of movement given for MCSs and extratropical cyclones (after Pellikka et al., 2022).

outcome was likely due to the local population's awareness of such oscillations, albeit typically of much weaker intensity, and the quick actions of an electrical company employee who immediately shut down the network upon detecting the first meteotsunami waves. This precaution likely saved many lives later, as the sea reached nearly the first floors of coastal homes in the inner part of the bay (Vučetić & Barčot, 2008; Vučetić et al., 2009).

Two other deadly meteotsunami events are also noteworthy: (a) The Mostaganem (Algeria) flood on 3 August 2007, where 12 people were killed by a sudden wave that struck beaches along a 40 km stretch of coastline, with an estimated maximum run-up of 7–10 m (Okal, 2021a), and (b) The Dayyer meteotsunami on 19 March 2017, which was measured with a height of approximately 2.5 m during high tide, affecting a 100 km stretch of the Iranian coastline between the cities of Dayyer and Asaluyeh. This event injured or killed 27 people (Heidarzadeh et al., 2020; Kazeminezhad et al., 2021; Salaree et al., 2018). No warning has been issued for any of listed events.

Instructively, even localized and moderate meteotsunami events can cause deaths and injuries in highly populated and macrotidal regions if no warning is in progress. At noon on 4 May 2008, there were many people fishing near the breakwater of the coastal city of Boryeong, western coast of South Korea, when a sudden 1.3-m high meteotsunami wave approached at the top of the tide and washed 36 people into the sea (Yoo et al., 2010), of which 9 were killed by the wave while 15 suffered serious injuries. The timing of the event was crucial, as a much stronger meteotsunami—with maximum measured wave height of up to 3 m—occurred along the western South

Korea coast a year before, 31 March 2007, but between midnight and dawn, causing only damage and no human casualties (M. S. Kim et al., 2019).

Currents induced by meteotsunamis can also cause fatalities. For example, the "abiki" (a local term for meteotsunamis in southeastern Japan) of 31 March 1979, caused the drowning of three people when their boat was damaged by meteotsunami-induced currents (Hibiya & Kajiura, 1982). Meteotsunamis can also generate rip currents in coastal regions. On 4 July 2003, and 18–21 July 2019, a sunny and calm day along the southern shores of Michigan, storm-generated meteotsunami waves traveled along the coastline as edge waves for a few hours, causing rip currents that drowned seven swimmers who were in the lake at the time (Linares et al., 2019; Y. L. Liu & Wu, 2022). Similar events have occurred in other locations during the summer, where there is sometimes a delay of several hours between the storm generating a meteotsunami and the waves reaching the coast. For example, during the Odessa meteotsunami on 27 June 2014, 12 people were injured on local beaches possibly due to a topographically modulated (by an underwater canyon) tsunami wave generated along the shelf break located hundreds of kilometers away (Šepić, Rabinovich, & Sytov, 2018). Further, along the US East Coast, a meteotsunami generated by a derecho on 13 June 2013, arrived 2–3 hr after the storm passed over the area, dragging the swimmers into the sea, with similar events occurring on multiple occasions due to reflection of the offshore propagating meteotsunami waves at the shelf edge and their subsequent "return" to the coast (Pasquet & Vilibić, 2013; Vennell, 2007, 2010; Wertman et al., 2014).

8.1.2. Coastal Flooding, Damage and Impact to Coastal Structures

In microtidal regions, such as the Mediterranean Sea, coastal flooding during meteotsunami events can be highly destructive, as the waves may be an order of magnitude larger than the tides (Monserrat et al., 2006; Vilibić et al., 2021). Because waterfronts in these regions are not designed to withstand such large sea level oscillations, the resulting damage from multi-meter sea level changes can be extensive. For instance, the estimated damage caused by the Vela Luka 1978 flood was approximately 7 million US dollars at the time (equaling ca. 35 million US dollars nowadays), equivalent to a quarter of the annual income of the entire island of Korčula (Orlić, 2015; Vučetić & Barčot, 2008; Vučetić et al., 2009). The sea inundated 188 households, not only those located on the waterfront, damaging furniture, electrical appliances, installations, and food supplies, including olive oil and wine (Figure 12). Additionally, the flood destroyed shops and markets, cars parked along the seaside, and boats moored in the harbor, which struck the seabed during the ebb of the meteotsunami. Indeed, this event was an extraordinary event, as the inhabitants of Vela Luka normally place a half-meter-high temporal protection at the house entrances to prevent flooding of the ground levels. However, the maximum sea level during the 1978 event was up to six times as high as the protections.

In contrast, meteotsunami floods in another Mediterranean hotspot, Ciutadella on the Balearic Islands—locally known as "rissaga"—typically do not cause significant damage to waterfront homes, as most of the town is situated on elevated ground several meters above sea level. However, the inlet serves as a mooring site for many boats and luxury yachts, which can be destroyed during meteotsunamis. for example, a number of luxury yachts broke their moorings and were swept into each other and into the coast during the meteotsunami of 15 June 2006. This event resulted in damages exceeding 10 million euros at that time (Jansà et al., 2007).

Along flat, sandy beaches, meteotsunami-induced coastal flooding can cause widespread panic, particularly during summer when good weather meteotsunamis occur, and beaches are crowded with people. Such incidents have been reported worldwide, including locations in Brazil, the Great Lakes, the US East Coast, the Dutch and the Italian coast (Candella & de Araujo, 2021; Memmola et al., 2024; Sibley et al., 2021). For example, squall lines traveling offshore generated 3-m-high waves on the flat, sandy beaches of Daytona Beach, Florida, on 3 July 1992. These waves struck during calm, clear weather, injuring about 75 people and severely damaging vehicles parked along the beach as well as beach infrastructure (Churchill et al., 1995; Sallenger et al., 1995). No warning was been issued at that time.

A particularly strong meteotsunami event is remembered by older residents of the village of Dwarskersbos on the western shores of South Africa. On the night of 27 August 1969, a 2.9-m-high meteotsunami wave (the height is obtained through interviews with older residents in 2010) flooded the waterfront of the village. Since the event occurred during nighttime, the wave's approach went unnoticed, and the flooding was only realized when seawater entered homes. The meteotsunami caused structural damage to some waterfront houses, and several light boats and poultry were lost (Okal et al., 2014).

10.1029/2024RG000867

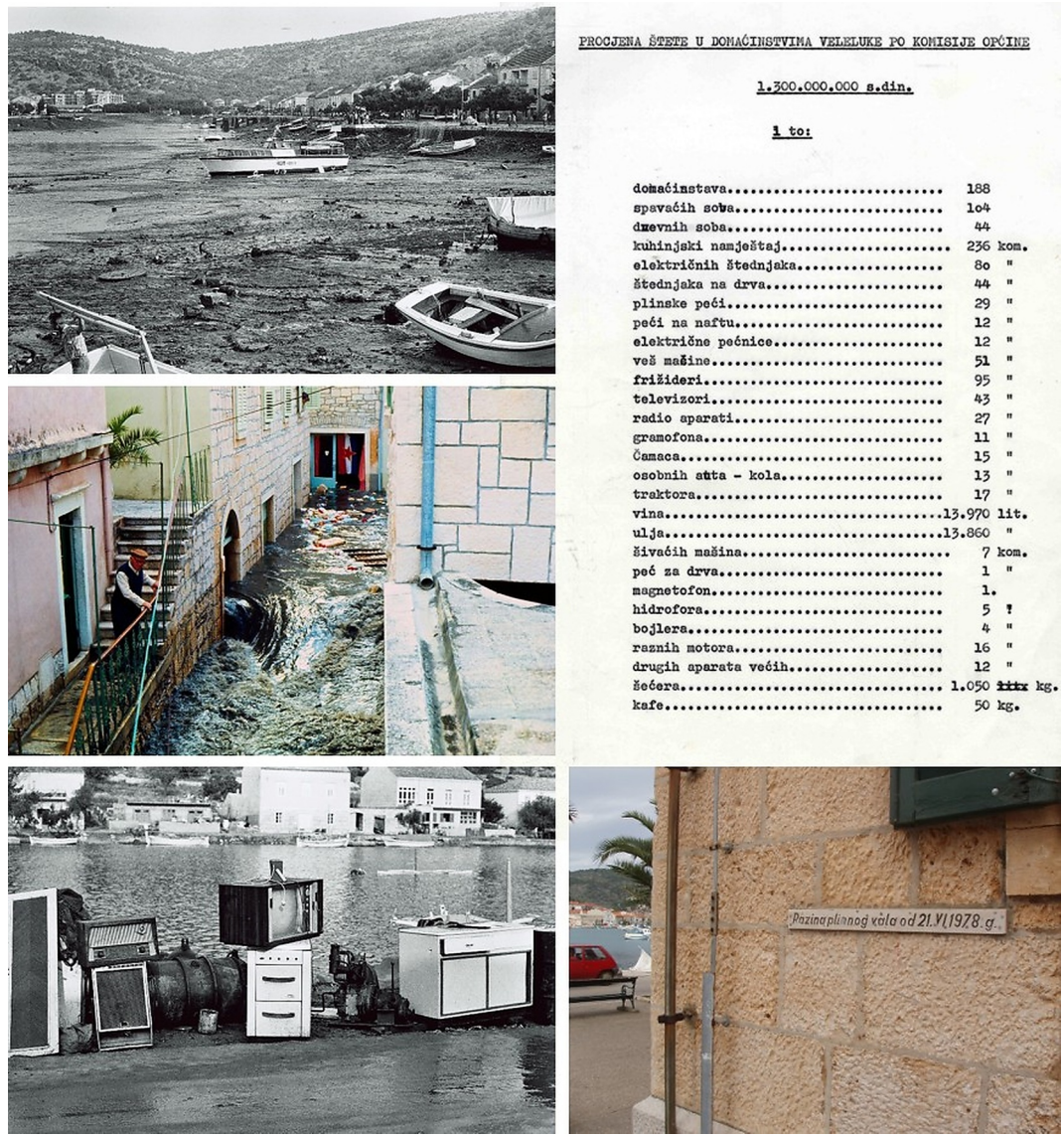

Figure 12. Photos of the Vela Luka meteotsunami and the damage: meteotsunami ebb with the emptied harbor (top left), retreat of sea from the flooded households (middle left), an "exhibition" of damaged household furniture and electrical appliances (bottom left), official list of damage in households (top right) and sign marking the maximum height of the meteotsunami wave at the school building (bottom right). Reproduced from Vučetić and Barčot (2008), with permission of the Dubrovnik State Archive (credit for left column photos: Vladimir Stanišić, archive number HR-DADU-SCKL-692).

In harbors, strong meteotsunamis can disrupt vessel maneuvering, with cargo ships potentially striking the seafloor due to a sudden drop of sea level. This can occur even when infragravity or meteotsunami waves originate from distant sources and generate only moderate sea level oscillations of a few tens of centimeters (Goring, 2009). Meteotsunami-induced currents, however, can be even more hazardous. On 17 August 2014, strong currents at Fremantle docks ripped a wharf free, where two cargo ships were moored. These ships collided with and severely damaged a nearby railway bridge—a critical connection in the Perth area—which was subsequently closed for 2 weeks (Pattiaratchi & Wijeratne, 2015), causing the multi-million cost due to rebuilding the line and redirecting the passenger and cargo traffics to longer routes. Along with storm surges, meteotsunamis can be responsible for closing of port harbors, particularly those with narrow entrances, like the harbor of Klaipeda, Lithuania (Nesteckytė et al., 2024), or the Port of Rotterdam (de Jong & Battjes, 2004; de Jong et al., 2003).

Strong meteotsunami currents can also cause damage in areas with constricted or complex bathymetry. For instance, in Mali Ston Bay, Croatia, known for its shellfish aquaculture farms, meteotsunami-induced currents on 27 July 2003, exceeded 150 cm/s (Vilibić et al., 2004)—an order of magnitude stronger than the average currents. These currents swept away moorings weighting over a thousand kilograms and associated shellfish-growing lines, resulting in damages exceeding a million euros. Following this event, aquaculture farms in that area have been relocated to more enclosed areas, where the currents are less intense.

8.1.3. Hazard and Risk Assessment Studies

Unlike tsunami studies, where probabilistic tsunami hazard and risk assessments have been developed over the past decades and implemented across many tsunami-prone coastlines (Behrens et al., 2021; Geist & Parsons, 2006; Grezio et al., 2017), the estimation of meteotsunami hazards and risks remains largely unexplored. Probabilistic approaches could estimate the probability of exceeding specific wave heights, maximum inundation levels, or associated risks. However, a significant constraint on such analyses is the lack of long-term data. Minute-resolution sea level data spans only a few decades at most, whereas the most hazardous meteotsunamis occur on centennial or longer time scales (e.g., the Vela Luka meteotsunami of 1978; Orlić, 2015). Additionally, height of meteotsunamis is strongly micro-location dependent, and many meteotsunami prone areas have very short measurements of sea level (e.g., for Vela Luka (Croatia) only 4 years of sea level 1-min sea level measurements are available) or no measurements at all.

The first study to conceptualize a methodology for probabilistic meteotsunami hazard estimation and test it was conducted by Geist et al. (2014) for the US East Coast. This study derived a probability density function using historical microbarograph records of atmospheric disturbances and Monte Carlo models to establish its continuous analytic distribution. Numerical modeling was then applied to compute maximum meteotsunami wave amplitudes near the coast. However, the probabilistic function was based on a limited data set of air pressure measurements spanning only 14 years. Repeating such a study in the future, as longer minute-resolution air pressure series become available, could yield more reliable and robust probabilistic threshold-exceeding estimates.

Another probabilistic approach has been attempted in meteotsunami forecasting systems (Denamiel, Šepić, Huan, et al., 2019). In this case, probability density functions for air pressure parameters were not derived from sparse measurements but instead a constant probability distribution within a prescribed range of variables was assumed. Further details on this warning system, including the variables and methodology used, are provided in Section 8.2.

An innovative approach was developed by Lewis et al. (2024), who constructed a meteotsunami intensity index incorporating both physical (hazard) variables (e.g., maximum wave height, currents, tidal stage at the time of the event) and "receptor" variables (e.g., shoreline geomorphology, slope and elevation, impacted assets, fatalities or injuries, and peak activity levels along the shore during the event). This index effectively reproduced meteotsunami risks along UK coastlines. However, as with probabilistic approaches, the greatest challenge lies in the lack of comprehensive data on used variables (maximum wave height, currents, maximum inland intrusion of seawater, additional or compound hazards, air pressure change, tidal regime, time of arrival of maximum wave at the shoreline, shoreline geomorphology, shoreline gradient, shoreline elevation, asset impact, fatality and/or injury).

Finally, a mitigation of meteotsunami hazards and risks has been explored by assessing the effects of coastal constructions to the coastal amplification of meteotsunami waves. A change in the harbor or bay bathymetry may strongly affect the wave height at the top (Denamiel et al., 2018), even in unexpected ways—e.g., dredging of a shallow harbor tops in the Vela Luka Bay may increase wave heights there for 20%–30%, as shown by numerical modeling. Similarly, prolonging the protecting pier of Vilanova harbor, Spain, resulted in additional amplification of the incoming meteotsunami waves (Monserrat et al., 2024). Still, some interventions in a harbor may dissipate the energy and lower oscillations, like installation of a number of radial piers (Rabinovich, 1993), construction of long shore-parallel, multichannel or offshore breakwaters (G. Y. Chen et al., 2004; Keuthen & Kraft, 2016; Maa et al., 2011) or other structures capable to reflect the incoming waves (Bayindir & Farazande, 2021; Gao et al., 2021).

8.2. Meteotsunami Forecasting and Early Warning Systems

Typically, coastal hazard early warning systems, such as those for tsunamis, are designed and implemented in response to major events. For example, the Pacific Tsunami Warning System was developed following the

devastating Pacific tsunamis of 1946 and 1960, caused by the Aleutian and Chilean earthquakes, which impacted many Pacific coastlines (Igarashi et al., 2011). Similarly, the Indian Ocean Tsunami Warning System was established after the 2004 Indian Ocean Boxing Day tsunami (Suppasri et al., 2015). At the national level, Japan has developed tsunami warning systems in response to the frequent occurrence of tsunamis reaching several tens of meters, which strike the country every few decades (Mulia & Satake, 2020).

The same principle applies to meteotsunamis. The first meteotsunami early warning system was created for the Balearic Islands, where 3-5-m "rissagas" (the local term for meteotsunamis) occur approximately every few decades, as in 1984 and 2006. Analyses of moderate events (several meters in wave height) from the 1970s and early 1980s revealed commonalities in specific synoptic patterns during these events (Jansà & Ramis, 2021; Ramis & Jansà, 1983). These patterns included (taken from Jansà & Ramis, 2021): (a) weakly cyclonic pattern at low levels (below 850 hPa), (b) a strong baroclinicity across the Western Mediterranean, southwesterly winds and advection of the warm air mass over and to the east of the Balearic Islands at around 850 hPa, (c) strong southwesterly flow at the eastern flank of a 500 hPa trough that is centered over the Iberian Peninsula, and (d) a jet stream close to the Mediterranean peninsular coasts with winds over the Balearics reaching 35–37 m/s at 300 hPa.

Consequently, the Spanish State Meteorological Agency (AEMET) established the rissaga warning system in 1985. This system involves a forecaster subjectively assessing synoptic products several days in advance and issuing qualitative rissaga warnings at various levels (e.g., no rissaga, potential weak rissaga, potentially moderate rissaga, or potentially strong/exceptional rissaga) (Jansà & Ramis, 2021). Since recently, the assessment of tsunamigenic conditions includes an assessment of the available high-resolution ocean models either those within the Balearic Rissaga Forecasting System (BRIFS, Mourre et al., 2021, https://www.socib.es/en/what-we-do/ocean-forecasting/brifs) or those based on the Triangle-based Regional Atmospheric Model TRAM (Romero, 2024, https://meteo.uib.es/tram). Periodic assessments of the system revealed a tendency to slightly overestimate weak events and moderately underestimate strong and exceptional events (Jansà & Ramis, 2021).

The synoptic patterns have also been quantitatively linked to rissagas through the development of a synoptic meteotsunami index (Šepić, Vilibić, & Monserrat, 2016). However, the link between the strongest rissagas and the index is not significant, limiting the capacity of the index to reliably forecast the strongest meteotsunami events. This is attributed to the critical role of mesoscale convective system positioning and time-space fluctuations (Villalonga et al., 2024), forecast of which remains challenging for operational weather prediction models (Plougonven & Zhang, 2014; Squitieri et al., 2023). Similar findings have been reported for the Adriatic Sea meteotsunamis, utilizing advanced k-medoid clustering methodologies (Ruić et al., 2024).

Alternative approaches have been developed to improve rissaga forecasting while reducing computational demands for real-time predictions. For instance, extracting key atmospheric processes that generate meteotsunamis (Romero et al., 2019) and employing neural networks to select warning levels based on vertical profiles of temperature, wind, and humidity from nearby stations (Vich & Romero, 2021). This neural network approach successfully forecasted 55%–75% of rissagas, though it produced an average false alarm rate of 30%, reaching over 50% for the strongest events. Still, such algorithms are quite fast—about an order of magnitude faster than full atmosphere-ocean numerical models. Notably, BRIFS (Renault et al., 2011) and TRAM operational model (Romero et al., 2019) integrate tide gauge and microbarograph measurements with the Weather and Research Forecasting (WRF) weather prediction model (Skaramock et al., 2005) at 4 to 2 km, respectively. The WRF output is then used to force the Regional Ocean Modeling System (ROMS, Shchepetkin & McWilliams, 2005, 2009) at 1 km or less. However, BRIFS and TRAM also tend to underestimate rissagas, presumably due to insufficient resolution (Jansà & Ramis, 2021; Mourre et al., 2021), which fails to capture atmospheric energy transfer at scales smaller than seven model resolution (Skamarock, 2004), despite the 2-min resolution of atmospheric model fields used to force the ocean model (Mourre et al., 2021). An ensemble of 22 BRIFS simulations in operational mode, with varying cumulus, microphysics, planetary boundary layer, and longwave/shortwave radiation schemes within the WRF model, was applied to 10 very high or extreme rissaga events (Mourre et al., 2021). Although the ensembles qualitatively reproduced the meteotsunami events, they did not reveal consistent parameterization preferences for achieving realistic magnitudes, which varied between different rissaga cases. Finally, at the Balearic Islands, pairing two observing sites—the recipient (where rissaga occurs, e.g., Ciutadella at Menorca Island) and another in which similar sea level signal has been recorded but being an hour in advance (e.g., a station at Mallorca Island)—was the basis for assessing if sea level measurements in advance of the meteotsunami hotspot may be used for forecast (Marcos et al., 2009). Still, this idea has not been

developed further, possibly because later studies showed that the majority of energy transfer from the atmosphere to the sea occurs on the shelf region between the islands of Mallorca and Menorca (Ličer et al., 2017) where there are no continuous sea level measurements.

Another advanced deterministic atmosphere-ocean model, the Adriatic Sea and Coast (AdriSC, Denamiel, Šepić, Ivanković, & Vilibić, 2019), was developed to reproduce and forecast Adriatic meteotsunamis. The AdriSC suite includes a high-resolution WRF model (Skaramrock et al., 2005) (3 km) coupled with ROMS (Shchepetkin & McWilliams, 2005, 2009) (1 km) and an unstructured Advanced Circulation model (ADCIRC, Luettich et al., 1991) for fine-scale resolution (up to 10 m) in complex coastal bathymetries where meteotsunamis normally occur. Despite its improvements, atmospheric model performance remains a limiting factor, with potential trajectory shifts of meteotsunamigenic disturbances by tens of kilometers or more and underestimated intensity of these disturbances. This results in underprediction of meteotsunami wave heights at vulnerable locations. Still, the capacity for operational forecasting of meteotsunami events is promising, even when multi-meteotsunami events comprising a series of atmospheric disturbances occur (Tojčić et al., 2021).

Due to the limited capacity of deterministic models to accurately forecast the intensity of meteotsunamis at their hotspots, a stochastic surrogate approach has been developed for the middle Adriatic Sea and tested for several Adriatic events (Denamiel, Šepić, Huan, et al., 2019). This system uses deterministic AdriSC forecasts of air pressure rates over the Adriatic. When a substantial percentage of threshold-exceeding air pressure rate values are detected, the system triggers an "event" mode in which six meteotsunami parameters are estimated from the model: the geographical location of disturbance initiation, propagation speed, direction of propagation, amplitude, period, and width of the disturbance. These parameters are then stochastically distributed over an interval using a probability density function optimized by generalized polynomial chaos expansion (Denamiel et al., 2020; Xiu & Karniadakis, 2002), with solutions compared against the best-describing pre-simulations weighted by a function. The surrogate stochastic system indicated that propagation speed for the Adriatic meteotsunamis is the most critical parameter, while the width of the disturbance is the least critical. Finally, evaluation of the stochastic surrogate operational system for the same Adriatic events as reproduced by the deterministic AdriSC forecast (Denamiel, Šepić, Ivanković, & Vilibić, 2019) resulted in a conservative assessment of meteotsunami occurrence but overestimated the probability of occurrence at some locations in the middle Adriatic.

The feasibility of combining operational atmospheric modeling and microbarograph observations in a meteotsunami early warning system has been tested along the Korean coastlines, which are also at risk from meteotsunamis of significant height (M. S. Kim et al., 2021). Along the 500 km of the Korean coastline, a network of 89 microbarographs has been employed for real-time estimation of the speed, propagation direction, and intensity of meteotsunamigenic disturbances (M. S. Kim et al., 2022). However, this number of microbarographs still results in spatially undersampled meteotsunami parameters, necessitating a network with a resolution of several kilometers (Monserrat & Thorpe, 1992; Rabinovich et al., 2021). For this reason, the operational atmospheric model of the Korean Meteorological Agency was also analyzed for its capacity to forecast air pressure jumps. The system was tested on a single meteotsunami event, where it was found that the model, on average, underestimated the pressure jumps, at various stations, by approximately 40% and exhibited a time mismatch of up to 1 hr, although it did reproduce the propagation of the pressure jump during the selected event.

Evidently, strategies for detecting and forecasting meteotsunamis encounter challenges at all stages due to the complexity and sensitivity of both the atmospheric processes that generate meteotsunamis and the energy transfer to the ocean. These challenges were already listed by Vilibić et al. (2016): (a) identifying tsunamigenic atmospheric synoptic conditions; (b) real-time detection of tsunamigenic atmospheric disturbances using a microbarograph network; (c) measurement and tracking of high-frequency sea level oscillations with high-resolution digital tide gauges and bottom pressure recorders; and (d) numerical simulation of meteotsunamis based on coupled atmosphere-ocean numerical models (Figure 13).

Although meteotsunami forecasting has improved over the last decade, development of an efficient, timely, and reliable meteotsunami warning system remains one of the key goals of the meteotsunami community. Achieving this may require more extensive weather and ocean observations, as well as a multi-level approach (Vilibić et al., 2016). Potential additional tools include, but are not limited to, operational weather radars capable of capturing tsunamigenic disturbances, which may correlate with radar reflectivity (Anderson et al., 2015; Kazeminezhad et al., 2021; Wertman et al., 2014; Williams, Schultz, et al., 2021), or satellite products that reliably estimate the speed of disturbances (Belušić & Strelec Mahović, 2009; Feng et al., 2021; Vilibić et al., 2010).

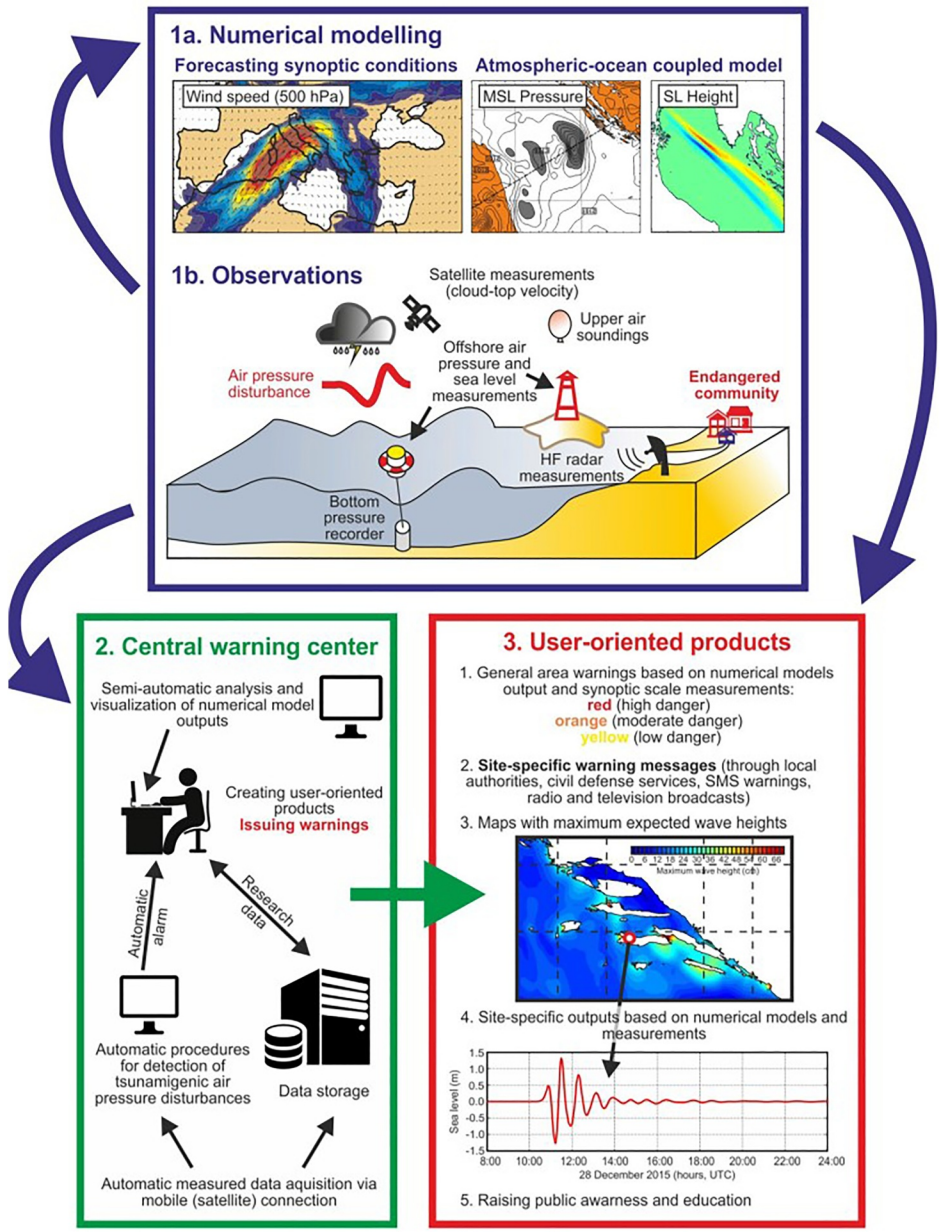

Figure 13. The proposed architecture of a meteotsunami warning system (after Vilibić et al., 2016).

8.3. Climate Change and Meteotsunamis

In the era of anthropogenic climate change—where one of the most prominent consequences is sea level rise combined with prolonged and more violent sea level extremes—hazards and risks in coastal regions are exponentially increasing (Hague et al., 2023). Despite this, the global assessment of meteotsunamis and high-frequency sea level oscillations has been largely neglected and primarily focused on specific locations (Pattiaratchi & Wijeratne, 2015). Projecting the intensity and frequency of meteotsunamis in future climates remains an open question, primarily because coupled atmosphere-ocean climate models are not yet capable of reproducing the generation of tsunamigenic atmospheric disturbances and their energy transfer to the sea. While atmospheric climate models and projections with kilometer-scale resolutions have only been tested in recent years (Ban et al., 2021; Fosser et al., 2024; Lagergren et al., 2024; Pichelli et al., 2021; Schär et al., 2020), to our knowledge no such models are currently coupled with the ocean models at kilometer-scale resolutions.

Despite this significant limitation, two studies have provided insights into future meteotsunami climates at specific hotspots, circumventing the limitations of full climate models. By using the connection between specific synoptic patterns and meteotsunamis, quantified for Ciutadella (Menorca, Spain) meteotsunami hotspot by Šepić, Vilibić, and Monserrat (2016), Vilibić et al. (2018) validated patterns generated by climate models against those of evaluation runs and existing reanalyzes (ERA-Interim at that time, Dee et al., 2011). Fine-tuning of the weighting coefficients during the index's construction yielded a good match between indexes derived from climate models and reanalysis synoptic patterns, enabling its extension to climate projections under scenarios RCP2.6, RCP4.5, and RCP8.5 (MED-11_CNRM-CM5 regional climate model, Panthou et al., 2016). More recently, Zemunik Selak et al. (2025) demonstrated that this connectivity is largely independent of whether ERA-Interim or the newer ERA5 reanalysis (Hersbach et al., 2020) is used, indicating that climate models—that are also capable to reproduce synoptic patterns—may be used for quantifying the meteotsunami climatology in the future climates, at least at some locations.

Unfortunately, the atmospheric climate model used by Vilibić et al. (2018) was the only one at the time archiving the nine synoptic variables required for the index construction at a reasonable time-space resolution, making uncertainty quantification of meteotsunami projections unfeasible. Nonetheless, the analysis revealed no significant change in meteotsunami frequency under scenario RCP2.6 and RCP4.5, while a 20% and 35% increase in days with meteotsunamis was detected for scenarios RCP8.5 during the mid- (2041–2070) and late- (2071–2100) 21st century. This increase was particularly pronounced in the spring-summer season when meteotsunamis are strongest in the Mediterranean (Vilibić et al., 2021). The rise in meteotsunami-prone days may result from a greater meandering of the jet stream at lower latitudes projected under scenario RCP8.5 (D. D. Ren & Leslie, 2024), which could lead to more southwesterly flows and meteotsunami-favorable conditions.

A different approach was adopted by Denamiel et al. (2022), who used the pseudo-global warming (PGW) methodology to simulate six Adriatic meteotsunami events under future climate conditions (2070–2100, scenario RCP8.5). This methodology involves repeating present-climate numerical simulations (conducted using the AdriSC atmosphere-ocean modeling suite, see Section 8.2) but forcing them with future climate boundary and initial conditions, which are derived from regional climate models like LMDZ4-NEMOMED8 (Beuvier et al., 2010). PGW essentially shifts the mean climate state while preserving system variability (Schär et al., 1996). Given the short duration of meteotsunami events (hours to a day), PGW simulations required minimal computational resources for the six investigated events.

The study suggested that small shifts in atmospheric patterns under future climates—specifically, changes in southwesterly to westerly flows in the mid-troposphere associated with meteotsunamis—could amplify the intensity of meteotsunamis in the middle Adriatic by approximately 30% or maintain their current intensity in the northern Adriatic. However, the study's reliance on only six events limits the reliability and robustness of its conclusions.

To address these limitations, a generalized approach has been developed for projecting meteotsunamis in future climates (Figure 14; Denamiel, Belušić, et al., 2023). This method involves performing a large number of short-term, high-resolution simulations of meteotsunami events selected via a synoptic meteotsunami index (see Section 7.1). This approach can generate robust statistics and provide uncertainty quantification while maintaining computational demands at reasonable levels. Conceptually, this methodology offers a promising solution for quantifying future meteotsunamis, as it has already been considered for projecting convective events (Hansen et al., 2024). However, it relies heavily on establishing reliable proxy relationships between synoptic patterns and meteotsunamis or high-frequency sea level oscillations, which have only been validated at a few locations (Zemunik, Denamiel, Williams, & Vilibić, 2022; Zemunik Selak et al., 2025). This remains one of the key challenges for eventual climate projections of meteotsunamis.

9. Planetary Meteotsunami Waves Driven by Explosive Volcanic Eruptions

One of the most commonly cited differences between seismic and meteorological tsunamis is that the former often spread across the ocean, and occasionally even around the globe, whereas the latter are usually local or, at most, regional phenomena (Monserrat et al., 2006; Rabinovich, 2020). This difference arises from their generation mechanisms and the amount of energy transferred to the tsunami waves (see Section 2 for more details). However, extremely strong explosive volcanic eruptions can trigger fast-moving atmospheric waves characterized by tsunamigenic rates of air pressure change. These waves can circumnavigate the Earth multiple times, generating

10.1029/2024RG000867

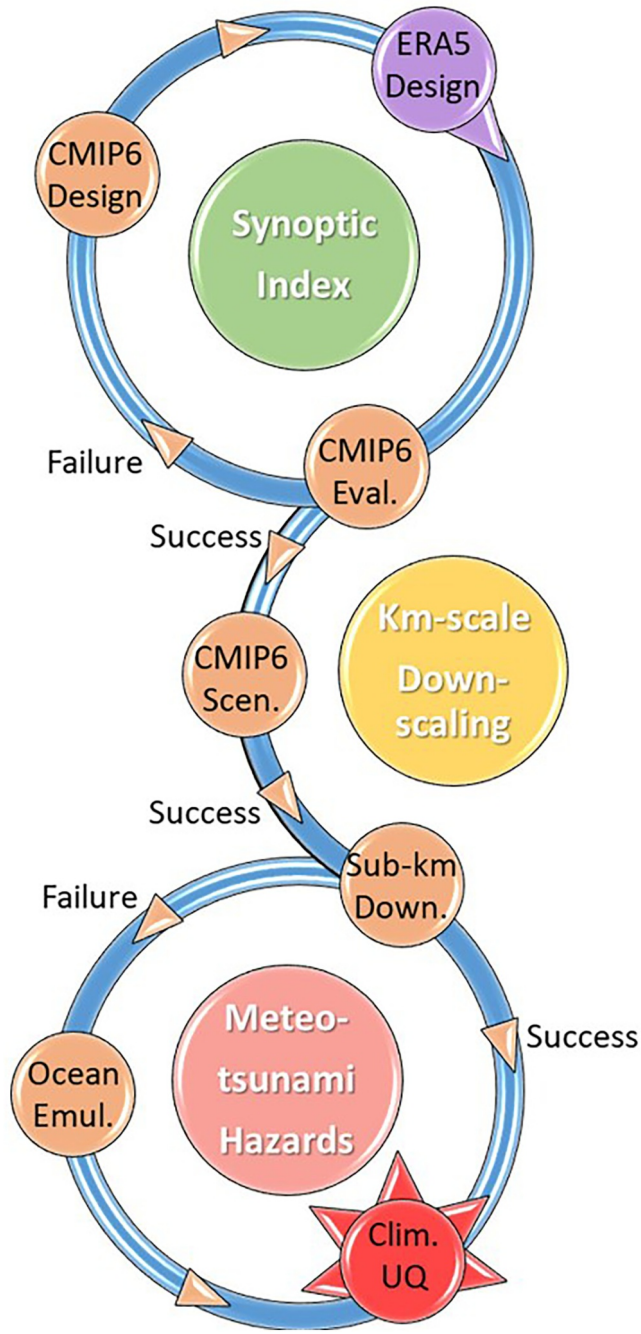

Figure 14. A workflow for robust estimations of meteotsunami hazard and its uncertainty: (1) establishing a reliable connection between meteotsunamis and synoptic patterns, (2) multi-nested model downscaling of extracted meteotsunami events, and (3) estimation of meteotsunami hazard and its uncertainty at a location (after Denamiel, Belušić, et al., 2023).

long ocean waves as they propagate. These are known as Lamb waves (Lamb, 1911), and they represent the eigenmode of atmospheric oscillations, confined by the Earth's surface. Lamb waves transport acoustic-gravity and gravity wave energy over vast distances, interacting weakly with topography. Their speed is slightly modulated by air temperature but is approximately equivalent to the speed of sound in an isothermal atmosphere at rest (about 312 m/s, Press & Harkrider, 1966; Kanamori et al., 1994). The Lamb waves are globally associated with intense air pressure jumps, which can reach several hPa over minutes but are limited by the energy of the explosion at the source.

Since the speed of Lamb waves is nearly always higher than the speed of tsunami waves in the ocean (for Lamb waves moving at 312 m/s, the ocean depth would need to be 9,900 m to reach full Proudman resonance; Proudman, 1929), long ocean waves are generated by traveling air pressure disturbances in conditions where the Froude number exceeds 1 (C. J. R. Garrett, 1970; Vilibić, 2008). This implies that the free wave travels slower than the forced wave (more in Section 4.1.1). Consequently, air-pressure-generated forced meteotsunami waves reach shorelines well in advance of any seismically or volcanically generated free tsunami waves related to volcanic eruption and initial water displacement.

Two such events have been recorded in modern history: the first occurred in 1883 during the eruption of the Krakatoa volcano, and the second in 2022 during the eruption of the Hunga Tonga-Hunga Ha'apai (HTHH) volcano.

The Krakatoa eruption peaked on 27 August 1883, when most of the island of Krakatoa collapsed into the sea, destroying the surrounding archipelago in a violent explosion (Self & Rampino, 1981). The eruption caused a landslide tsunami due to caldera collapse into the surrounding ocean (Paris et al., 2014), but it also resulted in unexpected tsunami waves observed in oceans where the tsunami waves which occurred because of caldera collapse could not arrive, such as along the Atlantic Ocean coastlines (M. Ewing & Press, 1955). Sparse tide gauge data from 1883 indicated that tsunami waves reached distant locations much earlier than predicted by theoretical travel times of free long ocean waves, as estimated from ocean bathymetry (their speed is given by $\sqrt{gh}$) (C. J. R. Garrett, 1970). Furthermore, the volcanic tsunami waves did not propagate beyond the Pacific Ocean (B. H. Choi et al., 2003). This suggests that the far-distant tsunami waves were generated by atmospheric Lamb waves, which circled the globe multiple times and were recorded by global air pressure sensors (Le Bras et al., 2024).

The HTHH eruption on 15 January 2022, was unexpected because the volcano is submerged, and no volcanic monitoring was in place. However, this event occurred during the modern era, benefiting from advancements in Earth observation systems. These now included satellites, autonomous sensors (e.g., dense tide gauge and microbarograph networks), atmospheric and oceanic models, and other integrated data products. Consequently, by December 2024, over 250 research papers had been published on the HTHH eruption (according to the Web of Science database), many of which documented local air pressure measurements attributed to the passage of the atmospheric Lamb wave (e.g., Harrison, 2022).

The HTHH eruption generated a prominent Lamb wave that circled the Earth for 6 days, with air pressure amplitudes ranging from 2 to 7 hPa during the first wave passage. The Lamb wave's speed slightly exceeded theoretical values (∼312 m/s), with robust global estimates ranging between 315 and 318 m/s (Horváth et al., 2024; Munaibari et al., 2023; Wright et al., 2022). In addition, the eruption produced numerous gravity waves in the stratosphere and higher altitudes, traveling at slower speeds (235–270 m/s) and dissipating more rapidly (Shinagawa & Miyoshi, 2024; Wright et al., 2022). One such mode, the Pekeris mode that caused weaker air pressure disturbances than the Lamb wave, represents an acoustic-gravity pseudo-mode of Earth's oscillations driven by strong atmospheric inversions (Pekeris, 1937). This mode traveled globally at an average speed of ∼230 m/s (Chau et al., 2024; Watanabe et al., 2022).

The volcanic caldera collapse generated a tsunami that spread across the Pacific Ocean (Figure 15; Heidarzadeh et al., 2022; Lynett et al., 2022; Pakoksung et al., 2022; Purkis et al., 2023). However, the Lamb wave triggered planetary meteotsunami waves that were observed in all major ocean basins (Anup et al., 2024; Dogan et al., 2023; Omira et al., 2022; Villalonga et al., 2023), and in enclosed seas like the Mediterranean (Heinrich et al., 2023). Wave heights typically ranged from a few centimeters to several tens of centimeters, occasionally exceeding 1 m, with amplification strongly influenced by local bathymetry and coastlines (P. L. F. Liu et al., 2023).

The meteotsunami waves were observed by global and regional tide gauge networks as well as high-frequency oceanographic radars (Lipa et al., 2023). Coastal observations indicated that these waves arrived concurrently with the Lamb wave in the atmosphere (Villalonga et al., 2023), underscoring their forced-wave nature. However, free long ocean waves generated by the Lamb wave have also been reported as significant along the coasts of the Pacific Ocean (Z. Y. Ren et al., 2023). Indeed, the deep Tonga Trench (with depths of up to 10,000 m)—over which both shock waves following the explosion (Hu et al., 2023) and the Lamb wave with its prominent air pressure amplitude (7 hPa or higher) were recorded—is recognized as a location where substantial amounts of Lamb wave

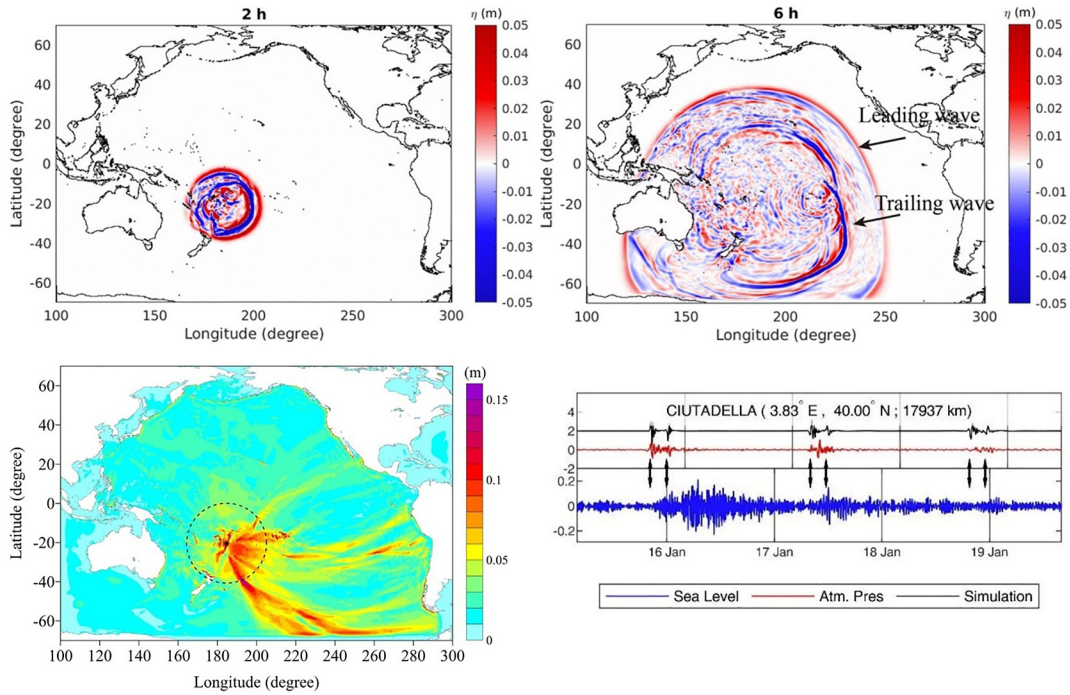

Figure 15. (up) Atmospheric Lamb wave-generated meteotsunami waves in the Pacific modeled 2 and 6 hr after the Hunga Tonga-Hunga Ha'apai explosive eruption of 15 January 2022, with (bottom left) maximum amplitudes (after Z. Y. Ren et al., 2023). The leading and trailing waves are representing the forced and free meteotsunami wave, respectively. (right bottom) Observed and simulated air pressure and measured sea level oscillations In Ciutadella (the Mediterranean Sea) with indicated arrival of Lamb waves (after Villalonga et al., 2023).

energy were transferred to the ocean through the Proudman resonance (Devlin et al., 2023). This occurs when the Froude number is slightly higher than or equal to 1. These forced waves then radiated out of the trench, mostly eastward, as free meteotsunami ocean waves (Yamashita & Kakimura, 2024). This phenomenon also applies to other deep trenches along the Pacific Rim, which potentially acted as sites for higher resonant energy transfer from the Lamb wave or as topographic amplifiers of the incoming meteotsunami waves (Devlin et al., 2023).

Notably, another forced meteotsunami wave generated by the slower Pekeris wave (traveling at approximately 230 m/s) in the atmosphere has also been documented along some Pacific shorelines, such as the Japanese coast (Suzuki et al., 2023). At some Japanese tide gauges, this wave was even larger, reaching 30 cm in crest-to-trough height and lagging approximately 2 hr behind the Lamb wave-generated forced meteotsunami wave. Although the Pekeris wave exhibited an order of magnitude weaker air pressure amplitude compared to the Lamb wave, its speed brought it into full Proudman resonance over oceans with depths of approximately 5,300 m, which is representative of substantial sections of the ocean between the HTHH volcano and Japan. As a result, a tenfold amplification of the Pekeris wave-generated meteotsunami through the Proudman resonance compensated for the tenfold lower air pressure of the Pekeris wave compared to the Lamb wave (Denamiel, Vasylkevych, et al., 2023).

Global and regional modeling and sensitivity studies have further provided intriguing insights into the HTHH 2022 event and beyond. Most studies aimed to reproduce the HTHH eruption-generated planetary meteotsunami wave event as accurately as possible, with some utilizing synthetic air pressure forcing functions fitted to observed amplitudes, periods, and propagation speeds of the atmospheric Lamb wave (Dogan et al., 2023; Omira et al., 2022; Yamashita & Kakimura, 2024). Others employed realistic atmospheric forcing for the ocean (Denamiel, Vasylkevych, et al., 2023), wherein the Lamb wave was simulated using atmospheric models that accounted for real air temperature variations and orography (Vasylkevych & Žagar, 2021), which influence wave dissipation, reflection, and refraction. These models almost perfectly replicated the timing of both Lamb and meteotsunami waves, and the modeled amplitudes were largely consistent with observed amplitudes at tide gauges. However, at locations with complex coastal bathymetry, meteotsunami amplitudes and sea level energy at higher frequencies were slightly underestimated, likely due to missing local bathymetry details in global models.

Using such a model and varying the speed of the atmospheric Lamb wave, the sensitivity of the world's oceans to resonance conditions has been quantified. Results suggest a tenfold increase in coastal runup from planetary meteotsunami waves—reaching levels of up to 10 m—if the atmospheric wave speed were 212 m/s (Denamiel, Vasylkevych, et al., 2023). At the speed of the Pekeris wave (230 m/s), the percentage of global oceans with Froude numbers between 0.9 and 1.1—conditions that substantially amplify forced meteotsunami waves through Proudman resonance—decreases by approximately 20% compared to a wave speed of 212 m/s. Under such conditions (a global Pekeris wave with an amplitude of several hectopascals), planetary meteotsunami waves could pose a significant hazard, with up to 4% of coastlines potentially experiencing maximum sea levels exceeding 1 m (Denamiel, Vasylkevych, et al., 2023). A simpler sensitivity study conducted by Yamashita & Kakimura (2023) derived global maximum wave maps based on bathymetry, reaching a similar conclusion: fully resonant conditions could significantly increase the global hazard posed by planetary meteotsunami waves, as observed during the HTHH event.

Regarding the depth of the ocean where the generation of planetary meteotsunami waves occurs, the effect of ocean compressibility can also be detected. However, this has little impact on solutions for a non-compressible ocean as represented by shallow-water equations (Das & Meylan, 2023; Pethiyagoda et al., 2024). It is also worth noting that atmospheric Lamb waves can be generated by other sources, such as bolides (ReVelle, 2008), asteroid explosions (Chyba et al., 1993), or thermonuclear bombs, and even by intrinsic atmospheric turbulence (Nishida et al., 2014). However, these sources typically produce amplitudes that are barely detectable by microbarographs and lack the potential to generate planetary meteotsunami waves.

10. Meteotsunami-Generated Vertically-Radiated Acoustic-Gravity Waves

As a tsunami propagates across the ocean, it generates atmospheric acoustic-gravity waves that propagate vertically (Artru et al., 2005; Figure 16). These waves travel vertically at a speed of approximately 50 m/s, amplify by several orders of magnitude, and reach the ionosphere (at heights of ∼350 km) in about 2 hr, causing perturbations in the electron density. Since such perturbations can be detected rapidly by ground-based Global Navigation Satellite Systems (GNSS), the detection of Total Electron Content (TEC) variability is currently being incorporated into early warning systems for natural hazards (Martire et al., 2023). The theory proposed by Godin et al. (2015) explains how long ocean waves generate acoustic-gravity waves, which must fall within a specific frequency range of 0.3–3 mHz (5–60 min) (Figure 16). At least in some geographical locations, it appears that the major contribution to thermosteric wave activity originates from long ocean waves (Zabotin et al., 2016).

Only a few studies have investigated the generation of vertical acoustic-gravity waves by strong meteotsunamis. Solovieva et al. (2021) documented that the multi-meteotsunami event that propagated over the Mediterranean between 23 and 27 June 2014 (as described by Šepić, Vilibić, Rabinovich, & Monserrat, 2015) was associated with strong ionization of the lower ionosphere. However, the authors did not attribute the generation of ionospheric waves solely to meteotsunami waves but also considered the upward propagation of acoustic-gravity waves triggered directly by strong convective storms accompanying the event, which can also generate significant ionospheric perturbations (Azeem & Barlage, 2018).

The first and only study to describe all phases of meteotsunami-generated upward propagation of acoustic-gravity waves, along with their observations using a variety of instruments and data sets, is by Vergados et al. (2023). Their observations showed an increase in wave amplitude as the waves approached the ionosphere, consistent with gravity wave linear theory (as described by Godin et al., 2015). This was accompanied by a progressive attenuation of higher frequencies and a clear detection of ∼15–25-min waves in TEC variability in the ionosphere (Figure 16). However, the travel time of such waves, from their generation to the ionosphere, was estimated to be approximately 8–9 hr, which is too long to make them viable for meteotsunami warning systems.

Regarding planetary meteotsunami waves generated by explosive volcanic eruptions, the HTHH event of 15 January 2022 was also associated with TEC variability lagging behind the ocean waves. Aside from the direct manifestations during the passage of Lamb waves (as discussed in Section 9), the delay between the atmospheric Lamb wave and the second peak in TEC (the first peak was associated with the Lamb wave) was approximately 2 hr around New Zealand. This supports the hypothesis that the delayed ionospheric response was caused by planetary meteotsunami waves triggering upward-propagating acoustic-gravity waves (Muafiry et al., 2023). Similar observations have been documented over China (Q. Z. Li et al., 2024). However, accurately quantifying these waves and distinguishing their effects from other TEC variability drivers remains a challenge.

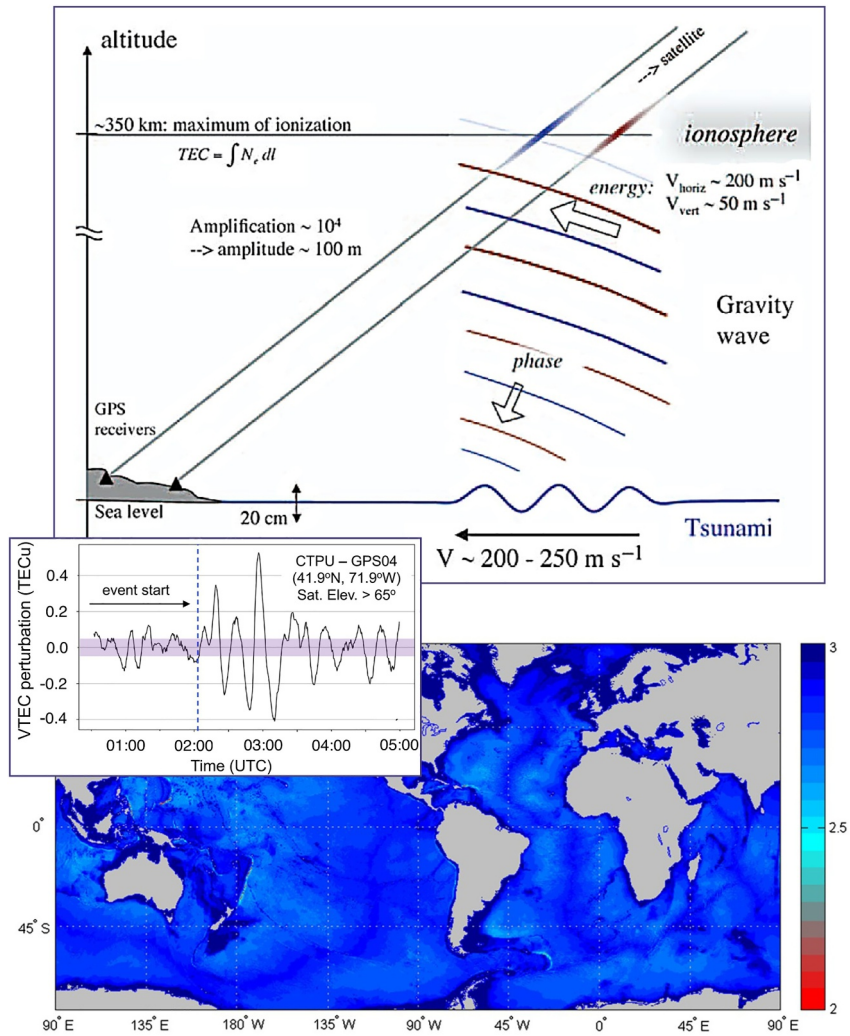

Figure 16. (up) A scheme of generation mechanism and propagation of acoustic-gravity waves radiated upward by tsunamis (after Artru et al., 2005). (bottom) The transition frequency (in mHz), that is, the frequency below which the long ocean waves are continuously radiating acoustic-gravity waves into the upper atmosphere (following the theory by and taken from Godin et al., 2015). Middle inset: Time series of Total Electron Content perturbations measured at a single Global Navigation Satellite Systems ground station on 13 June 2013, and being the consequence of a derecho-generated meteotsunami (after Vergados et al., 2023).

11. Research Gaps and Perspectives

As evident from the review, many aspects of research into meteotsunamis and high-frequency sea level oscillations remain underexplored or entirely unexamined. The current state-of-the-art in observations, modeling, data processing, and other challenges is hindering faster progress, similar to other scientific fields. Furthermore, each new discovery or answer about these natural phenomena raises additional questions for further investigation. In this context, we outline some of the most critical areas where advancements could significantly contribute to meteotsunami science, serving as a guide for future research activities within the community.

11.1. Challenges and Advancements in Observing Meteotsunamis

11.1.1. Sea Level Observations

Observing sea levels with a resolution of 1 minute or higher has become standard in many national monitoring systems (e.g., NOAA, Angove et al., 2021; Puertos del Estado, Pérez Gómez et al., 2022). The collection of minute-resolution sea level data was globally initiated in 2005 following the Sumatra-Andaman earthquake and

tsunami (Fujii & Satake, 2007) through the UNESCO IOC SLSMF portal (https://www.ioc-sealevelmonitoring.org, VLIZ/IOC, 2025). As of 9 January 2025, the portal hosted data from 1,249 active tide gauge stations. However, some national tide gauge networks still do not provide minute-resolution data, adhering instead to "traditional" sampling intervals. For example, the UK national sea level network continues to provide data with a 15-min resolution (NTSLF, 2025), which does not meet the standards required for meteotsunami research as it may significantly underestimate meteotsunami heights (Ozsoy et al., 2016; Tsimplis et al., 2009). Combining sea level measurements with varying sampling resolutions may lead to biased quantifications of meteotsunami and NSLOTT heights, necessitating careful consideration when merging such data sets (Heidarzadeh et al., 2024; Williams, Schultz, et al., 2021).

Another limitation of the SLSMF portal is the lack of quality control applied to the available data, as it is primarily designed for operational use (the portal currently develops automatic quality-control procedures to provide certain level of research-quality data). The creation of the MISELA quality-control data set (Zemunik et al., 2021a) revealed significant issues, such as spikes, offsets, reference shifts, scaling problems, and time shifts, particularly in data from stations maintained by agencies lacking resources for proper network upkeep. Many problematic stations are located in Africa and small oceanic islands—regions with generally sparse sea level measurements, even on an hourly scale. This highlights a key challenge for the sea level research community: densifying sea level networks in regions without existing stations (Woodworth, 1991; Woodworth et al., 2007).

The spatial undersampling of meteotsunamis by tide gauges is another limitation for observation-based studies. Tsunamigenic atmospheric disturbances typically occur over scales of a few to a few hundred kilometers, with coastal bathymetry significantly modulating the signal. Consequently, sea level oscillations can vary greatly over short distances, such as inside versus outside a bay or harbor. While no tide gauge network can capture all sea level variations, localized networks can be established using low-cost instruments (see Section 3.1), such as the VENOM network covering the Balearic Islands (Frank-Comas et al., 2021; Ramos-Alcántara et al., 2025). Similar approaches could be implemented in other meteotsunami hotspots, such as further densifying the MESSI tide gauge network in the middle Adriatic (Šepić et al., 2017; Vilibić et al., 2021), along the Korean coastline (J. Kim & Woo, 2021), or in other comparable locations.

Additionally, the longest minute-resolution data series span approximately 20 years, whereas the recurrence intervals of the most devastating meteotsunamis are on the scale of several decades or even centuries (Jansà & Ramis, 2021; Orlić, 2015). As a result, existing minute-resolution sea level data are insufficient for accurately quantifying meteotsunami hazards or estimating regional probability density functions (Geist et al., 2014).

Another challenge is the lack of public availability of minute-resolution sea level data from some providers. For instance, the Croatian Hydrographic Institute possesses high-quality, long-term minute-resolution data suitable for analyzing NSLOTTs (Ruić et al., 2023; Vilibić, Domijan, & Čupić, 2005; Vilibić, Orlić, et al., 2005), but this data is not publicly accessible. Similarly, minute-resolution data from Russian tide gauges (Kulikov et al., 2020), eastern Baltic tide gauges, and coastal China (S. W. Zhang et al., 2024) remain restricted. Adhering to FAIR (Findability, Accessibility, Interoperability, and Reuse) principles (Wilkinson et al., 2016) is essential for meaningful global or regional meteotsunami research.

In summary, regarding sea level observation standards for meteotsunami research, we recommend the following: (a) increasing the resolution of sea level measurements to 1 min or higher at all tide gauge stations, (b) ensuring the long-term maintenance of minute-resolution tide gauge networks (spanning at least several decades) with rigorous data quality control by providers, (c) making all sea level data accessible to the research community in alignment with FAIR principles, (d) establishing a centralized repository for accessing quality-controlled minute-resolution sea level data, incorporating additional harmonized quality-control procedures, and (e) conducting localized meteotsunami experiments with ultra-dense tide gauge networks wherever feasible.

11.1.2. "Classic" and Modern Atmospheric Observations

Since meteotsunamis are generated by rapid and intense changes in atmospheric pressure or wind disturbances traveling over a region, measuring these parameters at tide gauge sites should also be conducted with a sampling resolution of 1 min or higher. However, this requirement exceeds the current standards and recommendations for measurements at ground stations managed by national weather services, where data is typically stored at 10-min

or hourly intervals. This is despite the availability of technology capable of measuring and transmitting real-time meteorological information with minute-level resolution. Addressing the need to monitor meteotsunamigenic atmospheric disturbances could provide a compelling reason to push the World Meteorological Organization (WMO) to update standards for in situ measurements. Such updates would be particularly significant if operational forecasting of meteotsunamis were to become the responsibility of national weather services, as currently proposed by some committees (UNESCO/IOC, 2025).

In addition to national networks, many amateur meteorological networks have been developed in various regions and countries to study mesoscale phenomena. These networks often measure local meteorological parameters with lower quality and without the standardization of regular meteorological networks (Bell et al., 2013; Brousse et al., 2024; J. Y. Chen et al., 2021; Mitchell & Fry, 2024). While a wide range of instruments monitor meteorological parameters, some may be suitable for meteotsunami research if they meet the necessary precision and temporal resolution. For example, the BalearsMeteo amateur meteorological network (http://balearsmeteo.com) comprises approximately 55 stations across Mallorca Island that sample at sub-minute intervals with a resolution of 0.1 hPa. This level of precision and temporal resolution is sufficient to capture tsunamigenic air pressure disturbances and their spatial and temporal variability over small scales (a few kilometers) (Villalonga et al., 2024). Another example is the Victoria School network managed by schools in the Victoria area of British Columbia, Canada (https://www.victoriaweather.ca), which have been used to analyze tsunamigenic disturbances and improve the forcing of ocean models (Rabinovich et al., 2021). Establishing minimum requirements for both regular and amateur meteorological networks would enhance their utility in meteotsunami research.

Beyond ground-based stations, remote sensing techniques have recently been used to quantify tsunamigenic atmospheric disturbances. This includes the use of satellite imagery and weather radars to analyze strong convective systems, their speed, direction, and variability (Feng et al., 2021; Robledo et al., 2024). Recent studies have also linked tropical cyclones to meteotsunamis (e.g., Anarde et al., 2021; Heidarzadeh & Rabinovich, 2021; Rabinovich et al., 2023), suggesting that monitoring fine-scale features such as rainbands associated with atmospheric disturbances (Shi et al., 2020) could provide insights into mesoscale interactions between atmospheric and oceanic processes. Moreover, significant progress has been made in mapping upper atmosphere conditions, including the development of products for assessing electron content in the ionosphere (Martire et al., 2024). This may help evaluate whether meteotsunamis significantly affect electron variations or have negligible impacts.

To advance atmospheric measurements for meteotsunami research, we recommend the following: (a) establishing a standard sampling rate of 1 min at automatic meteorological stations, including those managed by national weather services and amateur networks, (b) further researching and developing methodologies to extract tsunamigenic parameters (or general wind and pressure changes) from remote sensing observations while aiming to reduce sampling intervals where feasible (e.g., achieving at least 5-min intervals for weather radar observations), and (c) building reliable connections and statistical frameworks to analyze the effects of meteotsunamis on the upper atmosphere and ionosphere, incorporating both atmospheric and sea level data products.

11.2. Reproducing Meteotsunamis for Efficient Forecasting and Hazard Assessment

11.2.1. Atmosphere-Ocean Numerical Modeling

Modeling meteotsunami events has always been challenging, as current atmospheric models struggle to adequately reproduce the relevant physical processes and meet the resolution requirements necessary for capturing the scales of atmospheric disturbances. The first successful reproduction of a tsunamigenic atmospheric disturbance was achieved in 2007 (Belušić et al., 2007). However, it only demonstrated the existence of the disturbance, while key characteristics such as pressure rates of change exceeding 2.5 hPa over 5 min—critical for driving meteotsunami intensity (Šepić & Vilibić, 2011)—were significantly underestimated. Furthermore, approximately half of the disturbance was missing in the simulations. This issue partly stems from selecting the appropriate parameterizations in atmospheric models (Horvath & Vilibić, 2014; Mourre et al., 2021) and is possibility also effected by inclusion or exclusion of air-sea coupling and waves into the modeling system (e.g., Rahimian et al., 2022). Additionally, insufficient resolution typically results in underestimation of energy for wavelengths below approximately seven times the horizontal resolution (Skamarock, 2004). Even when increasing resolution to 1 km or 500 m in widely used atmospheric models like the Weather Research and Forecasting (WRF) model (Skamarock et al., 2005), the reliability of simulations often remains inadequate for precisely simulating observed air pressure disturbances (Anderson & Mann, 2021; Denamiel, Šepić, Ivanković, &

Vilibić, 2019; Horvath et al., 2018; Rahimian et al., 2022). Consequently, the forcing of ocean models has often relied on synthetic forms of atmospheric pressure disturbances (e.g., cosine, bell-shaped, or boxcar functions) propagating with constant speed, direction, and rate of air pressure change (C. F. Huang et al., 2022; Ličer et al., 2017; Orlić et al., 2010; Vilibić, 2005).

Recent advancements leveraging GPU technology and machine learning algorithms have enabled downscaling to higher resolutions, improved physics—particularly microphysics—and reduced computational demands (Dowell et al., 2022; M. Huang et al., 2015; Kochkov et al., 2024; Muñoz-Esparza et al., 2022; Reynolds et al., 2023; Sauer et al., 2024; Welch et al., 2024). These advancements may overcome the challenges of accurately reproducing tsunamigenic disturbances. Additionally, stochastic surrogate modeling and machine learning algorithms offer potential improvements in meteotsunami reproduction (Denamiel, Šepić, Huan, et al., 2019; Metličić et al., 2024; Vich & Romero, 2021). However, these approaches face the challenge of limited data length. Probabilistic functions in surrogate modeling and machine learning-based meteotsunami forecasting struggle to align with observations due to the insufficient length of minute-resolution data or time spans of cataloged meteotsunami events relative to the return periods of significant meteotsunami events, predominantly underestimating the intensity of the strongest meteotsunami events.

Coastal regions with ridges or submarine canyons present challenges in ocean modeling, as wave transformation processes are highly dependent on rapidly changing nearshore topography. For tsunamis, coastal resolutions of 10–50 m are generally sufficient for reliable modeling along coastlines (Felix et al., 2024). However, even these resolutions may be inadequate for narrow bays just tens of meters wide, such as the Ciutadella inlet (Vilibić et al., 2008). Furthermore, bathymetric changes over small spatial scales can generate rip currents that pose safety risks to swimmers (Linares et al., 2019; Yuan et al., 2023). Accurate coastal modeling thus requires detailed and regularly updated bathymetry data (Latifah et al., 2024; Miyashita et al., 2022). Coastal variability may also exhibit strong interannual and decadal variations, necessitating quasi-continuous bathymetric surveys in meteotsunami-prone areas (Costa et al., 2023; Zhao & Bai, 2024). Open-ocean models with resolutions of O (100 m) or finer are needed to capture resonant processes in both oceanic and atmospheric domains. New-generation ocean models have these capabilities (e.g., Fan et al., 2024; Silvestri et al., 2024), making them suitable for coupling with high-resolution atmospheric models to realistically reproduce tsunamigenic atmospheric disturbances and the transfer of energy to meteotsunami waves.

Many of the numerical modeling approaches presented here require substantial computational resources. For example, running the full AdriSC operational modeling suite for a 3-day period—consisting of a basic module with innermost atmospheric and oceanic resolutions of 3 and 1 km, respectively, and a nearshore module with 1.5 km atmospheric resolution and an unstructured ocean grid of up to 10 m—required almost 22 hr on 260 CPUs at the supercomputing facilities of the European Center for Medium-Range Weather Forecasts (ECMWF; Denamiel, Šepić, Ivanković, & Vilibić, 2019). This raises the question of system efficiency, given that accuracy is still lacking—the same issue was encountered when implementing the BRIFS system in the Balearic Islands (Mourre et al., 2021). For that reason, simplified approaches to quantify tsunamigenic atmospheric disturbances may increase model efficiency (e.g., Romero et al., 2019).

In our view, downscaling fully coupled models to very high resolutions and including complex parameterization schemes is not a feasible option for operational systems. However, such approaches remain essential for advancing research into atmospheric and oceanic processes at high resolutions, which are crucial for understanding meteotsunami generation and dynamics. Indeed, because of their complexity, meteotsunamis—like other extreme and small-scale events (e.g., Hewitt et al., 2017; Lee et al., 2025)—offer an excellent framework for testing new modeling approaches in both the atmosphere and the ocean, such as parameterizations operable at fine temporal and spatial scales. In this way, high-resolution modeling can continue to improve.

To advance atmosphere-ocean numerical modeling of meteotsunamis, we recommend the following: (a) downscaling both atmospheric and ocean models to resolutions of at least O(100 m) in meteotsunami generation areas, ensuring the physics are preserved (in model parameterizations) at these resolutions. Ocean models should further resolve coastal processes with even higher resolutions O(10 m), (b) setting boundary conditions sufficiently far from the generation area, derived from global products with resolutions of at least O(10 km) or finer, (c) ensuring nearshore bathymetry data is of high quality and surveyed on a quasi-regular basis, tailored to local coastal morphology, (d) utilizing advanced computational technologies, such as GPUs, to optimize modeling efficiency and manage computational demands, (e) optimizing the efficiency and accuracy of various numerical

modeling setups for meteotsunamis through systematic comparison of approaches, with the aim of achieving the best performance while accounting for substantial computational demands, and (f) investing in stochastic, surrogate, and machine learning approaches to improve the estimation of threshold exceedance probabilities, particularly by refining input probability functions for meteotsunamigenic parameters.

11.2.2. Climate Modeling and Projecting Meteotsunamis

For climate projections, global climate models (GCMs) remain one to two orders of magnitude coarser than required for meteotsunami modeling, although advancements in resolution and physics are rapidly progressing (Planchat et al., 2023). For example, storm surge projections typically require resolutions of O(10 km) (Bernier et al., 2024; Muis et al., 2020). Meanwhile, regional climate projections have achieved atmospheric resolutions of approximately 1–3 km (Ban et al., 2021; Belušić et al., 2020; Lagergren et al., 2024), still falling short of meteotsunami modeling prerequisites. GPU-based models may offer a pathway to improving cloud process representation, a major uncertainty in climate simulations (Norman et al., 2022). Until climate models reach sub-kilometer resolutions, two approaches remain viable: (a) establishing reliable connections between synoptic patterns reproducible by climate models and meteotsunami events, and (b) conducting numerous short-term, high-resolution simulations using pseudo-global warming methodologies, as demonstrated in dynamic downscaling efforts (Hall et al., 2024). Such approaches have shown a potential for implementation in specific locations like the Adriatic Sea (Zemunik Selak et al., 2025). Initiatives like the Global Coastal Ocean Model Intercomparison Programme could also help establish standards for meteotsunami and process-oriented climate projections (NOC, 2025).

11.2.3. Establishing Operational Meteotsunami Early Warning Systems

Despite decades of progress in meteotsunami research, including geographic expansion, enhanced observational capabilities, and the use of modeling tools—the only fully operational meteotsunami forecasting and early warning systems remains these established in 1985 in the Balearic Islands by the national meteorological agency (AEMET) (Jansà & Ramis, 2021; UNESCO/IOC, 2025) and later upgraded using atmosphere-ocean models (BRIFS, Mourre et al., 2021; TRAM, Romero et al., 2019). While there have been attempts to establish reliable meteotsunami forecasting systems, these efforts have primarily been driven by research projects and have not resulted in long-term operational systems. For example, the MESSI project in the Adriatic (Šepić et al., 2017) and the TMEWS project along the U.S. East Coast (Angove et al., 2021; Vilibić, Monserrat, & Rabinovich, 2014) aimed to address this gap. However, the MESSI project lasted only 2 years, which was insufficient to develop all the necessary modules for a comprehensive Croatian meteotsunami forecasting and early warning system, and was not adopted by the national weather service for its maintenance. Similarly, the TMEWS project was discontinued after its first year due to budgetary constraints, leaving key components unimplemented.

Furthermore, the implementation of machine learning and neural network algorithms into meteotsunami forecasting systems has been tested (Vich & Romero, 2021) and has achieved reliability comparable to that of "classical" operational systems, offering another avenue for the development of operational early warning systems for meteotsunamis. In our view, however, the current level of data availability and process-oriented knowledge is not yet sufficient for the implementation of machine learning algorithms without human intervention and interpretation. Nevertheless, this remains a promising field of future research, already implemented in some hazards in geosciences (e.g., Flora et al., 2021; Z. F. Li et al., 2018), which may ultimately lead to a meteotsunami warning system capable of automatically forecasting events with an appropriate level of reliability.

To address these challenges, a clear set of recommendations can be derived from UNESCO/IOC (2025): (a) ensure the long-term sustainability of existing pilot meteotsunami warning systems (e.g., for the Adriatic, Denamiel, Šepić, Huan, et al., 2019; Denamiel, Šepić, Ivanković, & Vilibić, 2019; Denamiel et al., 2020) by integrating meteotsunami forecasting and early warning systems into the responsibilities of national weather services, (b) strengthen coordination between national weather services and the global tsunami warning system, (c) incorporate machine learning procedures for better forecasting of meteotsunami events, with its implementation into the decision-making process as well, and (d) develop and implement real-time standard operational procedures, including well-defined protocols for forecasting, detection, and the dissemination of meteotsunami forecasts to relevant services and the public.

11.2.4. Quantifying Reliability of Operational Meteotsunami Early Warning Systems

Once established, the reliability of operational early warning systems—such as the AEMET Balearic Islands system (Jansà & Ramis, 2021)—should be tested both at the outset and periodically to ensure optimal performance. This should also involve evaluating different system configurations for the same sets of events or within the same region, and comparing their performance—for example, a synoptic index–based approach versus a system relying on high-resolution atmosphere–ocean modeling, surrogate stochastic modeling, simplified numerical modeling, or machine learning algorithms. Some intercomparisons between deterministic and stochastic modeling approaches have been conducted for the Adriatic Sea (Denamiel, Šepić, Huan, et al., 2019), though only during the testing phase of the operational system. Further, the rissaga early warning system include both assessment of tsunamigenic atmospheric synoptic systems and atmosphere-ocean numerical modeling. However, no multi-architecture operational systems have been implemented or assessed at any other meteotsunami hotspot.

11.3. Process-Level Studies (a Selection)

As meteotsunami science has expanded in many directions over the last decades, the range of topics available for research has become quite broad. Some of these topics are already mentioned in Sections 11.1 and 11.2. Here, we extend the list and highlight some important aspects of meteotsunamis (this is by no means an exhaustive list) that we believe warrant further studies by the community.

11.3.1. Source Processes for Tsunamigenic Atmospheric Disturbances

Although the generation of AGWs (Plougonven & Zhang, 2014; Sibley et al., 2021; Vilibić, Horvath, et al., 2014), squall lines (Lu et al., 1997; Meng et al., 2013), mesoscale convective systems (Houze, 2004; Stensrud & Fritsch, 1994), and other atmospheric phenomena responsible for meteotsunamis is relatively well understood, the conditions necessary for their persistence over tens or hundreds of kilometers (e.g., wave ducting, Lindzen & Tung, 1976; Monserrat & Thorpe, 1996, or wave-CISK, Convective Instability of the Second Kind, Belušić et al., 2007; Xu & Clark, 1984) remain less explored. Observational and modeling limitations (discussed in Sections 11.1 and 11.2) hinder precise quantification of these phenomena, particularly their intensity and dissipation. Studying source mechanisms using state-of-the-art observational systems and atmospheric models could significantly enhance our understanding of meteotsunamigenic disturbances and their predictability.

11.3.2. Connecting Remote Sensing Measurements With Meteotsunamigenic Variables

Advances in weather radar performance and products (e.g., Michelson et al., 2020) allow for precise determination of the intensity, speed, and direction of potential tsunamigenic atmospheric disturbances (Anderson et al., 2015; Wertman et al., 2014). However, the connection between radar and satellite variables and ultra-dense microbarograph or meteorological networks has yet to be fully realized. This connection could now be established, as both dense ground networks and weather radars are becoming increasingly available (e.g., Hallali et al., 2016; J. J. Zhang et al., 2024). Successful calibration of these systems could facilitate tracking potential tsunamigenic atmospheric disturbances over coastal waters and help quantify meteotsunamigenic variables in areas lacking ground measurements (e.g., the 2017 Dayyer meteotsunami, Kazeminezhad et al., 2021). A similar approach could be applied to state-of-the-art satellite products, particularly those estimating cloud-top speeds, which may correspond to atmospheric disturbance velocities (Vilibić et al., 2010).

11.3.3. Quantifying Resonances and Bathymetry Effects

The theory underlying Proudman and Greenspan resonances was established decades ago. However, aside from few theoretical studies (e.g., Benjamin, 2015; Vennell, 2007, 2010; Williams, Horsburgh, et al., 2021), their roles in complex coastal environments remain poorly quantified. Many studies cite resonance mechanisms but lack computational evidence of their contributions. For instance, studies introducing the Proudman length (see Section 4.1.1) often reveal a mismatch between expected and modeled effects in complex environments such as the middle Adriatic Sea (Šepić, Međugorac, et al., 2016). When tsunamigenic atmospheric disturbances traverse coastal slopes with attached shelves (e.g., Bechle et al., 2015; Memmola et al., 2024; Wijeratne & Pattiaratchi, 2024) or when flat shelves transition to submarine slopes (Dusek et al., 2019; Šepić, Rabinovich, & Sytov, 2018), interactions between Greenspan and Proudman resonances, as well as eigen oscillations due to bathymetric changes, may occur. It is a question do we fully grasp the nature of resonant energy transfer in real-

world bathymetries, where multiple types of resonance may overlap and interact. Investigating these processes in greater detail could help explain why some regions are more prone to meteotsunamis than others.

11.3.4. Enhancing the Robustness of Meteotsunami Statistics

Robust statistics require long data sets. In the case of sea level observations at minute timescales, data sets spanning two decades now exist in some locations or local networks (see Section 3.1). Coarser-resolution data sets, such as 15-min data along the UK coastline, are even longer. Global coverage of such observations is also improving, while minute sea level research products (e.g., the MISELA data set, Zemunik et al., 2021a, 2021b) are becoming available and are planned to be extended. This growing data pool can enhance meteotsunami/NSLOTT statistics by extending analyses (documented in Sections 3 and 7) or by applying novel methods, such as Bayesian approaches to extreme sea level estimation (Calafat & Marcos, 2020; Choblet et al., 2014).

Additionally, clustering synoptic patterns globally, as performed for the Adriatic Sea (Ruić et al., 2024), may identify differences in intensity, frequency, and spatial coverage of meteotsunamis under varying conditions. Such clustering may globally document differences in the intensity, frequency and spatial distribution of so-called summer- or winter-type of meteotsunamis, or even reveal new types of meteotsunamis. Substantial number of global or regional cataloged events, such as these reported by Rabinovich (2020) or catalogs reported in Section 5.5, may be also used for clustering and end in a quantitative distinction between meteotsunami classes. Then, the synoptic clusters might be connected to source processes that normally differ between them (e.g., Pellikka et al., 2022). This is particularly important as meteotsunami hazard and risk is different for various meteotsunami classes and may help in developing class-based meteotsunami warning systems.

11.3.5. Developing Methodologies for Meteotsunamis Hazard and Risk Assessment

Estimating the level of coastal natural hazard at a specific location or along coastlines is challenging for hazards with large recurrence periods but is essential for many applications. For tsunamis, probabilistic tsunami hazard analysis has recently become a standard technique (e.g., Geist & Parsons, 2006; Grezio et al., 2017). For meteotsunamis, the only such study was conducted for the US East Coast (Geist et al., 2014), analyzing 14 years of data with a 6-min resolution. As minute-scale data series expand and achieve higher resolution in different ocean and coastal regions, this methodology could be extended and applied locally in areas where meteotsunami and high-frequency sea level data are regularly monitored. Stochastic surrogate modeling approaches might be particularly useful, as decreasing computational power needed for simulations while keeping the robustness of the hazard estimates (Denamiel, Šepić, Huan, et al., 2019, 2025). The same holds for machine learning techniques, which, e.g., outperform "classic" modeling approaches in storm surges forecasts (e.g., Rus et al., 2025), while being a promising tool in forecasting of NSLOTTs and meteotsunamis (Međugorac et al., 2025) although underestimating the strongest events.

11.3.6. Implementing Climate Projections of Meteotsunami Hazards

Assessing meteotsunami hazards in future climates largely depends on establishing a connection between meteotsunamis and synoptic patterns, as described in Section 7. A key prerequisite—outlined in Vilibić et al. (2018) and Denamiel, Belušić, et al. (2023)—is the establishment of a significant relationship between synoptic patterns and meteotsunamis/NSLOTTs. However, this connection is already known to be unreliable in certain parts of the Mediterranean and for the most severe events (Šepić, Vilibić, & Monserrat, 2016; Zemunik Selak et al., 2025). With progress in clustering synoptic patterns and meteotsunamis/NSLOTTs, the next logical step in the research presented in Section 8.3 would be the application of the proposed methodologies. This includes quantifying a synoptic-based meteotsunami index, with or without further downscaling of climate projections to (sub-)kilometer scales, in various regions of the world's oceans.

11.3.7. Hazard Assessment for Planetary Meteotsunami Events

The HTHH eruption in January 2022 confirmed the existence of planetary meteotsunami waves, which were already suspected to have followed after the 1883 Krakatau eruption (see Section 9). However, the HTHH event is the only one on which such research currently exists, while it might appear at many volcanic locations (Denamiel et al., 2025). Many questions emerge from this research, such as: (a) What conditions must be met to generate acoustic-gravity Lamb waves that can produce planetary meteotsunamis? (b) Does the shape of the explosion

impact the strength of planetary meteotsunami waves, particularly in relation to the rate of change in air pressure, which has been found to be important for other types of meteotsunamis? (c) How important is the geographical location of the explosion for determining the height of planetary meteotsunami waves? (d) Can explosive volcanic eruptions generate significantly stronger planetary meteotsunami waves? (e) Is it possible for the Pekeris mode of acoustic-gravity waves to become much more intense under certain atmospheric and eruption conditions, as its speed aligns with resonant conditions across much of the oceans? (f) Can other catastrophic natural hazards, such as asteroid explosions (e.g., Chicxulub; Range et al., 2022; Racki & Koeberl, 2024), generate planetary meteotsunami waves?

11.3.8. Assessing Connectivity Between Meteotsunamis and Ionospheric Processes

The connection between meteotsunamis and ionospheric disturbances is a relatively recent finding, with only one documented case of meteotsunami-generated vertical acoustic waves causing fluctuations in the total electron content (TEC) in the ionosphere (Vergados et al., 2023). Therefore, further case studies are needed to determine if this phenomenon occurs at other meteotsunami hotspots around the globe. Furthermore, global TEC products are continually improving in resolution and spatial coverage (Martire et al., 2024; Smith et al., 2024), while global and regional catalogs of meteotsunamis or repositories of NSLOTTs already exist (e.g., Dusek et al., 2019; Lewis et al., 2023; Šepić & Orlić, 2025a; Pasquet et al., 2013; Zemunik et al., 2021a, 2021b). This advancement enables research—at pointwise, regional, and global scales—to statistically evaluate the connectivity and quantify whether NSLOTTs, including meteotsunamis, are significant sources of TEC variability or not.

12. Summary and Outlook

In this review, we recapitulate the state-of-the-art across all segments of meteotsunami science—atmospherically induced long ocean waves in the tsunami frequency band. We hope this review will boost research activities on this phenomenon by presenting a (non-exhaustive) list of ideas for future progress in the meteotsunami community. Furthermore, since meteotsunamis significantly contribute to sea level extremes—reaching magnitudes comparable to other processes such as storm surges or seasonal sea level variations in some regions—this review aims to strengthen collaboration between the broader sea level and meteotsunami communities, which are currently sparse and non-systematic. The ultimate goal is to integrate meteotsunami estimates into global extreme sea level assessments, enabling a more comprehensive evaluation of all contributing processes in this era of rapid climate change and accelerated sea level rise (J. P. Wang et al., 2021).

Achieving this goal is challenging due to limitations in observations, numerical modeling tools, and the nature of meteotsunamis, which are highly variable in time and space. These challenges are influenced by several factors, such as (a) the resolution and parameterizations of atmospheric models—particularly climate models—which are not yet capable of reliably reproducing tsunamigenic atmospheric disturbances; and (b) inaccuracies in coastal bathymetry, which can significantly alter model predictions of meteotsunami wave amplification. Even minor changes (e.g., 5%–10%) in water depth or the speed of an atmospheric disturbance may double or halve the predicted meteotsunami wave height near shorelines. Developing improved modeling solutions for both the atmosphere and ocean will help address these challenges and enhance models' applicability to a wider range of unresolved processes. These include the reproduction of mesoscale convective systems in the atmosphere (Schumacher & Rasmussen, 2020) or the intensity and occurrence of oceanic surface currents and rip currents, which can pose risks to coastal safety.

This review is also directed at coastal engineers, managers, and operational services responsible for planning, governance, and alerting local populations about hazardous events in coastal zones. Building more resilient coastlines is of utmost importance in the era of climate change, and strategies for mitigating meteotsunami impacts—similar to those for other extreme sea level events—do exist. As with other meteorologically driven hazards, one of the key goals of meteotsunami science is to incorporate meteotsunamis into coastal hazard early warning systems, either through national and international ocean services (such as tsunami warning systems; Igarashi et al., 2011; Rafliana et al., 2022) or through national weather services. An expert group (UNESCO/IOC, 2025) has proposed that weather services are particularly suitable for this role, as they exist in all countries and have standardized procedures for forecasting and issuing hazard alerts (e.g., through the MeteoAlarm service, https://meteoalarm.org). We hope this review will help bridge the gap between meteotsunami research and its practical applications in coastal hazard and risk management.

Conflict of Interest

The authors declare no conflicts of interest relevant to this study.

Data Availability Statement

Sea level data presented in Figure 2 have been obtained from the IOC Sea Level Station Monitoring Facility (SLSMF, https://www.ioc-sealevelmonitoring.org). The time series presented in Figures 5 and 6 (Panama City Beach and Atlantic City tide gauges) were obtained from NOAA/NOS CO-OPS (https://tidesandcurrents.noaa.gov/tsunami). The Stari Grad and Vrboska time series were obtained from the Institute of Oceanography and Fisheries (Split, Croatia; http://faust.izor.hr/autodatapub/postaje). The Atlantic City air pressure series were obtained from the Automated Surface Observing Systems (ASOS; https://mesonet.agron.iastate.edu/request/download.phtml).

Acknowledgments
To all meteotsunami researchers for their seminal contributions through decades, which helped in understanding of this potentially destructive phenomenon. The thorough review carried out by two anonymous reviewers greatly improved the quality of the article. The research has been supported by Croatian Science Foundation through projects GLOMETS (Grant IP-2022-10-3064), C3PO (Grant IP-2022-10-9139), CroClimExtremes (Grant IP-2022-10-4144) and StVar-Adri (Grant IP-2019-04-5875), the Horizon 2020 project SHExtreme (Grant ERC-StG-853045) and Horizon Europe project MeD-Track (Grant ERC-PoC-101213756), and the project KLIMADRIA funded by the European Union—NextGenerationEU. Open access publishing facilitated by Institut Ruđer Bošković, as part of the Wiley - National and University Library in Zagreb Consortium Croatian Academic and Research Libraries Consortium agreement.

References

Airy, G. B. (1878). On the tides on Malta. *Philosophical Transactions of the Royal Society of London*, *169*, 123–138. https://doi.org/10.1098/rstl.1878.0006

Akamatsu, H. (1982). On seiches in Nagasaki Bay. *Papers in Meteorology and Geophysics*, *33*(2), 95–115. (in Japanese). https://doi.org/10.2467/mripapers.33.95

Alfonso-Sosa, E. (2016). Naples Meteotsunami on January 17, 2016. In *Ocean physics education, 16-Feb-16, technical report*. https://doi.org/10.13140/rg.2.2.26518.75840

Allan, J. C., Komar, P. D., Ruggiero, P., & Witter, R. (2012). The March 2011 Tohoku tsunami and its impacts along the US West Coast. *Journal of Coastal Research*, *28*, 1142–1153.

Amato, A. (2014). Some reflections on tsunami Early Warning Systems and their impact, with a look at the NEAMTWS. *Bolletino di Geofisica Teorica ed Applicata*, *61*, 403–420. https://doi.org/10.4430/bgta0329

Anarde, K., Cheng, W., Tissier, M., Figlus, J., & Horrillo, J. (2021). Meteotsunamis accompanying tropical cyclone rainbands during hurricane Harvey. *Journal of Geophysical Research: Oceans*, *126*(1), e2020JC016347. https://doi.org/10.1029/2020JC016347

Anderson, E. J., Bechle, A. J., Wu, C. H., Schwab, D. J., Mann, G. E., & Lombardy, K. A. (2015). Reconstruction of a meteotsunami in Lake Erie on May 27, 2012: Roles of atmospheric conditions on hydrodynamic response in enclosed basins. *Journal of Geophysical Research: Oceans*, *120*(12), 8020–8038. https://doi.org/10.1002/2015JC010883

Anderson, E. J., & Mann, G. E. (2021). A high-amplitude atmospheric inertia-gravity wave-induced meteotsunami in Lake Michigan. *Natural Hazards*, *106*(2), 1489–1501. https://doi.org/10.1007/s11069-020-04195-2

Angove, M., Kozlosky, L., Chu, P., Dusek, G., Mann, G., Anderson, E. J., et al. (2021). Addressing the meteotsunami risk in the United States. *Natural Hazards*, *106*(2), 1467–1487. https://doi.org/10.1007/s11069-020-04499-3

Anup, N., Rohith, B., Vijith, V., Rose, L., Sreeraj, P., Sabu, A., et al. (2024). Volcanic eruption triggers a rare meteotsunami in the Indian Ocean. *Geophysical Research Letters*, *51*(2), e2023GL108036. https://doi.org/10.1029/2023GL108036

Arbic, B. K., St-Laurent, P., Sutherland, G., & Garrett, C. (2007). On the resonance and influence of the tides in Ungava Bay and Hudson Strait. *Geophysical Research Letters*, *34*(17), L17606. https://doi.org/10.1029/2007GL030845

Artru, J., Ducic, V., Kanamori, H., Lognonné, P., & Murakami, M. (2005). Ionospheric detection of gravity waves induced by tsunamis. *Geophysical Journal International*, *160*(3), 840–848. https://doi.org/10.1111/j.1365-246X.2005.02552.x

Azeem, I., & Barlage, M. (2018). Atmosphere-ionosphere coupling from convectively generated gravity waves. *Advances in Space Research*, *61*(7), 1931–1941. https://doi.org/10.1016/j.asr.2017.09.029

Bailey, K., DiVeglio, C., & Welty, A. (2014). *An Examination of the June 2013 East Coast Meteotsunami Captured by NOAA Observing Systems. Maryland: NOAA Technical Report NOS CO-OPS 079* (p. 42). U.S. Department of Commerce, NOAA National Ocean Service, Silver Spring.

Ban, N., Caillaud, C., Coppola, E., Pichelli, E., Sobolowski, S., Adinolfi, M., et al. (2021). The first multi-model ensemble of regional climate simulations at kilometer-scale resolution, part I: Evaluation of precipitation. *Climate Dynamics*, *57*(1–2), 275–302. https://doi.org/10.1007/s00382-021-05708-w

Barnes, C. R., Best, M. M. R., Johnson, F. R., Pautet, L., & Pirenne, B. (2011). Challenges, benefits and opportunities in operating cabled ocean observatories: Perspectives from NEPTUNE Canada. In *2011 IEEE symposium on underwater technology and workshop on scientific use of submarine cables and related technologies, Tokyo, Japan, 2011* (pp. 1–7). https://doi.org/10.1109/UT.2011.5774134

Bayindir, C., & Farazande, S. (2021). The solution of the long-wave equation for various nonlinear depth and breadth profiles in the power-law form. *Dynamics of Atmospheres and Oceans*, *96*, 101254. https://doi.org/10.1016/j.dynatmoce.2021.101254

Bechle, A. J., Kristovich, D. A. R., & Wu, C. H. (2015). Meteotsunami occurrences and causes in Lake Michigan. *Journal of Geophysical Research: Oceans*, *120*(12), 8422–8438. https://doi.org/10.1002/2015JC011317

Bechle, A. J., & Wu, C. H. (2014). The Lake Michigan meteotsunamis of 1954 revisited. *Natural Hazards*, *74*(1), 155–177. https://doi.org/10.1007/s11069-014-1193-5

Bechle, A. J., Wu, C. H., Kristovich, D. A. R., Anderson, E. J., Schwab, D. J., & Rabinovich, A. B. (2016). Meteotsunamis in the Laurentian Great Lakes. *Scientific Reports*, *6*(1), 37832. https://doi.org/10.1038/srep37832

Behrens, J., Løvholt, F., Jalayer, F., Lorito, S., Salgado-Gálvez, M. A., Sørensen, M., et al. (2021). Probabilistic Tsunami hazard and risk analysis: A review of research gaps. *Frontiers in Earth Science*, *9*, 628772. https://doi.org/10.3389/feart.2021.628772

Bell, S., Cornford, D., & Bastin, L. (2013). The state of automated amateur weather observations. *Weather*, *68*(2), 36–41. https://doi.org/10.1002/wea.1980

Belušić, D., de Vries, H., Dobler, A., Landgren, O., Lind, P., Lindstedt, D., et al. (2020). HCLIM38: A flexible regional climate model applicable for different climate zones from coarse to convection-permitting scales. *Geoscientific Model Development*, *13*(3), 1311–1333. https://doi.org/10.5194/gmd-13-1311-2020

Belušić, D., Grisogono, B., & Bencetić Klaić, Z. (2007). Atmospheric origin of the devastating coupled air–sea event in the east Adriatic. *Journal of Geophysical Research*, *112*, D17111. https://doi.org/10.1029/2006JD008204

Belušić, D., & Strelec Mahović, N. (2009). Detecting and following atmospheric disturbances with a potential to generate meteotsunamis in the Adriatic. *Physics and Chemistry of the Earth*, *34*(17–18), 918–927. https://doi.org/10.1016/j.pce.2009.08.009

Benjamin, M. (2015). A mathematical study of meteo and landslide tsunamis: The Proudman resonance. *Nonlinearity*, *28*(11), 4037–4080. https://doi.org/10.1088/0951-7715/28/11/4037

Bernard, E., & Titov, V. V. (2015). Evolution of tsunami warning systems and products. *Philosophical Transaction of the Royal Society A*, *373*(2053), 20140371. https://doi.org/10.1098/rsta.2014.0371

Bernier, N. B., Hemer, M., Mori, N., Appendini, C. M., Breivik, O., de Camargo, R., et al. (2024). Storm surges and extreme sea levels: Review, establishment of model intercomparison and coordination of surge climate projection efforts (SurgeMIP). *Weather and Climate Extremes*, *45*, 100689. https://doi.org/10.1016/j.wace.2024.100689

Bertin, X., de Bakker, A., van Dongeren, A., Coco, G., André, G., Ardhuin, F., et al. (2018). Infragravity waves: From driving mechanisms to impacts. *Earth-Science Reviews*, *177*, 774–799. https://doi.org/10.1016/j.earscirev.2018.01.002

Beuvier, J., Sevault, F., Herrmann, M., Kontoyiannis, H., Ludwig, W., Rixen, M., et al. (2010). Modeling the Mediterranean Sea interannual variability during 1961–2000: Focus on the Eastern Mediterranean Transient. *Journal of Geophysical Research*, *115*(C8), C08017. https://doi.org/10.1029/2009JC005950

Bloemendaal, N., Haigh, I. D., de Moel, H., Muis, S., Haarsma, R. J., & Aerts, J. C. J. H. (2020). Generation of a global synthetic tropical cyclone hazard dataset using STORM. *Scientific Data*, *7*(1), 40. https://doi.org/10.1038/s41597-020-0381-2

Brousse, O., Simpson, C. H., Poorthuis, A., & Heaviside, C. (2024). Unequal distributions of crowdsourced weather data in England and Wales. *Nature Communications*, *15*(1), 4828. https://doi.org/10.1038/s41467-024-49276-z

Brüggeman, L. W. (1779). Ausfuerliche Beschreibung des Gegenwärtiges Zustandes des Koenigliesches Preußischen Herzogtums Vor-und Hinterpommern. *Stettin*.

Bryant, E. (2001). *Tsunami: The underrated hazard* (p. 350). Cambridge University Press.

Bubalo, M., Janeković, I., & Orlić, M. (2018). Chrystal and Proudman resonances simulated with three numerical models. *Ocean Dynamics*, *68*(4–5), 497–507. https://doi.org/10.1007/s10236-018-1146-8

Calafat, F. M., & Marcos, M. (2020). Probabilistic reanalysis of storm surge extremes in Europe. *Proceedings of the National Academy of Sciences of the United States of America*, *117*(4), 1877–1883. https://doi.org/10.1073/pnas.1913049117

Caloi, P. (1938). Sesse dell' alto Adriatico con particolare riguardo al Golfo di Trieste. *R Comit Talass Ital Mem*, *247*, 1–39. (in Italian).

Candela, J., Mazzola, S., Sammari, C., Limeburner, R., Lozano, C. J., Patti, B., & Bonnano, A. (1999). The "Mad Sea" phenomenon in the Strait of Sicily. *Journal of Physical Oceanography*, *29*(9), 2210–2231. https://doi.org/10.1175/1520-0485(1999)029<2210:TMSPIT>2.0.CO;2

Candella, R. N., & de Araujo, C. E. S. (2021). Meteotsunamis in Brazil: An overview of known occurrences from 1977 to 2020. *Natural Hazards*, *106*(2), 1563–1579. https://doi.org/10.1007/s11069-020-04331-y

Carvajal, M., Contreras-López, M., Winckler, P., & Sepúlveda, I. (2017). Meteotsunamis occurring along the Southwest Coast of South America during an intense storm. *Pure and Applied Geophysics*, *174*(8), 3313–3323. https://doi.org/10.1007/s00024-017-1584-0

Charney, J. G., & Eliasen, A. (1964). On the growth of the hurricane depression. *Journal of the Atmospheric Sciences*, *21*(1), 68–75. https://doi.org/10.1175/1520-0469(1964)021<0068:OTGOTH>2.0.CO;2

Chau, J. L., Poblet, F. L., Liu, H. L., Liu, A., Gulbrandsen, N., Jacobi, C., et al. (2024). Mesosphere and lower thermosphere wind perturbations due to the 2022 Hunga Tonga-Hunga Ha'apai eruption as observed by multistatic specular meteor radars. *Radio Science*, *59*(8), e2024RS008013. https://doi.org/10.1029/2024RS008013

Chen, G. Y., Chien, C. C., Su, C. H., & Tseng, H. M. (2004). Resonance induced by edge waves in Hua-Lien Harbor. *Journal of Oceanography*, *60*(6), 1035–1043. https://doi.org/10.1007/s10872-005-0011-9

Chen, J. Y., Saunders, K., & Whan, K. (2021). Quality control and bias adjustment of crowdsourced wind speed observations. *Quarterly Journal of the Royal Meteorological Society*, *147*, 3647–3664. https://doi.org/10.1002/qj.4146

Chen, Y. X., & Niu, X. J. (2018). Forced wave induced by an atmospheric pressure disturbance moving towards shore. *Continental Shelf Research*, *160*, 1–9. https://doi.org/10.1016/j.csr.2018.03.007

Cheng, W., Horillo, J., & Sunny, R. (2022). Numerical analysis of meteotsunamis in the Northeastern Gulf of Mexico. *Natural Hazards*, *110*(3), 1719–1734. https://doi.org/10.1007/s11069-021-05009-9

Cheung, K. F., Bai, Y. F., & Yamazaki, Y. (2013). Surges around the Hawaiian Islands from the 2011 Tohoku Tsunami. *Journal of Geophysical Research: Oceans*, *118*(10), 5703–5719. https://doi.org/10.1002/jgrc.20413

Cho, K.-H., Choi, J.-Y., Park, K.-S., Hyun, S.-K., Oh, Y., & Park, J. Y. (2013). A synoptic study on tsunami-like sea level oscillations along the west coast of Korea using an unstructured-grid ocean model. *Journal of Coastal Research*, *65*, 678–683. https://doi.org/10.2112/si65-115.1

Choblet, G., Husson, L., & Bodin, T. (2014). Probabilistic surface reconstruction of coastal sea level rise during the twentieth century. *Journal of Geophysical Research: Solid Earth*, *119*(12), 9206–9236. https://doi.org/10.1002/2014JB011639

Choi, B. H., Pelinovsky, E., Kim, K. O., & Lee, J. S. (2003). Simulation of the trans-oceanic tsunami propagation due to the 1883 Krakatau volcanic eruption. *Natural Hazards and Earth System Sciences*, *3*(5), 321–332. https://doi.org/10.5194/nhess-3-321-2003

Choi, B.-J., Hwang, C., & Lee, S.-H. (2014). Meteotsunami-tide interactions and high-frequency sea level oscillations in the eastern Yellow Sea. *Journal of Geophysical Research: Oceans*, *119*(10), 6725–6742. https://doi.org/10.1002/2013JC009788

Church, J. A., & White, N. J. (2006). A 20th century acceleration in global sea-level rise. *Geophysical Research Letters*, *33*(1), L01602. https://doi.org/10.1029/2005GL024826

Churchill, D. D., Houston, S. H., & Bond, N. A. (1995). The Daytona Beach wave of 3–4 July 1992: A shallow water gravity wave forced by a propagating squall line. *Bulletin of the American Meteorological Society*, *76*(1), 21–32. https://doi.org/10.1175/1520-0477(1995)076<0021:tdbwoj>2.0.co;2

Chyba, C. F., Thomas, P. J., & Zahnle, K. J. (1993). The 1908 Tunguska Explosion—Atmospheric disruption of a stony asteroid. *Nature*, *361*(6407), 40–44. https://doi.org/10.1038/361040a0

Colucci, P., & Michelato, A. (1976). An approach to study of the 'Marubbio' phenomenon. *Bolletino di Geofisica Teorica ed Applicata*, *13*(69), 3–10.

Costa, W. L. L., Bryan, K. R., & Coco, G. (2023). Modelling extreme water levels using intertidal topography and bathymetry derived from multispectral satellite images. *Natural Hazards and Earth System Sciences*, *23*(9), 3125–3146. https://doi.org/10.5194/nhess-23-3125-2023

Das, S., & Meylan, M. H. (2023). Effect of static compression on tsunami waves: Two-dimensional solution. *Physics of Fluids*, *35*(6), 066603. https://doi.org/10.1063/5.0154094

de Cámara, A., & Lott, F. (2015). A parameterization of gravity waves emitted by fronts and jets. *Geophysical Research Letters*, *42*(6), 2071–2078. https://doi.org/10.1002/2015GL063298

Dee, D. P., Uppala, S. M., Simmons, A. J., Berrisford, P., Poli, P., Kobayashi, S., et al. (2011). The ERA-Interim reanalysis: Configuration and performance of the data assimilation system. *Quarterly Journal of the Royal Meteorological Society*, *137*(656), 553–597. https://doi.org/10.1002/qj.828

Defant, A. (1961). *Physical oceanography* (Vol. 2, p. 598). Pergamon Press.

de Jong, M. P. C., & Battjes, J. A. (2004). Low-frequency sea waves generated by atmospheric convection cells. *Journal of Geophysical Research*, *109*, C01011. https://doi.org/10.1029/2003JC001931

de Jong, M. P. C., Holthuijsen, L. H., & Battjes, J. A. (2003). Generation of seiches by cold fronts over the southern North Sea. *Journal of Geophysical Research*, *108*, 3117. https://doi.org/10.1029/2002JC001422

de Jong, M. P. C., Reijmerink, S. P., & Beckers, J. V. L. (2021). Meteorologically generated long-period waves and their impact on the Dutch primary national flooding protection system. *Natural Hazards*, *106*(2), 1421–1443. https://doi.org/10.1007/s11069-020-04081-x

Denamiel, C., Belušić, D., Zemunik, P., & Vilibić, I. (2023). Climate projections of meteotsunami hazards. *Frontiers in Marine Science*, *10*, 1167863. https://doi.org/10.3389/fmars.2023.1167863

Denamiel, C., Ongaro, T. E., & Huan, X. (2025). Silent threat: Predicting acoustic meteotsunami global hazards. In *EGU General Assembly 2025, Vienna, Austria, 27 April–2 May 2025, EGU25-7820*. https://doi.org/10.5194/egusphere-egu25-7820

Denamiel, C., Šepić, J., Huan, X., Bolzer, C., & Vilibić, I. (2019). Stochastic surrogate model for meteotsunami early warning system in the eastern Adriatic Sea. *Journal of Geophysical Research: Oceans*, *124*(11), 8485–8499. https://doi.org/10.1029/2019JC015574

Denamiel, C., Šepić, J., Huan, X., & Vilibić, I. (2020). Uncertainty propagation using polynomial chaos expansions for extreme sea level hazard assessment: The case of the eastern Adriatic meteotsunamis. *Journal of Physical Oceanography*, *50*, 1005–2021. https://doi.org/10.1175/JPO-D-19-0147.1

Denamiel, C., Šepić, J., Ivanković, D., & Vilibić, I. (2019). The Adriatic Sea and coast modelling suite: Evaluation of the meteotsunami forecast component. *Ocean Modelling*, *135*, 71–93. https://doi.org/10.1016/j.ocemod.2019.02.003

Denamiel, C., Šepić, J., & Vilibić, I. (2018). Impact of geomorphological changes to harbor resonance during meteotsunamis: The Vela Luka Bay test case. *Pure and Applied Geophysics*, *175*, 3839–3859. https://doi.org/10.1007/978-3-030-11958-4_8

Denamiel, C., Tojčić, I., & Vilibić, I. (2022). Meteotsunamis in orography-free, flat bathymetry and warming climate conditions. *Journal of Geophysical Research: Oceans*, *127*(1), e2021JC017386. https://doi.org/10.1029/2021JC017386

Denamiel, C., Vasylkevych, S., Žagar, N., Zemunik, P., & Vilibić, I. (2023). Destructive potential of planetary meteotsunami waves beyond the Hunga Tonga–Hunga Ha'apai volcano eruption. *Bulletin of the American Meteorological Society*, *104*(1), E178–E191. https://doi.org/10.1175/BAMS-D-22-0164.1

Devlin, A. T., Jay, D. A., Talke, S. A., & Pan, J. (2023). Global water level variability observed after the Hunga Tonga-Hunga Ha'apai volcanic tsunami of 2022. *Ocean Science*, *19*(2), 517–534. https://doi.org/10.5194/os-19-517-2023

Ding, Y., Yu, H., Bao, X., Kuang, L., Wang, C., & Wang, W. (2011). Numerical study of the barotropic responses to a rapidly moving typhoon in the East China Sea. *Ocean Dynamics*, *61*(9), 1237–1259. https://doi.org/10.1007/s10236-011-0436-1

Dogan, G. G., Yalciner, A. C., Annunziato, A., Yalciner, B., & Necmioglu, O. (2023). Global propagation of air pressure waves and consequent ocean waves due to the January 2022 Hunga Tonga-Hunga Ha'apai eruption. *Ocean Engineering*, *267*, 113174. https://doi.org/10.1016/j.oceaneng.2022.113174

Dolgikh, S., Dolgikh, G., Zaytsev, A., & Pelinovsky, E. (2023). Long wave height distribution in the Sea of Japan caused by Typhoon Hinnamnor passage: Observations and modeling. *Physical Oceanography*, *30*(6), 747–759.

Domps, B., Marmain, J., & Guérin, C. A. (2022). A reanalysis of the October 2016 "meteotsunami" in British Columbia with help of high-frequency radars and autoregressive modeling. *IEEE Geoscience and Remote Sensing Letters*, *19*, 3505105. https://doi.org/10.1109/LGRS.2021.3066849

Donn, W. L., & Ewing, M. (1956). Stokes' edge waves in Lake Michigan. *Science*, *124*(3234), 1238–1242. https://doi.org/10.1126/science.124.3234.1238

Douglas, C. K. M. (1929). The line-squall and Channel wave of July 20th 1929. *The Meteorological Magazine*, *64*, 187–189.

Dowell, D. C., Alexander, C. R., James, E. P., Weygandt, S. S., Benjamin, S. G., Manikin, G. S., et al. (2022). The High-Resolution Rapid Refresh (HRRR): An hourly updating convection-allowing forecast model. Part I: Motivation and system description. *Weather and Forecasting*, *37*(8), 1371–1395. https://doi.org/10.1175/WAF-D-21-0151.1

Dragani, W. C., Mazio, C. A., & Nuñez, M. N. (2002). Sea level oscillations in coastal waters of the Buenos Aires province, Argentina. *Continental Shelf Research*, *22*(5), 779–790. https://doi.org/10.1016/S0278-4343(01)00096-6

Drago, A. (2009). Sea level variability and the 'Milghuba' seiche oscillations in the northern coast of Malta, Central Mediterranean. *Physics and Chemistry of the Earth*, *34*(17–18), 948–970. https://doi.org/10.1016/j.pce.2009.10.002

Dusek, G., DiVeglio, C., Licate, L., Heilman, L., Kirk, K., Paternostro, C., & Miller, A. (2019). A meteotsunami climatology along the US East Coast. *Bulletin of the American Meteorological Society*, *100*(7), 1329–1345. https://doi.org/10.1175/BAMS-D-18-0206.1

Dzvonkovskaya, A., Nikolić, D., Orlić, V., Perić, M. V., & Tošić, N. (2019). Remote observation of a small meteotsunami in the Bight of Benin using HF radar operating in lower HF band. *IEEE Access*, *7*, 88601–88608. https://doi.org/10.1109/ACCESS.2019.2926213

Ewing, M., & Press, F. (1955). Tide gauge disturbances from the great eruption of Krakatoa. *Eos Transactions American Geophysical Union*, *36*(1), 53–60. https://doi.org/10.1029/TR036i001p00053

Ewing, W. M., Press, F., & Donn, W. L. (1954). An explanation of the Lake Michigan wave of 26 June 1954. *Science*, *120*, 684–686. https://doi.org/10.1126/science.120.3122.6

Fan, X. Y., Fox-Kemper, B., Suzuki, N., Li, Q., Marchesiello, P., Sullivan, P. P., & Hall, P. S. (2024). Comparison of the Coastal and Regional Ocean COmmunity model (CROCO) and NCAR-LES in non-hydrostatic simulations. *Geoscientific Model Development*, *17*(10), 4095–4113. https://doi.org/10.5194/gmd-17-4095-2024

Felix, R., Hubbard, J., Wilson, K., & Switzer, A. (2024). Heatmap analysis of modeled coastal tsunamis using different bathymetry data resolutions. *Geoscience Letters*, *11*(1), 47. https://doi.org/10.1186/s40562-024-00362-6

Feng, Z., Leung, L. R., Liu, N. N., Wang, J. Y., Houze, R. A., Li, J. F., et al. (2021). A global high-resolution mesoscale convective system database using satellite-derived cloud tops, surface precipitation, and tracking. *Journal of Geophysical Research: Atmospheres*, *126*(8), e2020JD034202. https://doi.org/10.1029/2020JD034202

Ferrarin, C., Orlić, M., Bajo, M., Davolio, S., Umgiesser, G., & Lionello, P. (2023). The contribution of a mesoscale cyclone and associated meteotsunami to the exceptional flood in Venice on November 12, 2019. *Quarterly Journal of the Royal Meteorological Society*, *149*(756), 2929–2942. https://doi.org/10.1002/qj.4539

Fery, L., & Faranda, D. (2024). Analysing 23 years of warm-season derechos in France: A climatology and investigation of synoptic and environmental changes. *Weather and Climate Dynamics*, *5*(1), 439–461. https://doi.org/10.5194/wcd-5-439-2024

Fine, I. V., Rabinovich, A. B., Thomson, R. E., & Kulikov, E. A. (2003). Numerical modeling of tsunami generation by submarine and subaerial landslides. In A. C. Yalçiner, E. N. Pelinovsky, C. E. Synolakis, & E. Okal (Eds.), *Submarine landslides and tsunamis, NATO science series* (Vol. 21, pp. 69–88). Springer. https://doi.org/10.1007/978-94-010-0205-9_9

Flora, M. L., Potvin, C. K., Skinner, P. S., Handler, S., & McGovern, A. (2021). Using machine learning to generate storm-scale probabilistic guidance of severe weather hazards in the warn-on-forecast system. *Monthly Weather Review*, *149*(5), 1535–1557. https://doi.org/10.1175/MWR-D-20-0194.1

Fontserè, E. (1934). Les 'seixes de la costa catalana. In *Servei Meteorològic de Catalunya, Notes d'Estudi* (p. 58). (in Catalan).

Fosser, G., Gaetani, M., Kendon, E. J., Adinolfi, M., Ban, N., Belušić, D., et al. (2024). Convection-permitting climate models offer more certain extreme rainfall projections. *NPJ Climate and Atmospheric Science*, *7*(1), 51. https://doi.org/10.1038/s41612-024-00600-w

Frank-Comas, A., Puigdefàbregas, J., Tomàs-Ferrer, J., Font, A., Agulles, M., Soto-Navarro, J., et al. (2021). Implementation of a low-cost ultra-dense tide gauge network in the Balearic Islands. In *Marine Technology Workshop, Vigo, Spain* (p. 978).

Fritts, D. C. (1982). Shear excitation of atmospheric gravity waves. *Journal of the Atmospheric Sciences*, *39*(9), 1936–1952. https://doi.org/10.1175/1520-0469(1982)039<1936:SEOAGW>2.0.CO;2

Fritts, D. C. (1984). Shear excitation of atmospheric gravity waves. Part II: Nonlinear radiation from a free shear layer. *Journal of the Atmospheric Sciences*, *41*(4), 524–537. https://doi.org/10.1175/1520-0469(1984)041<0524:SEOAGW>2.0.CO;2

Fujii, Y., & Satake, K. (2007). Tsunami source of the 2004 Sumatra-Andaman earthquake inferred from tide gauge and satellite data. *Bulletin of the Seismological Society of America*, *97*(1A), S192–S207. https://doi.org/10.1785/0120050613

Gao, J. L., Ma, X. Z., Dong, G. H., Chen, H. Z., Liu, Q., & Zang, J. (2021). Investigation on the effects of Bragg reflection on harbor oscillations. *Coastal Engineering*, *170*, 103977. https://doi.org/10.1016/j.coastaleng.2021.103977

Garcies, M., Gomis, D., & Monserrat, S. (1996). Pressure-forced seiches of large amplitude in inlets of the Balearic Islands: 2. Observational study. *Journal of Geophysical Research*, *101*(C3), 6453–6467. https://doi.org/10.1029/95JC03626

Garrett, C. (1972). Tidal resonance in Bay of Fundy and Gulf of Maine. *Nature*, *238*(5365), 441–443. https://doi.org/10.1038/238441a0

Garrett, C. J. R. (1970). A theory of the Krakatoa tide gauge disturbances. *Tellus*, *22*(1), 43–52. https://doi.org/10.3402/tellusa.v22i1.10157

Gedzelman, S. D., & Rilling, R. A. (1977). Short-period atmospheric gravity waves: A study of their dynamic and synoptic features. *Monthly Weather Review*, *106*(2), 196–210. https://doi.org/10.1175/1520-0493(1978)106<0196:SPAGWA>2.0.CO;2

Geist, E. L., & Parsons, T. (2006). Probabilistic analysis of tsunami hazards. *Natural Hazards*, *37*(3), 277–314. https://doi.org/10.1007/s11069-005-4646-z

Geist, E. L., ten Brink, U. S., & Gove, M. (2014). A framework for the probabilistic analysis of meteotsunamis. *Natural Hazards*, *74*(1), 123–142. https://doi.org/10.1007/s11069-014-1294-1

Godin, O. A., Zabotin, N. A., & Bullett, T. W. (2015). Acoustic-gravity waves in the atmosphere generated by infragravity waves in the ocean. *Earth and Planetary Science*, *67*(1), 47. https://doi.org/10.1186/s40623-015-0212-4

Goring, D. G. (2009). Meteotsunami resulting from the propagation of synoptic-scale weather systems. *Physics and Chemistry of the Earth*, *34*(17–18), 1009–1015. https://doi.org/10.1016/j.pce.2009.10.004

Gossard, E. E., & Hooke, W. H. (1975). *Waves in the atmosphere: Atmospheric infrasound and gravity waves. Their generation and propagation* (p. 456). Elsevier.

Greenspan, H. P. (1956). The generation of edge waves by moving pressure disturbances. *Journal of Fluid Mechanics*, *1*(6), 574–592. https://doi.org/10.1017/S002211205600038X

Grezio, A., Babeyko, A., Baptista, M. A., Behrens, J., Costa, A., Davies, G., et al. (2017). Probabilistic Tsunami Hazard analysis: Multiple sources and global applications. *Reviews of Geophysics*, *55*(4), 1158–1198. https://doi.org/10.1002/2017RG000579

Grue, J., Pedersen, G. K., & Saetra, O. (2022). Free wave effects in meteotsunamis. *Journal of Geophysical Research: Oceans*, *127*(2), e2021JC017669. https://doi.org/10.1029/2021JC017669

Guastini, C. T., & Bosart, L. F. (2016). Analysis of a progressive derecho climatology and associated formation environments. *Monthly Weather Review*, *144*(4), 1363–1382. https://doi.org/10.1175/MWR-D-15-0256.1

Gusiakov, V. K. (2019). Global occurrence of large tsunamis and tsunami-like waves within the last 120 years (1900–2019). *Pure and Applied Geophysics*, *177*(3), 1261–1266. https://doi.org/10.1007/s00024-020-02437-9

Gusiakov, V. K. (2021). Meteotsunamis at global scale: Problems of event identification, parameterization and cataloguing. *Natural Hazards*, *106*(2), 1105–1123. https://doi.org/10.1007/s11069-020-04230-2

Hague, B., Mcgregor, S., Jones, D. A., Reef, R., Jakob, D., & Murphy, B. F. (2023). The global drivers of chronic coastal flood hazards under sea-level rise. *Earth's Future*, *11*(8), e2023EF003784. https://doi.org/10.1029/2023EF003784

Haigh, I. D., Marcos, M., Talke, S. A., Woodworth, P. L., Hunter, J. R., Hague, B., et al. (2023). GESLA Version 3: A major update to the global higher-frequency sea-level dataset. *Geoscience Data Journal*, *10*(3), 293–314. https://doi.org/10.1002/gdj3.174

Hall, A., Rahimi, S., Norris, J., Ban, N., Siler, N., Leung, L. R., et al. (2024). An evaluation of dynamical downscaling methods used to project regional climate change. *Journal of Geophysical Research: Atmospheres*, *24*, e2023JD040591. https://doi.org/10.1029/2023JD040591

Hallali, R., Dalaudier, F., & du Chatelet, J. P. (2016). Comparison between radar and automatic weather station refractivity variability. *Boundary-Layer Meteorology*, *160*(2), 299–317. https://doi.org/10.1007/s10546-016-0145-x

Hansen, F., Belušić, D., & Wyser, K. (2024). Relationship between circulation types and extreme precipitation over Scandinavia is stable under climate change. *Geophysical Research Letters*, *52*(12), e2024GL109704. https://doi.org/10.1029/2024GL109704

Harrison, G. (2022). Pressure anomalies from the January 2022 Hunga Tonga-Hunga Ha'apai eruption. *Weather*, *77*(3), 87–90. https://doi.org/10.1002/wea.4170

Haslett, S. K., & Bryant, E. A. (2009). Meteorological tsunamis in southern Britain: An historical review. *Geographical Review*, *99*(2), 146–163. https://doi.org/10.1111/j.1931-0846.2009.tb00424.x

Haslett, S. K., Mellor, H. E., & Bryant, E. A. (2009). Meteo-tsunami hazard associated with summer thunderstorms in the United Kingdom. *Physics and Chemistry of the Earth*, *34*(17–18), 1016–1022. https://doi.org/10.1016/j.pce.2009.10.005

Heidarzadeh, M., Gusman, A. R., Ishibe, T., Sabeti, R., & Šepić, J. (2022). Estimating the eruption-induced water displacement source of the 15 January 2022 Tonga volcanic tsunami from tsunami spectra and numerical modelling. *Ocean Engineering*, *261*, 112165. https://doi.org/10.1016/j.oceaneng.2022.112165

Heidarzadeh, M., & Rabinovich, A. B. (2021). Combined hazard of typhoon-generated meteorological tsunamis and storm surges along the coast of Japan. *Natural Hazards*, *106*(2), 1639–1672. https://doi.org/10.1007/s11069-020-04448-0

Heidarzadeh, M., Šepić, J., & Iwamoto, T. (2024). Long-duration storm surges due to 2023 successive UK storms Ciarán and Domingos: Generation, field surveys, and numerical modelling. *Ocean Modelling*, *194*, 102487. https://doi.org/10.1016/j.ocemod.2024.102487

Heidarzadeh, M., Šepić, J., Rabinovich, A., Allahyar, M., Soltanpour, A., & Tavakoli, F. (2020). Meteorological tsunami of 19 March 2017 in the Persian Gulf: Observations and analyses. *Pure and Applied Geophysics*, *177*(3), 1231–1259. https://doi.org/10.1007/s00024-019-02263-8

Heinrich, P., Gailler, A., Dupont, A., Rey, V., Hebert, H., & Listowski, C. (2023). Observations and simulations of the meteotsunami generated by the Tonga eruption on 15 January 2022 in the Mediterranean Sea. *Geophysical Journal International*, *234*(2), 903–914. https://doi.org/10.1093/gji/ggad092

Heron, M., & Dzvonkovskaya, A. (2015). Conceptual view of reflection and transmission of a tsunami wave at a step in bathymetry. In *Oceans 2015—MTS/IEEE Washington*. https://doi.org/10.23919/OCEANS.2015.7404520

Hersbach, H., Bell, B., Berrisford, P., Hirahara, S., Horányi, A., Muñoz-Sabater, J., et al. (2020). The ERA5 global reanalysis. *Quarterly Journal of the Royal Meteorological Society*, *146*(730), 1999–2049. https://doi.org/10.1002/qj.3803

Hewitt, H. T., Bell, M. J., Chassignet, E. P., Czaja, A., Ferreira, D., Griffies, S. M., et al. (2017). Will high-resolution global ocean models benefit coupled predictions on short-range to climate timescales? *Ocean Modelling*, *120*, 120–136. https://doi.org/10.1016/j.ocemod.2017.11.002

Hibiya, T., & Kajiura, K. (1982). Origin of the*Abiki* phenomenon (a kind of seiche) in Nagasaki Bay. *Journal of the Oceanographic Society of Japan*, *38*(3), 172–182. https://doi.org/10.1007/bf02110288

Hodžić, M. (1979/1980). Occurrences of exceptional sea level oscillations in the Vela Luka Bay (in Croatian). *Priroda*, *68*(2–3), 52–53.

Honda, K., Terada, T., Yoshida, Y., & Isitani, D. (1908). An investigation on the secondary undulations of oceanic tides. *Journal of College Sciences, Imperial University Tokyo*, *108*, 1–110.

Horváth, A., Vadas, S. L., Stephan, C. C., & Buehler, S. A. (2024). One-minute resolution GOES-R observations of Lamb and gravity waves triggered by the Hunga Tonga-Hunga Ha'apai eruptions on 15 January 2022. *Journal of Geophysical Research: Atmospheres*, *129*(3), e2023JD039329. https://doi.org/10.1029/2023JD039329

Horvath, K., Šepić, J., & Telišman Prtenjak, M. (2018). Atmospheric forcing conducive for the Adriatic 25 June 2014 meteotsunami event. *Pure and Applied Geophysics*, *175*(11), 3817–3837. https://doi.org/10.1007/s00024-018-1902-1

Horvath, K., & Vilibić, I. (2014). Atmospheric mesoscale conditions during the Boothbay meteotsunami: A numerical sensitivity study using a high-resolution mesoscale model. *Natural Hazards*, *74*(1), 55–74. https://doi.org/10.1007/s11069-014-1055-1

Houze, R. A., Jr. (2004). Mesoscale convective systems. *Review of Geophysics*, *42*(4), RG4003. https://doi.org/10.1029/2004RG000150

Hu, G., Li, L. L., Ren, Z. Y., & Zhang, K. (2023). The characteristics of the 2022 Tonga volcanic tsunami in the Pacific Ocean. *Natural Hazards and Earth System Sciences*, *23*(2), 675–691. https://doi.org/10.5194/nhess-23-675-2023

Huang, C. F., Anderson, E., Liu, Y., Ma, G. F., Mann, G., & Xue, P. F. (2022). Evaluating essential processes and forecast requirements for meteotsunami-induced coastal flooding. *Natural Hazards*, *110*(3), 1693–1718. https://doi.org/10.1007/s11069-021-05007-x

Huang, M., Huang, B., Gu, L. J., Huang, H. L. A., & Goldberg, M. D. (2015). Parallel GPU architecture framework for the WRF single moment 6-class microphysics scheme. *Computers & Geosciences*, *83*, 17–26. https://doi.org/10.1016/j.cageo.2015.06.014

Igarashi, Y., Kong, L., Yamamoto, M., & McCreery, C. S. (2011). Anatomy of historical Tsunamis: Lessons learned for tsunami warning. *Pure and Applied Geophysics*, *168*(11), 2043–2063. https://doi.org/10.1007/s00024-011-0287-1

Iglesias, O., Lastras, G., Souto, C., Costa, S., & Canals, M. (2014). Effects of coastal submarine canyons on tsunami propagation and impact. *Marine Geology*, *350*, 39–51. https://doi.org/10.1016/j.margeo.2014.01.013

Jansà, A. (1986). Respuesta marina a perturbaciones meso-meteorológicas: La rissaga de 21 de junio de 1984 en Ciutadella (in Spanish). *Revista de meteorología*, *3*(7), 5–29.

Jansà, A., & Jansà, X. (1980). Oceanografia. In *enciclopèdia de Menorca (in Spanish)* (Vol. 1, pp. 161–235). Obra Cultural de Menorca.

Jansà, A., Monserrat, S., & Gomis, D. (2007). The rissaga of 15 June 2006 in Ciutadella (Menorca), a meteorological tsunami. *Advances in Geosciences*, *12*, 1–4. https://doi.org/10.5194/adgeo-12-1-2007

Jansà, A., & Ramis, C. (2021). The Balearic rissaga: From pioneering research to present-day knowledge. *Natural Hazards*, *106*(2), 1269–1297. https://doi.org/10.1007/s11069-020-04221-3

Johns, R. H., & Hirt, W. D. (1987). Derechos: Widespread convectively induced windstorms. *Weather and Forecasting*, *2*(1), 32–49. https://doi.org/10.1175/1520-0434(1987)002<0032:DWCIW>2.0.CO;2

JRC. (2025). WEBCRITECH. European Commission joint research Centre—ISPRA—Space, security and migration directorate. Retrieved from https://webcritech.jrc.ec.europa.eu

Juries of the Island of Menorca. (1465). Als molt honorables e de gran saviesa Mossenyors los Jurats de la Illa de Mallorca (To the very honourable and of great wisdom Monsignors the Juries of the Mallorca Island, in old Catalan Language) Document ARM (Archive of the Mallorcan Kingdom, Col·lecció Pasqual, num. 872). Localisation and transcription: Andreu Murillo. Published in Les rissagues de Ciutadella i altres oscil·lacions de nivell de la mar de gran amplitud a la Mediterrània, textos de les comunicacions presentades a les I Jornades, Ciutadella de Menorca, del 14 al 16 de maig de 1987. *IME Col·lecció Recerca*, *2*(7), 1990.

Kakinuma, T., & Kosugi, J. (2024). Numerical study on the excitation and propagation of surface/internal waves due to air pressure waves over topography. *Water Waves*, *7*(2), 315–348. https://doi.org/10.1007/s42286-024-00099-x

Kanamori, H., Mori, J., & Harkrider, D. G. (1994). Excitation of atmospheric oscillations by volcanic-eruptions. *Journal of Geophysical Research*, *99*(B11), 21947–21961. https://doi.org/10.1029/94JB01475

Kazeminezhad, M. H., Vilibić, I., Denamiel, C., Ghafarian, P., & Negah, S. (2021). Weather radar and ancillary observations of the convective system causing the northern Persian Gulf meteotsunami on 19 March 2017. *Natural Hazards*, *106*(2), 1747–1769. https://doi.org/10.1007/s11069-020-04208-0

Ke, Z., & Yankovsky, A. E. (2011). Relative role of subinertial and superinertial modes in the coastal long wave response forced by the landfall of a tropical cyclone. *Continental Shelf Research*, *31*(9), 929–938. https://doi.org/10.1016/j.csr.2011.02.015

Keliher, T. E. (1975). The occurrence of microbarograph-detected gravity waves compared with the existence of dynamically unstable wind shear layers. *Journal of Geophysical Research*, *80*(21), 2967–2976. https://doi.org/10.1029/JC080i021p02967

Keuthen, M., & Kraft, D. (2016). Shape optimization of a breakwater. *Inverse Problems in Science and Engineering*, *24*(6), 936–956. https://doi.org/10.1080/17415977.2015.1077522

Kim, J., Choi, B. J., & Omira, R. (2022). On the Greenspan resurgence of meteotsunamis in the Yellow Sea-insights from the newly discovered 11-12 June 2009 event. *Natural Hazards*, *114*(2), 1323–1340. https://doi.org/10.1007/s11069-022-05427-3

Kim, J., & Omira, R. (2024). Combined surge-meteotsunami dynamics: A numerical model for hurricane Leslie on the coast of Portugal. *Ocean Modelling*, *189*, 102368. https://doi.org/10.1016/j.ocemod.2024.102368

Kim, M. S., Kim, H., Eom, H. M., You, S. H., & Woo, S. B. (2019). Occurrence of hazardous meteotsunamis coupled with pressure disturbance traveling in the Yellow Sea, Korea. *Journal of Coastal Research*, *91*(sp1), 71–75. https://doi.org/10.2112/SI91-015.1

Kim, M.-S., Kim, H., Kim, Y.-K., Yoo, S.-H., Eom, H.-M., & Woo, S.-B. (2017). Determination of accurate arrival time of meteotsunami event in Yellow Sea. *Journal of Coastal Research*, *79*, 149–153. https://doi.org/10.2112/SI79-031.1

Kim, M.-S., & Woo, S.-B. (2021). Propagation and amplification of meteotsunamis in multiple harbours along the eastern Yellow Sea coast. *Continental Shelf Research*, *225*, 104474. https://doi.org/10.1016/j.csr.2021.104474

Kim, M. S., Woo, S. B., Eom, H., & You, S. H. (2021). Occurrence of pressure-forced meteotsunami events in the eastern Yellow Sea during 2010–2019. *Natural Hazards and Earth System Sciences*, *21*(11), 3323–3337. https://doi.org/10.5194/nhess-21-3323-2021
Kim, M. S., Woo, S. B., Eom, H., You, S. H., & Lee, H. M. (2022). Towards observation- and atmospheric model-based early warning systems for meteotsunami mitigation: A case study of Korea. *Weather and Climate Extremes*, *37*, 100463. https://doi.org/10.1016/j.wace.2022.100463
Kochkov, D., Yuval, J., Langmore, I., Norgaard, P., Smith, J., Mooers, G., et al. (2024). Neural general circulation models for weather and climate. *Nature*, *632*, 8027–8066. https://doi.org/10.1038/s41586-024-07744-y
Kowalik, Z., Horrillo, J., Knight, W., & Logan, T. (2008). Kuril Islands tsunami of November 2006: 1. Impact at Crescent city by distant scattering. *Journal of Geophysical Research*, *113*(C1), C01020. https://doi.org/10.1029/2007JC004402
Kubota, T., Saito, T., Chikasada, N. Y., & Sandanbata, O. (2021). Meteotsunami observed by the deep-ocean seafloor pressure gauge network off northeastern Japan. *Geophysical Research Letters*, *48*(21), e2021GL094255. https://doi.org/10.1029/2021GL094255
Kulikov, M. E., Medvedev, I. P., & Kondrin, A. T. (2020). Features of seasonal variability of tidal sea-level oscillations in the Russian Arctic seas. *Russian Meteorology and Hydrology*, *45*(6), 411–421. https://doi.org/10.3103/S1068373920060047
Kwon, K., Choi, B. J., Myoung, S. G., & Sim, H. S. (2021). Propagation of a Meteotsunami from the Yellow Sea to the Korea Strait in April 2019. *Atmosphere*, *12*(8), 1083. https://doi.org/10.3390/atmos12081083
Lagergren, F., Björk, R. G., Andersson, C., Belušić, D., Björkman, M. P., Kjellström, E., et al. (2024). Kilometre-scale simulations over Fennoscandia reveal a large loss of tundra due to climate warming. *Biogeosciences*, *21*(5), 1093–1116. https://doi.org/10.5194/bg-21-1093-2024
Lam, R., Sanchez-Gonzalez, A., Willson, M., Wirnsberger, P., Fortunato, M., Alet, F., et al. (2023). Learning skillful medium-range global weather forecasting. *Science*, *382*(6677), 1416–1421. https://doi.org/10.1126/science.adi2336
Lamb, H. (1911). On atmospheric oscillations. *Proceedings of the Royal Society A*, *84*, 551–572. https://doi.org/10.1098/rspa.1911.0008
Lamb, H. (1932). *Hydrodynamics* (6th ed., p. 738). Cambridge University Press.
Lander, J. F., Lockridge, P. A., & Kozuch, M. J. (1993). *Tsunamis affecting the West Coast of the United States 1806–1992* (p. 242). U.S. Department of Commerce, NOAA National Geophysical Data Center.
Latifah, A. L., Hariyanto, H. L., & Ismanto, R. D. (2024). Effect of bathymetry data on tsunami wave ray tracing in the western Banten Sea. *Continental Shelf Research*, *277*, 105247. https://doi.org/10.1016/j.csr.2024.105247
Le Bras, R., Bittner, P., Kusmierczyk-Michulec, J., Mialle, P., & Rambolamanana, G. (2024). TIMING analysis of the multiple passages of the pressure wave generated by the 2022 Hunga Tonga-Hunga Ha'apai and comparison with the 1883 Krakatoa pressure wave. *Pure and Applied Geophysics*, *182*(1), 1–28. https://doi.org/10.1007/s00024-024-03507-y
Lee, M., Oh, D., Kim, J. Y., & Kim, C. K. (2025). Simulating near-surface winds in Europe with the WRF model: Assessing parameterization sensitivity under extreme wind conditions. *Atmosphere*, *16*(6), 665. https://doi.org/10.3390/atmos16060665
Lewis, C., Smyth, T., Neumann, J., & Cloke, H. (2024). Proposal for a new meteotsunami intensity index. *Natural Hazards and Earth System Sciences*, *24*(1), 121–131. https://doi.org/10.5194/nhess-24-121-2024
Lewis, C., Smyth, T., Williams, D., Neumann, J., & Cloke, H. (2023). Meteotsunami in the United Kingdom: The hidden hazard. *Natural Hazards and Earth System Sciences*, *23*(7), 2531–2546. https://doi.org/10.5194/nhess-23-2531-2023
Li, Q. Z., Xu, J. Y., Gusman, A. R., Liu, H. L., Yuan, W., Liu, W. J., et al. (2024). Upper-atmosphere responses to the 2022 Hunga Tonga-Hunga Ha′apai volcanic eruption via acoustic gravity waves and air-sea interaction. *Atmospheric Chemistry and Physics*, *24*(14), 8343–8361. https://doi.org/10.5194/acp-24-8343-2024
Li, Z. F., Meier, M. A., Hauksson, E., Zhan, Z. W., & Andrews, J. (2018). Machine learning seismic wave discrimination: Application to earthquake early warning. *Geophysical Research Letters*, *45*(10), 4773–4779. https://doi.org/10.1029/2018GL077870
Ličer, M., Mourre, B., Troupin, C., Krietemeyer, A., Jansá, A., & Tintoré, J. (2017). Numerical study of Balearic meteotsunami generation and propagation under synthetic gravity wave forcing. *Ocean Modelling*, *111*, 38–45. https://doi.org/10.1016/j.ocemod.2017.02.001
Lin, L. C., Liu, W. C., & Wu, C. H. (2024a). A 16-year meteotsunami climatology in the coastal areas of southern Asia-Pacific Ocean. *Frontiers in Marine Science*, *10*, 1333843. https://doi.org/10.3389/fmars.2023.1333843
Lin, L. C., Liu, W. C., & Wu, C. H. (2024b). Meteotsunamis in the Tamsui River estuary, Taiwan. *Estuarine, Coastal and Shelf Science*, *299*, 108704. https://doi.org/10.1016/j.ecss.2024.108704
Lin, L. C., & Wu, C. H. (2021). Unexpected meteotsunamis prior to Typhoon Wipha and Typhoon Neoguri. *Natural Hazards*, *106*(2), 1673–1686. https://doi.org/10.1007/s11069-020-04313-0
Linares, Á., Bechle, A. J., & Wu, C. H. (2016). Characterization and assessment of the meteotsunami hazard in northern Lake Michigan. *Journal of Geophysical Research Oceans*, *121*(9), 7141–7158. https://doi.org/10.1002/2016JC011979
Linares, Á., Wu, C. H., Bechle, A. J., Anderson, E. J., & Kristovich, D. A. R. (2019). Unexpected rip currents induced by a meteotsunami. *Scientific Reports*, *9*(1), 2105. https://doi.org/10.1038/s41598-019-38716-2
Lindzen, R. S. (1974). Wave-CISK in the tropics. *Journal of the Atmospheric Sciences*, *31*(1), 156–179. https://doi.org/10.1175/1520-0469(1974)031<0156:WCITT>2.0.CO;2
Lindzen, R. S., & Tung, K.-K. (1976). Banded convective activity and ducted gravity waves. *Monthly Weather Review*, *104*, 1602–1617. https://doi.org/10.1029/2018JD029523
Lipa, B., Barrick, D., Whelan, C., Losekoot, M., & Parikh, H. (2023). First open-coast HF radar observations of a 2-phase volcanic tsunami, Tonga 2022. *Remote Sensing*, *15*(9), 2325. https://doi.org/10.3390/rs15092325
Lipa, B., Parikh, H., Barrick, D., Roarty, H., & Glenn, S. (2014). High-frequency radar observations of the June 2013 US East Coast meteotsunami. *Natural Hazards*, *74*(1), 109–122. https://doi.org/10.1007/s11069-013-0992-4
Liu, P. L. F., Higuera, P., & Lo, P. H. Y. (2023). Scattering of moving atmospheric pressure induced tsunamis by bathymetry and coastline. *Physics of Fluids*, *35*(10), 106605. https://doi.org/10.1063/5.0164300
Liu, Y. L., & Wu, C. H. (2022). Drowning incidents and conditions due to hidden flash rips in Lake Michigan. *Science of the Total Environment*, *827*, 154314. https://doi.org/10.1016/j.scitotenv.2022.154314
Lu, C. G., Ciesielski, P. E., & Schubert, W. H. (1997). Geostrophic and ageostrophic circulations in midlatitude squall lines. *Journal of the Atmospheric Sciences*, *54*(9), 1218–1230. https://doi.org/10.1175/1520-0469(1997)054<1218:GAACIM>2.0.CO;2
Luettich, R. A., Birkhahn, R. H., & Westerink, J. J. (1991). Application of ADCIRC-2DDI to Masonboro Inlet, North Carolina: A brief numerical modeling study. In *Contractors report to the US army engineer waterways experiment station*. Retrieved from https://adcirc.org/wp-content/uploads/sites/2255/2018/11/1991_Luettich02.pdf
Lynett, P., McCann, M., Zhou, Z. L., Renteria, W., Borrero, J., Greer, D., et al. (2022). Diverse tsunamigenesis triggered by the Hunga Tonga-Hunga Ha'apai eruption. *Nature*, *609*(7928), 728–733. https://doi.org/10.1038/s41586-022-05170-6
Ma, Z., Han, G., & de Young, B. (2015). Oceanic responses to Hurricane Igor over the Grand Banks: A modeling study. *Journal of Geophysical Research: Oceans*, *120*(2), 1276–1295. https://doi.org/10.1002/2014JC010322

Maa, J. P. Y., Tsai, C. H., Juang, W. J., & Tseng, H. M. (2011). A preliminary study on Typhoon Tim induced resonance at Hualien Harbor, Taiwan. *Ocean Dynamics*, *61*(4), 411–423. https://doi.org/10.1007/s10236-010-0355-6

Maramai, A., Brizuela, B., & Graziani, L. (2014). The Euro-Mediterranean tsunami catalogue. *Annals of Geophysics*, *37*(4), S0435. https://doi.org/10.4401/ag-6437

Marcos, M., Calafat, F. M., Berihuete, A., & Dangendorf, S. (2015). Long-term variations in global sea level extremes. *Journal of Geophysical Research: Oceans*, *120*(12), 8115–8134. https://doi.org/10.1002/2015JC011173

Marcos, M., Monserrat, M., Medina, R., Orfila, A., & Olabarrieta, M. (2009). External forcing of meteorological tsunamis at the coast of the Balearic Islands. *Physics and Chemistry of the Earth*, *34*(17–18), 938–947. https://doi.org/10.1016/j.pce.2009.10.001

Martire, L., Krishnamoorthy, S., Vergados, P., Romans, L. J., Szilágyi, B., Meng, X., et al. (2023). The GUARDIAN system-a GNSS upper atmospheric real-time disaster information and alert network. *GPS Solutions*, *27*(1), 32. https://doi.org/10.1007/s10291-022-01365-6

Martire, L., Runge, T. F., Meng, X., Krishnamoorthy, S., Vergados, P., Mannucci, A. J., et al. (2024). The JPL-GIM algorithm and products: Multi-GNSS high-rate global mapping of total electron content. *Journal of Geodesy*, *98*(5), 44. https://doi.org/10.1007/s00190-024-01860-3

Matoza, R. S., Fee, D., Assink, J. D., Iezzi, A. M., Green, D. N., Kim, K., et al. (2022). Atmospheric waves and global seismo-acoustic observations of the January 2022 Hunga eruption, Tonga. *Science*, *377*(6601), 95–100. https://doi.org/10.1126/science.abo7063

Mecking, J. V., Fogarty, C. T., Greatbatch, R. J., Sheng, J., & Mercer, D. (2009). Using atmospheric model output to simulate the meteorological tsunami response to Tropical Storm Helene (2000). *Journal of Geophysical Research*, *114*(C10). https://doi.org/10.1029/2009JC005290

Međugorac, I., Metličić, N., Rus, M., Čupić, S., Mihanović, H., Šepić, J., et al. (2025). Deep-learning models for predicting high-frequency sea-level oscillations in the Adriatic Sea, EGU General Assembly 2025, Vienna, Austria, 27 April–2 May 2025, EGU25-4952. https://doi.org/10.5194/egusphere-egu25-4952

Medvedev, I. P., Rabinovich, A. B., & Šepić, J. (2022). Destructive coastal sea level oscillations generated by Typhoon Maysak in the Sea of Japan in September 2020. *Scientific Reports*, *12*(1), 8463. https://doi.org/10.1038/s41598-022-12189-2

Medvedev, I. P., Vilibić, I., & Rabinovich, A. B. (2020). Tidal resonance in the Adriatic Sea: Observational evidence. *Journal of Geophysical Research: Oceans*, *125*(8), e2020JC016168. https://doi.org/10.1029/2020JC016168

Memmola, F., Vilibić, I., Coluccelli, A., Brocchini, M., Corvaro, S., Penna, P., & Falco, P. (2024). On the generation of a meteotsunami, the case study of supercell storm, over Adriatic Sea, EMS Annual Meeting 2024, Barcelona, Spain, 1–6 Sep 2024, EMS2024-799. https://doi.org/10.5194/ems2024-799

Meng, Z. Y., Yan, D. C., & Zhang, Y. J. (2013). General features of squall lines in East China. *Monthly Weather Review*, *141*(5), 1629–1647. https://doi.org/10.1175/MWR-D-12-00208.1

Mercer, D., Sheng, J., Greatbatch, J., & Bobanović, J. (2002). Barotropic waves generated by storms moving rapidly over shallow water. *Journal of Geophysical Research*, *107*(C10), 3152. https://doi.org/10.1029/2001JC001140

Metličić, N., Rus, M., Međugorac, I., Šepić, J., & Ličer, M. (2024). Predicting high-frequency sea level oscillations using deep convolutional networks. In *Abstract book, 3rd world conference on Meteotsunamis, Bodrum, 13-17 October 2024*. Retrieved from https://3rdmeteotsunami.org

Metzner, M., Gade, M., Hennings, I., & Rabinovich, A. B. (2000). The observation of seiches in the Baltic Sea using a multi data set of water levels. *Journal of Marine Systems*, *24*(1–2), 67–84. https://doi.org/10.1016/S0924-7963(99)00079-2

Michelson, M., Hansen, B., Jacques, D., Lemay, F., & Rodriguez, P. (2020). Monitoring the impacts of weather radar data quality control for quantitative application at the continental scale. *Meteorological Applications*, *27*(4), e1929. https://doi.org/10.1002/met.1929

Miles, J., & Munk, W. (1961). Harbor paradox. *Journal of the Waterways and Harbors Division ASCE*, *87*(3), 111–132. https://doi.org/10.1061/jwheau.0000223

Mitchell, T. D., & Fry, M. J. (2024). The importance of crowdsourced observations for urban climate services. *International Journal of Climatology*, *44*(5), 1409–1422. https://doi.org/10.1002/joc.8390

Miyashita, T., Mori, N., & Gómez-Ramos, O. (2022). Local tsunami amplification factors due to the bathymetric effect and its application to approximate hazard assessment on the Zihuatanejo coast. *Pure and Applied Geophysics*, *179*(12), 4301–4322. https://doi.org/10.1007/s00024-022-03177-8

Monecke, K., Finger, W., Klarer, D., Kongko, W., McAdoo, B. G., Moore, A. L., & Sudrajat, S. U. (2008). A 1,000-year sediment record of tsunami recurrence in northern Sumatra. *Nature*, *455*(7217), 1232–1234. https://doi.org/10.1038/nature07374

Monserrat, S., Ibberson, A., & Thorpe, A. J. (1991). Atmospheric gravity waves and the "rissaga" phenomenon. *Quarterly Journal of the Royal Meteorological Society*, *117*(499), 553–570. https://doi.org/10.1002/qj.49711749907

Monserrat, S., Rabinovich, A. B., & Casas, B. (1998). On the reconstruction of the transfer function for atmospherically generated seiches. *Geophysical Research Letters*, *25*(12), 2197–2200. https://doi.org/10.1029/98GL01506

Monserrat, S., Ramis, C., & Thorpe, A. J. (1991). Large-amplitude pressure oscillations in the Western Mediterranean. *Geophysical Research Letters*, *18*(2), 183–186. https://doi.org/10.1029/91GL00234

Monserrat, S., & Thorpe, A. J. (1992). Gravity-wave observations using an array of microbarographs in the Balearic Islands. *Quarterly Journal of the Royal Meteorological Society*, *118*(504), 259–282. https://doi.org/10.1002/qj.49711850405

Monserrat, S., & Thorpe, A. J. (1996). Use of ducting theory in an observed case of gravity waves. *Journal of the Atmospheric Sciences*, *53*(12), 17242–21736. https://doi.org/10.1175/1520-0469(1996)053<1724:uodtia>2.0.co;2

Monserrat, S., Vilibić, I., & Rabinovich, A. B. (2006). Meteotsunamis: Atmospherically induced destructive ocean waves in the tsunami frequency band. *Natural Hazards and Earth System Sciences*, *6*, 1035–1051. https://doi.org/10.5194/nhess-6-1035-2006

Monserrat, S., Villalonga, V., Puigdefabregas, J., & Jordà, G. (2024). Another port, after undergoing significant works in its entrance, competing with Ciutadella for the "Western Mediterranean meteotsunami hotspot contest". In *Abstract book, 3rd world conference on Meteotsunamis, Bodrum, 13-17 October 2024*. Retrieved from https://3rdmeteotsunami.org/

Mourre, B., Santana, A., Builes, A., Gautreau, L., Ličer, M., Jansà, A., et al. (2021). On the potential of ensemble forecasting for the prediction of meteotsunamis in the Balearic Islands: Sensitivity to atmospheric model parameterizations. *Natural Hazards*, *106*(2), 1315–1336. https://doi.org/10.1007/s11069-020-03908-x

Muafiry, I. N., Wijaya, D. D., Meilano, I., & Heki, K. (2023). Diverse ionospheric disturbances by the 2022 Hunga Tonga-Hunga Ha'apai eruption observed by a dense GNSS array in New Zealand. *Journal of Geophysical Research: Space Physics*, *128*(11), e2023JA031486. https://doi.org/10.1029/2023JA031486

Muis, S., Apecechea, M. I., Dullaart, J., Rego, J. D., Madsen, K. S., Su, J., et al. (2020). A high-resolution global dataset of extreme sea levels, tides, and storm surges, including future projections. *Frontiers in Marine Science*, *7*, 263. https://doi.org/10.3389/fmars.2020.00263

Mulia, I. E., & Satake, K. (2020). Developments of tsunami observing systems in Japan. *Frontiers in Earth Science*, *145*, 145. https://doi.org/10.3389/feart.2020.00145

Munaibari, E., Rolland, L., Sladen, A., & Delouis, B. (2023). Anatomy of the tsunami and Lamb waves-induced ionospheric signatures generated by the 2022 Hunga Tonga volcanic eruption. *Pure and Applied Geophysics*, *180*(5), 1751–1764. https://doi.org/10.1007/s00024-023-03271-5

Munk, W. H. (1962). *Long waves, the Sea* (pp. 647–663). John Wiley.

Munk, W. H., Snodgrass, F., & Carrier, G. (1956). Edge waves on the continental shelf. *Science*, *123*(3187), 127–132. https://doi.org/10.1126/science.123.3187.127

Muñoz-Esparza, D., Sauer, J. A., Jensen, A. A., Xue, L., & Grabowski, W. W. (2022). The FastEddy® resident-GPU accelerated large-eddy simulation framework: Moist dynamics extension, validation and sensitivities of modeling non-precipitating shallow cumulus clouds. *Journal of Advances in Modeling Earth Systems*, *14*(4), e2021MS002904. https://doi.org/10.1029/2021MS002904

Nappo, C. J. (2002). *An introduction to atmospheric gravity waves* (p. 276). Academic Press, Elsevier Science.

Necmioglu, O., Chang Seng, D., Annunziato, A., & Imperiali, O. (2023). *JRC/DG-ECHO/UNESCO-IOC joint hybrid-workshop on local tsunami warning in the context of multi-hazard disaster risk mitigation*. Publications Office of the European Union. https://doi.org/10.2760/398065

Needham, H. F., & Keim, B. D. (2012). A storm surge database for the US Gulf Coast. *International Journal of Climatology*, *32*(14), 2108–2123. https://doi.org/10.1002/joc.2425

Needham, H. F., Keim, B. D., & Sathiaraj, D. (2015). A review of tropical cyclone-generated storm surges: Global data sources, observations, and impacts. *Reviews of Geophysics*, *53*(2), 545–591. https://doi.org/10.1002/2014RG000477

Nesteckytė, L., Stankūnavičius, L., Kelpšaitė-Rimkienė, L., & Šepić, J. (2024). 2023 November storm in the port of Klaipeda; why was the port closed? *Pure and Applied Geophysics*, *181*(11), 3173–3188. https://doi.org/10.1007/s00024-024-03596-9

Niedda, M., & Greppi, M. (2007). Tidal, seiche and wind dynamics in a small lagoon in the Mediterranean Sea. *Estuarine, Coastal and Shelf Science*, *74*(1–2), 21–30. https://doi.org/10.1016/j.ecss.2007.03.022

Nishida, K., Kobayashi, N., & Fukao, Y. (2014). Background Lamb waves in the Earth's atmosphere. *Geophysical Journal International*, *196*(1), 312–316. https://doi.org/10.1093/gji/ggt413

Niu, X. J. (2020). Conditions for the occurrence of notable edge waves due to atmospheric disturbances. *Applied Ocean Research*, *101*, 102255. https://doi.org/10.1016/j.apor.2020.102255

Niu, X. J. (2021). Resonance of long waves around a circular island and its relation to edge waves. *European Journal of Mechanics B: Fluids*, *86*, 15–24. https://doi.org/10.1016/j.euromechflu.2020.11.007

Niu, X. J., & Chen, Y. X. (2020). Energy accumulation during the growth of forced wave induced by a moving atmospheric pressure disturbance. *Coastal Engineering Journal*, *62*(1), 23–34. https://doi.org/10.1080/21664250.2019.1682747

NOAA. (2025). Tides & currents. Retrieved from https://tidesandcurrents.noaa.gov/1mindata.html

NOC. (2025). Future Coastal Ocean climates (FLAME). Retrieved from https://projects.noc.ac.uk/flame

Nolan, D. S., & Zhang, J. A. (2017). Spiral gravity waves radiating from tropical cyclones. *Geophysical Research Letters*, *44*(8), 3924–3931. https://doi.org/10.1002/2017GL073572

Nomitsu, T. (1935). A theory of tsunamis and seiches produced by wind and barometric gradient. *Memoirs of the College of Science Imperial University Kyoto A*, *18*(4), 201–214.

Norman, M. R., Bader, D. A., Eldred, C., Hannah, W. M., Hillman, B. R., Jones, C. R., et al. (2022). Unprecedented cloud resolution in a GPU-enabled full-physics atmospheric climate simulation on OLCF's summit supercomputer. *International Journal of High-Performance Computing Applications*, *36*(1), 93–105. https://doi.org/10.1177/10943420211027539

NTSLF. (2025). *National tidal and Sea level facility*. National Oceanographic Centre & University of Liverpool. Retrieved from https://ntslf.org

Okal, E. A. (2021a). On the possibility of seismic recording of meteotsunamis. *Natural Hazards*, *106*(2), 1125–1147. https://doi.org/10.1007/s11069-020-04146-x

Okal, E. A. (2021b). Snell's Law applied to tsunamis: Simulations and observations. *Pure and Applied Geophysics*, *178*(12), 4969–4983. https://doi.org/10.1007/s00024-021-02703-4

Okal, E. A., Visser, J. N. J., & de Beer, C. H. (2014). The Dwarskersbos, South Africa local tsunami of August 27, 1969: Field survey and simulation as a meteorological event. *Natural Hazards*, *74*(1), 251–268. https://doi.org/10.1007/s11069-014-1205-5

Olabarrieta, M., Valle-Levinson, A., Martinez, C. J., Pattiaratchi, C., & Shi, L. (2017). Meteotsunamis in the northeastern Gulf of Mexico and their possible link to El Niño Southern Oscillation. *Natural Hazards*, *88*(3), 1325–1346. https://doi.org/10.1007/s11069-017-2922-3

Omira, R., Ramalho, R. S., Kim, J., González, P. J., Kadri, U., Miranda, J. M., et al. (2022). Global Tonga tsunami explained by a fast-moving atmospheric source. *Nature*, *609*(7928), 734–740. https://doi.org/10.1038/s41586-022-04926-4

Orlić, M. (1980). About a possible occurrence of the Proudman resonance in the Adriatic. *Thalassia Jugoslavica*, *16*, 79–88.

Orlić, M. (2015). The first attempt at cataloguing tsunami-like waves of meteorological origin in Croatian coastal waters. *Acta Adriatica*, *56*(1), 83–96.

Orlić, M., Belušić, D., Janeković, I., & Pasarić, M. (2010). Fresh evidence relating the great Adriatic surge of 21 June 1978 to mesoscale atmospheric forcing. *Journal of Geophysical Research*, *115*(C6), C06011. https://doi.org/10.1029/2009JC005777

Ozsoy, O., Haigh, I. D., Wadey, M. P., Nicholls, R. J., & Wells, N. C. (2016). High-frequency sea level variations and implications for coastal flooding: A case study of the Solent, UK. *Continental Shelf Research*, *122*, 1–13. https://doi.org/10.1016/j.csr.2016.03.021

Pakoksung, K., Suppasri, A., & Imamura, F. (2022). The near-field tsunami generated by the 15 January 2022 eruption of the Hunga Tonga-Hunga Ha'apai volcano and its impact on Tongatapu, Tonga. *Scientific Reports*, *12*(1), 15187. https://doi.org/10.1038/s41598-022-19486-w

Panthou, G., Vrac, M., Drobinski, P., Bastin, S., & Li, L. (2016). Impact of model resolution and Mediterranean Sea coupling on hydrometeorological extremes in RCMs in the frame of HyMeX and MED-CORDEX. *Climate Dynamics*, *51*(3), 915–932. https://doi.org/10.1007/s00382-016-3374-2

Paris, R., Wassmer, P., Lavigne, F., Belousov, A., Belousova, M., Iskandarsyah, Y., et al. (2014). Coupling eruption and tsunami records: The Krakatau 1883 case study, Indonesia. *Bulletin of Volcanology*, *76*(4), 814. https://doi.org/10.1007/s00445-014-0814-x

Pasquet, S., & Vilibić, I. (2013). Shelf edge reflection of atmospherically generated long ocean waves along the central U.S. East Coast. *Continental Shelf Research*, *66*, 1–8. https://doi.org/10.1016/j.csr.2013.06.007

Pasquet, S., Vilibić, I., & Šepić, J. (2013). A survey of strong high frequency sea level oscillations along the US East Coast between 2006 and 2011. *Natural Hazards and Earth System Sciences*, *13*(2), 473–482. https://doi.org/10.5194/nhess-13-473-2013

Pattiaratchi, C. B., & Wijeratne, E. M. S. (2014). Observations of meteorological tsunamis along the south-west Australian coast. *Natural Hazards*, *74*(1), 281–303. https://doi.org/10.1007/s11069-014-1263-8

Pattiaratchi, C. B., & Wijeratne, E. M. S. (2015). Are meteotsunamis an underrated hazard? *Philosophical Transactions of the Royal Society A*, *373*(2053), 20140377. https://doi.org/10.1098/rsta.2014.0377

Paxton, C. H., & Sobien, D. A. (1998). Resonant interaction between an atmospheric gravity wave and shallow water wave along Florida's west coast. *Bulletin of the American Meteorological Society*, *79*(12), 2727–2732. https://doi.org/10.1175/1520-0477(1998)079<2727:RIBAAG>2.0.CO;2

Paxton, L. D. (2016). Development of a forecast process for meteotsunami events in the Gulf of Mexico. In *Master thesis, school of geosciences, college of arts and sciences* (p. 76). University of South Florida.
Pekeris, C. L. (1937). Atmospheric oscillations. *Proceedings of the Royal Society of London*, *158*(A895), 650–671. https://doi.org/10.1098/rspa.1937.0046
Pellikka, H., Laurila, T. K., Boman, H., Karjalainen, A., Björkqvist, J. V., & Kahma, K. K. (2020). Meteotsunami occurrence in the Gulf of Finland over the past century. *Natural Hazards and Earth System Sciences*, *20*(9), 2535–2546. https://doi.org/10.5194/nhess-20-2535-2020
Pellikka, H., Rauhala, J., Kahma, K. K., Stipa, T., Boman, H., & Kangas, A. (2014). Recent observations of meteotsunamis on the Finnish coast. *Natural Hazards*, *74*(1), 197–215. https://doi.org/10.1007/s11069-014-1150-3
Pellikka, H., Šepić, J., Lehtonen, I., & Vilibić, I. (2022). Meteotsunamis in the northern Baltic Sea and their relation to synoptic patterns. *Weather and Climate Extremes*, *38*, 100527. https://doi.org/10.1016/j.wace.2022.100527
Perez, I., Dragani, W., Oreirio, F., & Fiore, M. (2022). Meteotsunamis at the Río de la Plata estuary. *Estuarine, Coastal and Shelf Science*, *277*, 108064. https://doi.org/10.1016/j.ecss.2022.108064
Pérez Gómez, B., García-León, M., García-Valdecasas, J., Clementi, E., Mösso Aranda, C., Pérez-Rubio, S., et al. (2021). Understanding sea level processes during western Mediterranean storm Gloria. *Frontiers in Marine Science*, *8*, 647437. https://doi.org/10.3389/fmars.2021.647437
Pérez Gómez, B., Vilibić, I., Šepić, J., Međugorac, I., Ličer, M., Testut, L., et al. (2022). Coastal sea level monitoring in the Mediterranean and Black seas. *Ocean Science*, *18*(4), 997–1053. https://doi.org/10.5194/os-18-997-2022
Pethiyagoda, R., Das, S., Bonham, M., & Meylan, M. H. (2024). Atmospheric pressure-induced three-dimensional surface wave propagation in the compressible ocean: Effect of static compression. *Physics of Fluids*, *36*(9), 096618. https://doi.org/10.1063/5.0223048
Pichelli, E., Coppola, E., Sobolowski, S., Ban, N., Giorgi, F., Stocchi, P., et al. (2021). The first multi-model ensemble of regional climate simulations at kilometer-scale resolution part 2: Historical and future simulations of precipitation. *Climate Dynamics*, *56*(11–12), 3581–3602. https://doi.org/10.1007/s00382-021-05657-4
Piotrowski, A., Szczucinski, W., Sydor, P., Kotrys, B., Rzodkiewicz, M., & Krzyminska, J. (2017). Sedimentary evidence of extreme storm surge or tsunami events in the southern Baltic Sea (Rogowo area, NW Poland). *Geological Quaternary*, *61*, 973–985. https://doi.org/10.7306/gq.1385
Planchat, A., Kwiatkowski, L., Bopp, L., Torres, O., Christian, J. R., Butenschön, M., et al. (2023). The representation of alkalinity and the carbonate pump from CMIP5 to CMIP6 Earth system models and implications for the carbon cycle. *Biogeosciences*, *20*(7), 1195–1257. https://doi.org/10.5194/bg-20-1195-2023
Platzman, G. W. (1958). A numerical computation of the surge of 26 June 1954 on Lake Michigan. *Geophysica*, *6*, 407–438.
Platzman, G. W. (1965). The predictions of surges in the southern basin of Lake Michigan. Part I. The dynamical basis for prediction. *Monthly Weather Review*, *93*(5), 275–281. https://doi.org/10.1175/1520-0493(1965)093<0275:tposit>2.3.co;2
Plougonven, R., & Zhang, F. (2014). Internal gravity waves from atmospheric jets and fronts. *Reviews of Geophysics*, *52*(1), 33–76. https://doi.org/10.1002/2012RG000419
Press, F., & Harkrider, D. (1966). Air-sea waves from the explosion of Krakatoa. *Science*, *154*(3754), 1325–1327. https://doi.org/10.1126/science.154.3754.1325
Pringle, W. J., Wirasaet, D., Roberts, K. J., & Westerink, J. J. (2021). Global storm tide modeling with ADCIRC v55: Unstructured mesh design and performance. *Geoscientific Model Development*, *14*(2), 1125–1145. https://doi.org/10.5194/gmd-14-1125-2021
Proudman, J. (1929). The effects on the sea of changes in atmospheric pressure. *Geophysical Supplements to the Monthly Notices of the Royal Astronomical Society*, *2*(4), 197–209. https://doi.org/10.1111/j.1365-246x.1929.tb05408.x
Pugh, D., & Woodworth, P. L. (2014). *Sea-level science: Understanding tides, surges, tsunamis and mean sea-level changes*. Cambridge University Press.
Pupić Vurilj, M., Brnac, T., Ruić, K., Šepić, J., & Balić, M. (2023). Mediterranean meteotsunamis of May 2021 and June 2022: Observations, data analysis and synoptic background. *Geofizika*, *40*(2), 179–205. https://doi.org/10.15233/gfz.2023.40.8
Purkis, S. J., Ward, S. N., Fitzpatrick, N. M., Garvin, J. B., Slayback, D., Cronin, S. J., et al. (2023). The 2022 Hunga-Tonga megatsunami: Near-field simulation of a once-in-a-century event. *Science Advances*, *9*(15), adf5493. https://doi.org/10.1126/sciadv.adf5493
Rabinovich, A. B. (1993). Long Ocean gravity waves: Trapping, resonance, and leaking (Gidrometeoizdat, St. Petersburg, 1993) (p. 325). (in Russian).
Rabinovich, A. B. (2009). Seiches and harbor oscillations. In Y. C. Kim (Ed.), *Handbook of coastal and ocean engineering* (pp. 193–236). World Scientific Publishers. https://doi.org/10.1142/9789812819307_0009
Rabinovich, A. B. (2020). Twenty-seven years of progress in the science of meteorological tsunamis following the 1992 Daytona Beach event. *Pure and Applied Geophysics*, *177*(3), 1193–1230. https://doi.org/10.1007/s00024-019-02349-3
Rabinovich, A. B., & Monserrat, S. (1996). Meteorological tsunamis near the Balearic and Kuril Islands: Descriptive and statistical analysis. *Natural Hazards*, *13*(1), 55–90. https://doi.org/10.1007/BF00156506
Rabinovich, A. B., & Monserrat, S. (1998). Generation of meteorological tsunamis (large amplitude seiches) near the Balearic and Kuril Islands. *Natural Hazards*, *18*(1), 27–55. https://doi.org/10.1023/A:1008096627047
Rabinovich, A. B., Šepić, J., Medvedev, I. P., & Thomson, R. E. (2025). A triple jeopardy flood event: Coincident arrival of the 2022 Tonga tsunami with a storm surge and meteotsunami on the East Coast of the United States. *Bulletin of the American Meteorological Society*, *106*(2), E290–E309. https://doi.org/10.1175/BAMS-D-24-0040.1
Rabinovich, A. B., Šepić, J., & Thomson, R. E. (2021). The meteorological tsunami of 1 November 2010 in the southern strait of Georgia: A case study. *Natural Hazards*, *106*(2), 1503–1544. https://doi.org/10.1007/s11069-020-04203-5
Rabinovich, A. B., Šepić, J., & Thomson, R. E. (2023). Strength in numbers: The tail end of Typhoon Songda combines with local cyclones to generate extreme sea level oscillations on the British Columbia and Washington coasts during mid-October 2016. *Journal of Physical Oceanography*, *53*(1), 131–155. https://doi.org/10.1175/JPO-D-22-0096.1
Racki, G., & Koeberl, C. (2024). Impact catastrophism versus mass extinctions in retrospective, perspective and prospective: Toward a Phanerozoic impact event stratigraphy. *Earth-Science Reviews*, *259*, 104904. https://doi.org/10.1016/j.earscirev.2024.104904
Rafliana, I., Jalayer, F., Cerase, A., Cugliari, L., Baiguera, M., Salmanidou, D., et al. (2022). Tsunami risk communication and management: Contemporary gaps and challenges. *International Journal of Disaster Risk Reduction*, *70*, 102771. https://doi.org/10.1016/j.ijdrr.2021.102771
Rahimian, M., Beyramzadeh, M., & Siadatmousavi, S. M. (2022). The skill assessment of Weather and Research Forecasting and WAVEWATCH-III models during recent meteotsunami event in the Persian Gulf. *Frontiers in Marine Science*, *9*, 834151. https://doi.org/10.3389/fmars.2022.834151
Raichlen, F. (1966). Harbor resonance. In A. T. Ippen (Ed.), *Estuary and coastline hydrodynamics* (pp. 281–340). McGraw Hill Book Company.
Ramis, C., & Jansà, A. (1983). Condiciones meteorológicas simultáneas a la aparición de oscilaciones del nivel del mar de amplitud extraordinaria en el Mediterráneo Occidental (in Spanish). *Revista Geofísica*, *39*, 35–42.

Ramos-Alcántara, J., Agulles, M., Gomis, D., & Jordà, G. (2025). Quantifying the contributors to extreme sea level events in a Mediterranean microtidal region at high spatio-temporal resolution. *Climate Dynamics*, *63*(3), 167. https://doi.org/10.1007/s00382-025-07653-4

Range, M. M., Arbic, B. K., Johnson, B. C., Moore, T. C., Titov, V., Adcroft, A. J., et al. (2022). The Chicxulub impact produced a powerful global tsunami. *AGU Advances*, *3*(5), e2021AV000627. https://doi.org/10.1029/2021AV000627

Rawat, A., Ardhuin, F., Ballu, V., Crawford, W., Corela, C., & Aucan, J. (2014). Infragravity waves across the oceans. *Geophysical Research Letters*, *41*(22), 7957–7963. https://doi.org/10.1002/2014GL061604

Ren, D. D., & Leslie, L. M. (2024). Implications for extreme midlatitude weather events of secondary flow associated with polar jets. *International Journal of Climatology*, *44*(14), 4925–4941. https://doi.org/10.1002/joc.8615

Ren, Z. Y., Higuera, P., & Liu, P. L. F. (2023). On tsunami waves induced by atmospheric pressure shock waves after the 2022 Hunga Tonga-Hunga Ha'apai volcano eruption. *Journal of Geophysical Research: Oceans*, *128*(4), e2022JC019166. https://doi.org/10.1029/2022JC019166

Renault, L., Vizoso, G., Jansà, A., Wilkin, J., & Tintoré, J. (2011). Toward the predictability of meteotsunamis in the Balearic Sea using regional nested atmosphere and ocean models. *Geophysical Research Letters*, *38*(10), L10601. https://doi.org/10.1029/2011gl047361

Renqvist, H. (1926). Ein Seebär in Finnland. Zur Frage Nach der Entstehung der Seebären. *Geografiska Annaler*, *8*(3), 230–236. https://doi.org/10.1080/20014422.1926.11881133

Resio, D. T., & Westerink, J. J. (2008). Hurricanes and the physics of surges. *Physics Today*, *61*(9), 33–38. https://doi.org/10.1063/1.2982120

ReVelle, D. O. (2008). Acoustic-gravity waves from bolide sources. *Earth, Moon, and Planets*, *102*(1–4), 345–356. https://doi.org/10.1007/s11038-007-9181-3

Reynolds, D., Gutmann, E., Kruyt, B., Haugeneder, M., Jonas, T., Gerber, F., et al. (2023). The High-resolution Intermediate Complexity Atmospheric Research (HICAR v1.1) model enables fast dynamic downscaling to the hectometer scale. *Geoscientific Model Development*, *15*(17), 5049–5068. https://doi.org/10.5194/gmd-16-5049-2023

Robledo, V., Henao, J. J., Mejía, J. F., Ramírez-Cardona, A., Hernández, K. S., Gómez-Ríos, S., & Rendón, A. M. (2024). Climatological tracking and lifecycle characteristics of mesoscale convective systems in northwestern South America. *Journal of Geophysical Research: Atmospheres*, *129*(19), e2024JD041159. https://doi.org/10.1029/2024JD041159

Romero, R. (2024). TRAM: A new non-hydrostatic fully compressible numerical model suited for all kinds of regional atmospheric predictions. *Quarterly Journal of the Royal Meteorological Society*, *150*(759), 1124–1156. https://doi.org/10.1002/qj.4639

Romero, R., Vich, M., & Ramis, C. (2019). A pragmatic approach for the numerical prediction of meteotsunamis in Ciutadella harbour (Balearic Islands). *Ocean Modelling*, *142*, 101441. https://doi.org/10.1016/j.ocemod.2019.101441

Ruić, K., Šepić, J., Mlinar, M., & Međugorac, I. (2023). Contribution of high-frequency (T < 2 h) sea level oscillations to the Adriatic sea level maxima. *Natural Hazards*, *116*(3), 3747–3777. https://doi.org/10.1007/s11069-023-05834-0

Ruić, K., Šepić, J., & Vojković, M. (2024). Synoptic patterns associated with high-frequency sea level extremes in the Adriatic Sea. *Ocean Science*, *21*(3), 1183–1203. https://doi.org/10.5194/os-21-1183-2025

Rus, M., Mihanović, H., Ličer, M., & Kristan, M. (2025). HIDRA3: A deep-learning model for multipoint ensemble sea level forecasting in the presence of tide gauge sensor failures. *Geoscientific Model Development*, *18*(3), 605–620. https://doi.org/10.5194/gmd-18-605-2025

Salaree, A., Mansouri, R., & Okal, E. A. (2018). The intriguing tsunami of 19 March 2017 at Bandar Dayyer, Iran: Field survey and simulations. *Natural Hazards*, *90*(3), 1277–1307. https://doi.org/10.1007/s11069-017-3119-5

Sallenger, A. H., Jr., List, J. H., Gelfenbaum, G., Stumpf, R. P., & Hansen, M. (1995). Large wave at Dayton Beach, Florida, explained as a squall-line surge. *Journal of Coastal Research*, *11*, 1383–1388.

Sammari, C., Koutitonsky, V. G., & Moussa, M. (2006). Sea level variability and tidal resonance in the Gulf of Gabes, Tunisia. *Continental Shelf Research*, *26*(3), 338–350. https://doi.org/10.1016/j.csr.2005.11.006

Satake, K., & Atwater, B. F. (2007). Long-term perspectives on giant earthquakes and tsunamis at subduction zones. *Annual Review of Earth and Planetary Sciences*, *35*(1), 349–374. https://doi.org/10.1146/annurev.earth.35.031306.140302

Sauer, J., Munoz-Esparza, D., & Prestopnik, J. (2024). FastEddy-model software release [Software]. *Zenodo*. https://doi.org/10.5281/ZENODO.11042755

Schär, C., Frei, C., Luthi, D., & Davies, H. C. (1996). Surrogate climate-change scenarios for regional climate models. *Geophysical Research Letters*, *23*(6), 669–672. https://doi.org/10.1029/96GL00265

Schär, C., Fuhrer, O., Arteaga, A., Ban, N., Charpilloz, C., Di Girolamo, S., et al. (2020). Kilometer-scale climate models: Prospects and challenges. *Bulletin of the American Meteorological Society*, *101*(5), E567–E587. https://doi.org/10.1175/BAMS-D-18-0167.1

Schumacher, R. S., & Rasmussen, K. L. (2020). The formation, character and changing nature of mesoscale convective systems. *Nature Review Earth & Environment*, *1*(6), 300–314. https://doi.org/10.1038/s43017-020-0057-7

Seelam, J. K., Murali, R. M., & Baldock, T. E. (2016). Effect of submarine canyons on tsunami heights, currents and run-up off the southeast coast of India. *Current Science*, *111*(12), 1990–2004. https://doi.org/10.18520/cs/v111/i12/1990-2004

Self, S., & Rampino, M. R. (1981). The 1883 eruption of Krakatau. *Nature*, *284*(5843), 699–704. https://doi.org/10.1038/294699a0

Seo, S. N., & Liu, P. L. F. (2014). Edge waves generated by atmospheric pressure disturbances moving along a shoreline on a sloping beach. *Coastal Engineering*, *85*, 43–59. https://doi.org/10.1016/j.coastaleng.2013.12.002

Šepić, J., Međugorac, I., Janeković, I., Dunić, N., & Vilibić, I. (2016). Multi-meteotsunami event in the Adriatic Sea generated by atmospheric disturbances of 25–26 June 2014. *Pure and Applied Geophysics*, *173*(12), 4117–4138. https://doi.org/10.1007/s00024-016-1249-4

Šepić, J., & Orlić, M. (2025a). Adriatic meteotsunami catalogue. Retrieved from https://projekti.pmfst.unist.hr/floods/meteotsunamis/adriatic-catalogue/

Šepić, J., & Orlić, M. (2025b). Legend of March Friday, adriatic meteotsunami catalogue. Retrieved from https://projekti.pmfst.unist.hr/floods/meteotsunamis/cultural-heritage

Šepić, J., Orlić, M., & Vilibić, I. (2008). The Bakar Bay seiches and their relationship with atmospheric processes. *Acta Adriatica*, *49*(2), 107–123.

Šepić, J., & Rabinovich, A. B. (2014). Meteotsunami in the Great Lakes and on the Atlantic coast of the United States generated by the ''derecho'' of June 29–30, 2012. *Natural Hazards*, *74*(1), 75–107. https://doi.org/10.1007/s11069-014-1310-5

Šepić, J., Rabinovich, A. B., & Sytov, V. N. (2018). Odessa tsunami of 27 June 2014: Observations and numerical modelling. *Pure and Applied Geophysics*, *175*(4), 1545–1572. https://doi.org/10.1007/s00024-017-1729-1

Šepić, J., & Vilibić, I. (2011). The development and implementation of a real-time meteotsunami warning network for the Adriatic Sea. *Natural Hazards and Earth System Sciences*, *11*(1), 83–91. https://doi.org/10.5194/nhess-11-83-2011

Šepić, J., Vilibić, I., Beg Paklar, G., Dadić, V., Denamiel, C., Dunić, N., et al. (2017). Towards an understanding and operational early warning of the Adriatic meteotsunamis: Project MESSI. In *Coastal and maritime Mediterranean conference, split, Croatia*. https://doi.org/10.5150/cmcm.2017.033

Šepić, J., Vilibić, I., & Belušić, D. (2009). Source of the 2007 Ist meteotsunami (Adriatic Sea). *Journal of Geophysical Research*, *114*, C03016. https://doi.org/10.1029/2008JC005092

Šepić, J., Vilibić, I., & Fine, I. (2015). Northern Adriatic meteorological tsunamis: Assessment of their potential through ocean modeling experiments. *Journal of Geophysical Research: Oceans*, *120*(4), 2993–3010. https://doi.org/10.1002/2015JC010795

Šepić, J., Vilibić, I., Lafon, A., Macheboeuf, L., & Ivanović, Z. (2015). High-frequency sea level oscillations in the Mediterranean and their connection to synoptic patterns. *Progress in Oceanography*, *137*, 284–298. https://doi.org/10.1016/j.pocean.2015.07.005

Šepić, J., Vilibić, I., & Monserrat, S. (2009). Teleconnections between the Adriatic and the Balearic meteotsunamis. *Physics and Chemistry of the Earth*, *34*(17–18), 928–937. https://doi.org/10.1016/j.pce.2009.08.007

Šepić, J., Vilibić, I., & Monserrat, S. (2016). Quantifying the probability of meteotsunami occurrence from synoptic atmospheric patterns. *Geophysical Research Letters*, *43*(19), 10377–10410. https://doi.org/10.1002/2016GL070754

Šepić, J., Vilibić, I., Rabinovich, A. B., & Monserrat, S. (2015). Widespread tsunami-like waves of 23–27 June in the Mediterranean and Black Seas generated by high-altitude atmospheric forcing. *Scientific Reports*, *5*(1), 11682. https://doi.org/10.1038/srep11682

Šepić, J., Vilibić, I., Rabinovich, A. B., & Tinti, S. (2018). Meteotsunami ("Marrobbio") of 25–26 June 2014 on the southwestern coast of Sicily, Italy. *Pure and Applied Geophysics*, *175*(4), 1573–1593. https://doi.org/10.1007/s00024-018-1827-8

Šepić, J., Vilibić, I., & Strelec Mahović, N. (2012). Northern Adriatic meteorological tsunamis: Observations, link to the atmosphere, and predictability. *Journal of Geophysical Research*, *117*, C02002. https://doi.org/10.1029/2011JC007608

Shchepetkin, A. F., & McWilliams, J. C. (2005). The regional oceanic modeling system: A split-explicit, free-surface, topography-following-coordinate ocean model. *Ocean Modelling*, *9*(4), 347–404. https://doi.org/10.1016/j.ocemod.2004.08.002

Shchepetkin, A. F., & McWilliams, J. C. (2009). Correction and commentary for "ocean forecasting in terrain-following coordinates: Formulation and skill assessment of the regional ocean modeling system" by Haidvogel et al., J. Comput. Phys., 227, pp. 3595–3624. *Journal of Computational Physics*, *228*, 8985–9000. https://doi.org/10.1016/j.jcp.2009.09.002

Sheremet, A., Gravois, U., & Shrira, V. (2016). Observations of meteotsunami on the Louisiana shelf: A lone soliton with a soliton pack. *Natural Hazards*, *84*(S2), 471–492. https://doi.org/10.1007/s11069-016-2446-2

Shi, L., Olabarrieta, M., Nolan, D. S., & Warner, J. C. (2020). Tropical cyclone rainbands can trigger meteotsunamis. *Nature Communications*, *11*(1), 678. https://doi.org/10.1038/s41467-020-14423-9

Shi, L., Olabarrieta, M., Valle-Levinson, A., & Warner, J. C. (2019). Relevance of wind stress and wave-dependent ocean surface roughness on the generation of winter meteotsunamis in the Northern Gulf of Mexico. *Ocean Modelling*, *140*, 101408. https://doi.org/10.1016/j.ocemod.2019.101408

Shinagawa, H., & Miyoshi, Y. (2024). Simulation study of atmosphere-ionosphere variations driven by the eruption of Hunga Tonga-Hunga Ha'apai on 15 January 2022. *Earth Planets and Space*, *76*(1), 15. https://doi.org/10.1186/s40623-024-01960-6

Sibley, A. W., Cox, D., & Tappin, D. R. (2021). Convective rear-flank downdraft as driver for meteotsunami along English Channel and North Sea coasts 28–29 May 2017. *Natural Hazards*, *106*(2), 1445–1465. https://doi.org/10.1007/s11069-020-04328-7

Silvestri, S., Wagner, G. L., Campin, J. M., Constantinou, N. C., Hill, C. N., Souza, A., & Ferrari, R. (2024). A new WENO-based momentum advection scheme for simulations of ocean mesoscale turbulence. *Journal in Advances in Modelling Earth Systems*, *16*(7), e2023MS004130. https://doi.org/10.1029/2023MS004130

Skamarock, W. C. (2004). Evaluating mesoscale NWP models using kinetic energy spectra. *Monthly Weather Review*, *132*(12), 3019–3032. https://doi.org/10.1175/MWR2830.1

Skamarock, W. C., Klemp, J. B., Dudhia, J., Gill, D. O., Barker, D. M., Wang, W., & Powers, J. G. (2005). A description of the advanced research WRF version 2. In *NCAR, technical note NCAR/TN-468+STR*. https://doi.org/10.5065/D6DZ069T

Smith, J., Kast, A., Geraschenko, A., Morton, Y. J., Brenner, M. P., van Diggelen, F., & Williams, B. P. (2024). Mapping the ionosphere with millions of phones. *Nature*, *635*(8038), 365–369. https://doi.org/10.1038/s41586-024-08072-x

Soloviev, S. L., Solovieva, O. N., Go, C. N., Kim, K. S., & Shchetnikov, N. A. (2000). Tsunamis in the Mediterranean Sea 2000 B.C.–2000 A.D. *Advances in Natural and Technological Hazards Research*, *13*, 1–239. https://doi.org/10.1007/978-94-015-9510-0

Solovieva, M., Rozhnoi, A., Shalimov, S., Shevchenko, G., Biagi, P. F., & Fedum, V. (2021). The lower ionosphere disturbances observed during the chain of the meteotsunamis in the Mediterranean sea in June 2014. *Natural Hazards*, *106*(2), 1383–1396. https://doi.org/10.1007/s11069-020-04223-1

Squitieri, B. J., Wade, A. R., & Jirak, I. L. (2023). A historical overview on the science of derechos. *Bulletin of the American Meteorological Society*, *104*(10), E1734–E1763. https://doi.org/10.1175/BAMS-D-22-0278.1

Stensrud, D. J., & Fritsch, J. M. (1994). Mesoscale convective systems in weakly forced large-scale environments: 2. Generation of a mesoscale initial condition. *Monthly Weather Review*, *122*(9), 2068–2083. https://doi.org/10.1175/1520-0493(1994)122<2068:MCSIWF>2.0.CO;2

Stull, R. (2017). *Practical meteorology: An algebra-based survey of atmospheric sciences* (p. 940). University of British Columbia.

Sun, Q. Y., & Niu, X. J. (2021). Harbor resonance triggered by atmospherically driven edge waves. *Ocean Engineering*, *224*, 108735. https://doi.org/10.1016/j.oceaneng.2021.108735

Suppasri, A., Goto, K., Muhari, A., Ranasinghe, P., Riyaz, M., Affan, M., et al. (2015). A decade after the 2004 Indian Ocean tsunami: The progress in disaster preparedness and future challenges in Indonesia, Sri Lanka, Thailand and the Maldives. *Pure and Applied Geophysics*, *172*(12), 3313–3341. https://doi.org/10.1007/s00024-015-1134-6

Suursaar, Ü., Kullas, T., Otsmann, M., Saaremäe, I., Kuik, J., & Merilain, M. (2006). Cyclone Gudrun in January 2005 and modelling its hydrodynamic consequences in the Estonian coastal waters. *Boreal Environment Research*, *11*, 143–159.

Suzuki, T., Nakano, M., Watanabe, S., Tatebe, H., & Takano, Y. (2023). Mechanism of a meteorological tsunami reaching the Japanese coast caused by Lamb and Pekeris waves generated by the 2022 Tonga eruption. *Ocean Modelling*, *181*, 102153. https://doi.org/10.1016/j.ocemod.2022.102153

Tabain, T., & Tabain, N. (1994). Razgovor o poplimajima u Veloj luci. *Luško Libro*, *2*, 71–85. (in Croatian).

Tanaka, H. K. M., Aichi, M., Balogh, S. J., Bozza, C., Coniglione, R., Gluyas, J., et al. (2022). Periodic sea-level oscillation in Tokyo Bay detected with the Tokyo-Bay seafloor hyper-kilometric submarine deep detector (TS-HKMSDD). *Scientific Reports*, *12*(1), 6097. https://doi.org/10.1038/s41598-022-10078-2

Tanaka, K. (2010). Atmospheric pressure-wave bands around a cold front resulted in a meteotsunami in the East China Sea in February 2009. *Natural Hazards and Earth System Sciences*, *10*(12), 2599–2610. https://doi.org/10.5194/nhess-10-2599-2010

Tanaka, K. (2012). On meteotsunamis around Tsushima Strait generated by the Baiu front. *Natural Hazards*, *63*(2), 805–822. https://doi.org/10.1007/s11069-012-0186-5

Tappin, D., Sibley, A., Horsburgh, K., Daubord, C., Cox, D., & Long, D. (2013). The English Channel tsunami of 27 June 2011—A probable meteorological source. *Weather*, *68*(6), 144–152. https://doi.org/10.1002/wea.2061

Thiebaut, S., & Vennell, R. (2011). Resonance of long waves generated by storms obliquely crossing shelf topography in a rotating ocean. *Journal of Fluid Dynamics*, *682*, 261–288. https://doi.org/10.1017/jfm.2011.221

Thompson, J., Renzi, E., Sibley, A., & Tappin, D. R. (2020). UK meteotsunamis: A revision and update on events and their frequency. *Weather*, *75*(9), 281–287. https://doi.org/10.1002/wea.3741

Thomson, R. E., Rabinovich, A. B., & Krassovski, M. V. (2007). Double jeopardy: Concurrent arrival of the 2004 Sumatra tsunami and storm-generated waves on the Atlantic coast of the United States and Canada. *Geophysical Research Letters*, *34*(15), L15607. https://doi.org/10.1029/2007GL030685

Tinti, S., Maramai, A., & Graziani, L. (2004). The new catalogue of the Italian tsunamis. *Natural Hazards*, *33*(3), 439–465. https://doi.org/10.1023/B:NHAZ.0000048469.51059.65

Tintoré, J., Gomis, D., Alonso, S., & Wang, D. P. (1988). A theoretical study of large sea level oscillations in the Western Mediterranean. *Journal of Geophysical Research*, *93*(C9), 10797–10803. https://doi.org/10.1029/JC093iC09p10797

Titov, V., & Moore, C. (2021). Meteotsunami model forecast: Can coastal hazard be quantified in real time? *Natural Hazards*, *106*(2), 1545–1561. https://doi.org/10.1007/s11069-020-04450-6

Titov, V., Rabinovich, A. B., Mofjeld, H. O., Thomson, R. E., & González, F. I. (2005). The global reach of the 26 December 2004 Sumatra tsunami. *Science*, *309*(5743), 2045–2048. https://doi.org/10.1126/science.1114576

Tojčić, I., Denamiel, C., & Vilibić, I. (2021). Performance of the Adriatic early warning system during the multi-meteotsunami event of 11-19 May 2020: An assessment using energy banners. *Natural Hazards and Earth System Sciences*, *21*(8), 2427–2446. https://doi.org/10.5194/nhess-21-2427-2021

Tonegawa, T., & Fukao, Y. (2022). Wave propagation of meteotsunamis and generation of free tsunamis in the sloping area of the Japan Trench for the 2022 Hunga-Tonga volcanic eruption. *Earth and Planets Science*, *74*(1), 159. https://doi.org/10.1186/s40623-022-01727-x

Tsimplis, M. N., Marcos, M., Pérez, B., Challenor, P., Garcia-Fernandez, M. J., & Raicich, F. (2009). On the effect of the sampling frequency of sea level measurements on return period estimate of extremes-southern European examples. *Continental Shelf Research*, *29*(18), 2214–2221. https://doi.org/10.1016/j.csr.2009.08.015

UNESCO/IOC. (1985). Manual on sea level measurement and interpretation. Volume I—Basic procedures. In *IOC manual and guides* (Vol. 14). https://doi.org/10.25607/OBP-1420.83.

UNESCO/IOC. (2020). Quality control of in situ sea level observations: A review and progress towards automated quality control. In *IOC manual and guides* (Vol. 83, p. 70). https://doi.org/10.25607/OBP-854

UNESCO/IOC. (2025). Meteotsunamis: Definition, detection and alerting services investigation. In *IOC Technical Series, 200* (p. 31). Retrieved from https://unesdoc.unesco.org/ark:/48223/pf0000392653

Ursell, F. (1952). Edge waves on a sloping beach. *Proceedings of the Royal Society of London*, *214*, 79–97. https://doi.org/10.1098/rspa.1952.0152

Vasylkevych, S., & Žagar, N. (2021). A high-accuracy global prognostic model for the simulation of Rossby and gravity wave dynamics. *Quarterly Journal of the Royal Meteorological Society*, *147*(736), 1989–2007. https://doi.org/10.1002/qj.4006

Vennell, R. (2007). Long barotropic waves generated by a storm crossing topography. *Journal of Physical Oceanography*, *37*(12), 2809–2823. https://doi.org/10.1175/2007JPO3687.1

Vennell, R. (2010). Resonance and trapping of topographic transient ocean waves generated by a moving atmospheric disturbance. *Journal of Fluid Dynamics*, *650*, 427–442. https://doi.org/10.1017/S0022112009993739

Vergados, P., Krishnamoorthy, S., Martire, L., Mrak, S., Komjáthy, A., Morton, Y. T. J., & Vilibić, I. (2023). Prospects for meteotsunami detection in Earth's atmosphere using GNSS observations. *GPS Solutions*, *27*(4), 169. https://doi.org/10.1007/s10291-023-01492-8

Vich, M. M., & Romero, R. (2021). Forecasting meteotsunamis with neural networks: The case of Ciutadella harbour (Balearic Islands). *Natural Hazards*, *106*(2), 1299–1314. https://doi.org/10.1007/s11069-020-04041-5

Vilibić, I. (2005). Numerical study of the Middle Adriatic coastal waters sensitivity to the various air pressure travelling disturbances. *Annales Geophysicae*, *23*(12), 3569–3578. https://doi.org/10.5194/angeo-23-3569-2005

Vilibić, I. (2008). Numerical simulations of the Proudman resonance. *Continental Shelf Research*, *28*(4–5), 574–581. https://doi.org/10.1016/j.csr.2007.11.005

Vilibić, I., Bubalo, M., Zemunik Selak, P., Pranić, P., Radovan, A., Mihanović, H., & Dominović, I. (2025). High-frequency water level oscillations in a coastal shallow lake. *Natural Hazards*. https://doi.org/10.1007/s11069-025-07506-7

Vilibić, I., Denamiel, C., Zemunik, P., & Monserrat, S. (2021). The Mediterranean and Black Sea meteotsunamis: An overview. *Natural Hazards*, *106*(2), 1223–1267. https://doi.org/10.1007/s11069-020-04306-z

Vilibić, I., Domijan, N., & Čupić, S. (2005). Wind versus air pressure seiche triggering in the Middle Adriatic coastal waters. *Journal of Marine Systems*, *57*(1–2), 189–200. https://doi.org/10.1016/j.jmarsys.2005.04.007

Vilibić, I., Domijan, N., Orlić, M., Leder, N., & Pasarić, M. (2004). Resonant coupling of a traveling air-pressure disturbance with the east Adriatic coastal waters. *Journal of Geophysical Research*, *109*(C10), C10001. https://doi.org/10.1029/2004JC002279

Vilibić, I., Horvath, K., Strelec Mahović, N., Monserrat, S., Marcos, M., Amores, A., & Fine, I. (2014). Atmospheric processes responsible for generation of the 2008 Boothbay meteotsunami. *Natural Hazards*, *74*(1), 25–53. https://doi.org/10.1007/s11069-013-0811-y

Vilibić, I., Monserrat, S., & Rabinovich, A. B. (2014). Meteorological tsunamis on the US East Coast and in other regions of the World Ocean. *Natural Hazards*, *74*, 1–9. https://doi.org/10.1007/s11069-014-1350-x

Vilibić, I., Monserrat, S., Rabinovich, A. B., & Mihanović, H. (2008). Numerical modelling of the destructive meteotsunami of 15 June 2006 on the coast of the Balearic Islands. *Pure and Applied Geophysics*, *165*(11–12), 2169–2195. https://doi.org/10.1007/s00024-008-0426-5

Vilibić, I., Orlić, M., Čupić, S., Domijan, N., Leder, N., Mihanović, H., et al. (2005). A new approach to sea level observations in Croatia. *Geofizika*, *22*, 21–57.

Vilibić, I., & Šepić, J. (2009). Destructive meteotsunamis along the eastern Adriatic coast: Overview. *Physics and Chemistry of the Earth*, *34*, 904–917. https://doi.org/10.1016/j.pce.2009.08.004

Vilibić, I., & Šepić, J. (2017). Global mapping of nonseismic sea level oscillations at tsunami timescales. *Scientific Reports*, *7*(1), 40818. https://doi.org/10.1038/srep40818

Vilibić, I., Šepić, J., Dunić, N., Sevault, F., Monserrat, S., & Jordà, G. (2018). Proxy-based assessment of strength and frequency of meteotsunamis in future climate. *Geophysical Research Letters*, *45*(19), 10501–10510. https://doi.org/10.1029/2018GL079566

Vilibić, I., Šepić, J., Rabinovich, A. B., & Monserrat, S. (2016). Modern approaches in meteotsunami research and early warning. *Frontiers in Marine Science*, *3*, 57. https://doi.org/10.3389/fmars.2016.00057

Vilibić, I., Šepić, J., Ranguelov, J., Strelec-Mahović, N., & Tinti, S. (2010). Possible atmospheric origin of the 7 May 2007 western Black Sea shelf tsunami event. *Journal of Geophysical Research*, *115*, C07006. https://doi.org/10.1029/2009JC005904

Villalonga, J., Amores, À., Monserrat, S., Marcos, M., Gomis, D., & Jordà, G. (2023). Observational study of the heterogeneous global meteotsunami generated after the Hunga Tonga–Hunga Ha'apai Volcano eruption. *Scientific Reports*, *13*(1), 8649. https://doi.org/10.1038/s41598-023-35800-6

Villalonga, J., Monserrat, S., Gomis, D., & Jordà, G. (2024). Observational characterization of atmospheric disturbances generating meteotsunamis in the Balearic Islands. *Journal of Geophysical Research: Oceans*, *129*(6), e2024JC020910. https://doi.org/10.1029/2024JC020910

VLIZ/IOC. (2025). Sea level station monitoring facility. https://doi.org/10.14284/482

von Storch, H., & Woth, K. (2008). Storm surges: Perspectives and options. *Sustainability Science*, *3*(1), 33–43. https://doi.org/10.1007/s11625-008-0044-2

Vučetić, T., & Barčot, T. (2008). Records on ''tidal wave" that hit Vela Luka on 21 June 1978. In *Municipality of Vela Luka and Institute of Oceanography and Fisheries, Vela Luka–Split* (p. 80). (in Croatian).

Vučetić, T., Vilibić, I., Tinti, S., & Maramai, A. (2009). The Great Adriatic flood of 21 June 1978 revisited: An overview of the reports. *Physics and Chemistry of the Earth*, *34*(17–18), 894–903. https://doi.org/10.1016/j.pce.2009.08.005

Wächter, J., Babeyko, A., Fleischer, J., Häner, R., Hammitzsch, M., Kloth, A., & Lendholt, M. (2012). Development of tsunami early warning systems and future challenges. *Natural Hazards and Earth System Sciences*, *12*(6), 1923–1935. https://doi.org/10.5194/nhess-12-1923-2012

Wang, J. P., Church, J. A., Zhang, X. B., & Chen, X. Y. (2021). Reconciling global mean and regional sea level change in projections and observations. *Nature Communications*, *12*(1), 990. https://doi.org/10.1038/s41467-021-21265-6

Wang, X., Li, K., Yu, Z., & Wu, J. (1987). Statistical characteristics of seiches in Longkou Harbour. *Journal of Physical Oceanography*, *17*(7), 1963–1966. https://doi.org/10.1175/1520-0485(1987)017<1063:SCOSIL>2.0.CO;2

Watanabe, S., Hamilton, K., Sakazaki, T., & Nakano, M. (2022). First detection of the Pekeris internal global atmospheric resonance: Evidence from the 2022 Tonga eruption and from global reanalysis data. *Journal of the Atmospheric Sciences*, *79*(11), 3027–3043. https://doi.org/10.1175/JAS-D-22-0078.1

Welch, B. M., Horel, J. D., & Sauer, J. A. (2024). Application of the NCAR FastEddy® microscale model to a lake breeze front. *Atmosphere*, *15*(7), 809. https://doi.org/10.3390/atmos15070809

Wertman, C. A., Yablonsky, R. M., Shen, Y., Merrill, J., Kincaid, C. R., & Pockalny, R. A. (2014). Mesoscale convective system surface pressure anomalies responsible for meteotsunamis along the U.S. East Coast on June 13th, 2013. *Scientific Reports*, *4*(1), 7143. https://doi.org/10.1038/srep07143

Whitmore, P., & Knight, B. (2014). Meteotsunami forecasting: Sensitivities demonstrated by the 2008 Boothbay, Maine, event. *Natural Hazards*, *74*(1), 11–23. https://doi.org/10.1007/s11069-014-1056-0

Wijeratne, E. M. S., & Pattiaratchi, C. B. (2024). Meteotsunamis generated by thunderstorms. *Journal of Geophysical Research: Oceans*, *129*(8), e2023JC020662. https://doi.org/10.1029/2023JC020662

Wilkinson, M. D., Dumontier, M., Aalbersberg, I. J., Appleton, G., Axton, M., Baak, A., et al. (2016). The FAIR Guiding Principles for scientific data management and stewardship. *Scientific Data*, *3*(1), 160018. https://doi.org/10.1038/sdata.2016.18

Williams, D. A., Horsburgh, K. J., Schultz, D. M., & Hughes, C. W. (2021). Proudman resonance with tides, bathymetry and variable atmospheric forcings. *Natural Hazards*, *106*(2), 1169–1194. https://doi.org/10.1007/s11069-020-03896-y

Williams, D. A., Schultz, D. M., Horsburgh, K. J., & Hughes, C. W. (2021). An 8-yr meteotsunami climatology across Northwest Europe: 2010-17. *Journal of Physical Oceanography*, *51*(4), 1145–1161. https://doi.org/10.1175/JPO-D-20-0175.1

Wilson, B. (1972). Seiches. *Advances in Hydroscience*, *8*, 1–94. https://doi.org/10.1016/b978-0-12-021808-0.50006-1

Woodworth, P. L. (1991). The permanent service for mean sea level and the global sea-level observing system. *Journal of Coastal Research*, *7*, 699–710.

Woodworth, P. L., Aman, A., & Aarup, T. (2007). Sea level monitoring in Africa. *African Journal of Marine Science*, *29*(3), 321–330. https://doi.org/10.2989/AJMS.2007.29.3.2.332

Woodworth, P. L., & Player, R. (2003). The Permanent Service for Mean Sea Level: An update to the 21st century. *Journal of Coastal Research*, *19*, 287–295.

Wright, C. J., Hindley, N. P., Alexander, M. J., Barlow, M., Hoffmann, L., Mitchell, C. N., et al. (2022). Surface-to-space atmospheric waves from Hunga Tonga-Hunga Ha'apai eruption. *Nature*, *609*(7928), 741–746. https://doi.org/10.1038/s41586-022-05012-5

Xiong, M. J., Wang, G., Zheng, J. H., Gao, J. L., & Thanh, N. V. (2017). Analytic arrival-time prediction method for the largest wave of tsunami trapped by parabolic oceanic ridges. *Journal of Earthquake and Tsunami*, *11*(1), 1740004. https://doi.org/10.1142/S1793431117400048

Xiu, D., & Karniadakis, G. E. (2002). The Wiener–Askey polynomial chaos for stochastic differential equations. *SIAM Journal on Scientific Computing*, *24*(2), 619–644. https://doi.org/10.1137/S1064827501387826

Xu, Q., & Clark, J. H. E. (1984). Wave CISK and mesoscale convective systems. *Journal of the Atmospheric Sciences*, *41*(13), 2089–2107. https://doi.org/10.1175/1520-0469(1984)041<2089:WCAMCS>2.0.CO;2

Yamashita, K., & Kakimura, T. (2024). Interpretation of the global tsunami amplitude distribution due to the air pressure waves from the 2022 Hunga Tonga–Hunga Ha`apai volcanic eruption. *Applied Ocean Research*, *151*, 104168. https://doi.org/10.1016/j.apor.2024.104168

Yankovsky, A. E. (2008). Long-wave response of the West Florida Shelf to the landfall of Hurricane Wilma, October 2005. *Journal of Coastal Research*, *24*, 33–39. https://doi.org/10.2112/06-0824.1

Yankovsky, A. E. (2009). Large-scale edge waves generated by hurricane landfall. *Journal of Geophysical Research*, *114*(C3), C03014. https://doi.org/10.1029/2008JC005113

Yoo, J., Lee, D.-Y., Ha, T.-M., Cho, Y.-S., & Woo, S.-B. (2010). Characteristics of abnormal large waves measured from coastal videos. *Natural Hazards and Earth System Sciences*, *10*(4), 947–956. https://doi.org/10.5194/nhess-10-947-2010

Yoon, S. B. (2002). Propagation of distant tsunamis over slowly varying topography. *Journal of Geophysical Research*, *107*(C10), 3140. https://doi.org/10.1029/2001JC000791

Yuan, Y., Yang, H., Yu, F., Gao, Y., Li, B., & Xing, C. (2023). A wave-resolving modeling study of rip current variability, rip hazard, and swimmer escape strategies on an embayed beach. *Natural Hazards and Earth System Sciences*, *23*(11), 3487–3507. https://doi.org/10.5194/nhess-23-3487-2023

Zabotin, N. A., Godin, O. A., & Bullett, T. W. (2016). Oceans are a major source of waves in the thermosphere. *Journal of Geophysical Research: Space Physics*, *121*(4), 3452–3463. https://doi.org/10.1002/2016JA022357

Zemunik, P., Bonanno, A., Mazzola, S., Giacalone, G., Fontana, I., Genovese, S., et al. (2021). Observing meteotsunamis ("Marrobbio") on the southwestern coast of Sicily. *Natural Hazards*, *106*(2), 1337–1363. https://doi.org/10.1007/s11069-020-04303-2

Zemunik, P., Denamiel, C., Šepić, J., & Vilibić, I. (2022). High-frequency sea-level analysis: Global distributions. *Global and Planetary Change*, *210*, 103775. https://doi.org/10.1016/j.gloplacha.2022.103775

Zemunik, P., Denamiel, C., Williams, J., & Vilibić, I. (2022). High-frequency sea-level extremes: Global correlations to synoptic atmospheric patterns. *Weather and Climate Extremes*, *38*, 100516. https://doi.org/10.1016/j.wace.2022.100516

Zemunik, P., Vilibić, I., Šepić, J., Pellikka, H., & Čatipović, L. (2021a). MISELA: 1-minute sea-level analysis global dataset. *Earth System Science Data*, *13*, 4121–4132. https://doi.org/10.5194/essd-13-4121-2021

Zemunik, P., Vilibić, I., Šepić, J., Pellikka, H., & Čatipović, L. (2021b). MISELA: Minute sea-level analysis [Dataset]. *Marine Data Archive*. https://doi.org/10.14284/456

Zemunik Selak, P., Vilibić, I., Denamiel, C., & Pranić, P. (2025). Synoptic-based model for reconstructing and forecasting high-frequency sea-level extremes in the Mediterranean. *Weather and Climate Extremes*, *48*, 100775. https://doi.org/10.1016/j.wace.2025.100775

Zhang, J. J., Bai, L. Q., Li, Z. M., Du, Y., & Zhang, S. S. (2024). High-frequency microbarograph-observed pressure variations associated with gust fronts during an extreme rainfall event. *Remote Sensing*, *16*(1), 101. https://doi.org/10.3390/rs16010101

Zhang, S. W., Li, Y. X., Feng, J. L., Jin, Y. Y., Zhang, J., & Zhao, L. (2024). Comprehensive comparative analysis of reconstructed sea level datasets in the China Seas: Insights from tide gauge and satellite altimetry. *Frontiers in Marine Science*, *11*, 1469173. https://doi.org/10.3389/fmars.2024.1469173

Zhao, L., & Bai, Y. (2024). Joint-optimized coverage path planning framework for USV-assisted offshore bathymetric mapping: From theory to practice. *Knowledge-Based Systems*, *304*, 112449. https://doi.org/10.1016/j.knosys.2024.112449

Erratum

The originally published version of this article contained an error in Equation 9. The equation has been corrected as follows:

$$H^2(f) = \frac{1}{\left[1 - \left(f/f_0\right)^2\right]^2 + Q^{-2}\left(f/f_0\right)^2}, \tag{9}$$

This may be considered the authoritative version of record.